MONTHLY NOTICES

OF THE

ROYAL ASTRONOMICAL SOCIETY

Vol. 116 No. 4 1956

Published and Sold by the
ROYAL ASTRONOMICAL SOCIETY
BURLINGTON HOUSE
LONDON, W.1

Price Thirteen Shillings and Sixpence

NOTICE TO AUTHORS

1. *Communications.*—Papers must be communicated to the Society by a Fellow. They should be accompanied by a summary at the *beginning* of the paper conveying briefly the content of the paper, and drawing attention to important new information and to the main conclusions. The summary should be intelligible in itself, without reference to the paper, to a reader with some knowledge of the subject; it should not normally exceed 200 words in length. **Authors are requested to submit MSS. in duplicate. These should be typed using double spacing and leaving a margin of not less than one inch on the left-hand side. Corrections to the MSS. should be made in the text and not in the margin.** Unless a paper reaches the Secretaries more than seven days before a Council meeting it will not normally be considered at that meeting. By Council decision, MSS. of accepted papers are retained by the Society for one year after publication; unless their return is then requested by the author, they are destroyed.

2. *Presentation.*—Authors are allowed considerable latitude, but they are requested to follow the general style and arrangement of *Monthly Notices*. References to literature should be given in the standard form, including a date, for printing either as footnotes or in a numbered list at the end of the paper. Each reference should give the **name and initials** of the author cited, irrespective of the occurrence of the name in the text (some latitude being permissible, however, in the case of an author referring to his own work). The following examples indicate the style of reference appropriate for a paper and a book, respectively :—

A. Corlin, *Zs. f. Astrophys.*, **15**, 239, 1938.
H. Jeffreys, *Theory of Probability*, 2nd edn., section 5.45, p. 258, Oxford, 1948.

Alternatively, the Harvard reference system may be used.

3. *Notation.*—For technical astronomical terms, authors should conform closely to the recommendations of Commission 3 of the International Astronomical Union (*Trans. I.A.U.*, Vol. VI, p. 345, 1938). Council has decided to adopt the I.A.U. 3-letter abbreviations for constellations where contraction is desirable (Vol. IV, p. 221, 1932). In general matters, authors should follow the recommendations in *Symbols, Signs and Abbreviations* (London : Royal Society, 1951) except where these conflict with I.A.U. practice.

4. *Diagrams.*—**These should be designed to appear upright on the page, drawn about twice the size required in print and prepared for direct photographic reproduction except for the lettering, which should be inserted in pencil. Legends should be given in the manuscript indicating where in the text the figure should appear.** Blocks are retained by the Society for 10 years; unless the author requires them before the end of this period they are then destroyed.

5. *Tables.*—**These should be arranged so that they can be printed upright on the page.**

6. *Proofs.*—Costs of alteration exceeding 5 per cent of composition must be borne by the author. Fellows are warned that such costs have risen sharply in recent years, and it is in their own and the Society's interests to seek the maximum conciseness and simplification of symbols and equations consistent with clarity.

7. *Revised Manuscripts.*—When papers are submitted in revised form it is especially requested that they be accompanied by the original MSS.

Reading of Papers at Meetings

8. When submitting papers authors are requested to indicate whether they will be willing and able to read the paper at the next or some subsequent meeting, and approximately how long they would like to be allotted for speaking.

9. Postcards giving the programme of each meeting are issued some days before the meeting concerned. Fellows wishing to receive such cards whether for Ordinary Meetings or for the Geophysical Discussions or both should notify the Assistant Secretary.

MONTHLY NOTICES

OF THE

ROYAL ASTRONOMICAL SOCIETY

Vol. 116 No. 4

MEETING OF 1956 MAY 11

Professor Sir Harold Jeffreys, President, in the Chair

The election by the Council of the following Fellows was duly confirmed ;—

George Allison Eiby, M.Sc., 2 Shortland Street, Khandallah, Wellington, New Zealand (proposed by K. D. Adams);

*Michael Godfrey Fisher, B.Sc., West Wood, Carleton, Pontefract, Yorkshire (proposed by C. W. Allen);

Rev. Walter J. Miller, S. J., Fordham University Astronomical Laboratory, New York, U.S.A. (proposed by R. v. d. R. Woolley);

Walter Orr Roberts, Director of the High Altitude Observatory, Boulder, Colorado, U.S.A. (proposed by S. Chapman); and

Henry Peter Francis Swinnerton-Dyer, M.A., Trinity College, Cambridge (proposed by B. E. J. Pagel).

The election by the Council of the following Junior Member was duly confirmed :—

John Keith Welwyn Davies, 101 Slade Lane, Levenshulme, Manchester (proposed by Z. Kopal).

Seventy-four presents were announced as having been received since the last meeting, including :—

G. de Vaucouleurs, *Physics of the Planet Mars* (presented by the author).

* Transferred from Junior Membership.

THE DAMPING OF THE VARIATION OF LATITUDE

Harold Jeffreys

(Received 1956 February 27)

Summary

Bondi and Gold have pointed out a mistake in an estimate of the viscosity of the Earth's core based on the damping of the 14-monthly variation of latitude. The full force of this criticism is diminished when account is taken of a second serious mistake, and correction of this leads to the conclusion that the damping might just be due to dissipation in the core, but for other reasons it cannot be due to viscosity there. The damping could be due to elastico-viscosity in the shell at depths greater than 700 km, in which case the viscosity would be about 10^{20} c.g.s. units, or to elastic afterworking. In the latter case a wide range of parameters in the law is permissible.

In the third edition of *The Earth* I used three data relevant to the admissible viscosity of the Earth's core.

(*a*) The transmission of sharp longitudinal pulses through the core forbids a kinematic viscosity greater than 10^8 cm^2/sec.*

(*b*) An extrapolation based on Bridgman's work suggested that 1 cm^2/sec is probably of the right order of magnitude.†

(*c*) On the assumption that damping of the 14-monthly variation of latitude is due to viscosity in the core, I found a viscosity of about 10^5 cm^2/sec.‡

(*d*) I found also that within a wide range of possibilities elastic afterworking in the shell could account for the damping.

Bondi and Gold in an interesting paper§ have argued that no type of dissipation in the core can account for the damping of the variation of latitude. They say, however, in the first paragraph on p. 42 that I considered it "probable, or at any rate possible" that viscosity in the core accounts for it; in view of the above comparison this statement seems exaggerated. In particular, if we accept (*b*), and I see no reason to doubt it, their result so far as it concerns viscosity is an immediate consequence.

As they point out, there is a serious mistake in (*c*). They are correct in saying that my discussion confuses two meanings of (l, m), which at first denote direction cosines of the instantaneous axis with respect to the geographic axis and later denote those of the geographic axis with respect to the mean frame of reference. However, the argument contains a second mistake, which they mention but do not explain in detail. This is worth attention, particularly because it will be relevant to further discussions. In the simple case of a rigid shell and a homogeneous core I took‖ a general rotation of the shell, referred to mean rotating axes, expressed by direction cosines (l, m), and put $\zeta = l + im$. The additional motion of the core is represented by a complex quantity ζ. This does

*H. Jeffreys, *The Earth*, 1952, p. 244. †*Ibid.*, p. 244. ‡*Ibid.*, p. 246.
§*M.N.*, **115**, 41–46, 1955. ‖ H. Jeffreys, *M.N.*, **109**, 670–686, 1949.

not give a simple rotation, being affected by the ellipticity, but the resulting displacements differ from those given by a rotation within a factor of order ϵ, where ϵ is the ellipticity of the core boundary. The ratio ζ/ζ' is $-(1-\epsilon)+O(\epsilon^2)$. The slip depends only on ζ. Thus with an oblate boundary ellipticity decreases the slip, but prolateness would increase it. In any case the ellipticity is quite unimportant. (This is not true for precession and nutation; there the ellipticity has a dominating effect on account of the proximity of two free periods.)

For an elastic shell the elastic displacements of the boundary produce similar normal displacements to those produced by a rotation of the shell, and it was convenient to introduce a fictitious rotation ζ'' that would produce the same normal displacements as the actual rotation and the elastic displacements together. Unfortunately I supposed in *The Earth* that it would also produce the same tangential displacements, and this is false. The motion of the core is the resultant of those produced by ζ'' and ζ, with ζ now about $-(1-\epsilon)\zeta''$. In the case I solved for an elastic shell ζ'' was about $0{\cdot}14\zeta'$. With a factor ϵ the slip is equal to that produced by a rotation $\zeta'-(\zeta''+\zeta)$ and hence to the same accuracy to that produced by ζ'. For an elastic shell as for a rigid one, therefore, the slip is practically the same as if the core did not move. Consequently the factor $0{\cdot}14$ should be suppressed in the ratio of the slip to ζ'. Incidentally Bondi and Gold (second paragraph on p. 45) are wrong in supposing that the rotation of the shell varies from ζ' to ζ'' with radius; the mean rotation of a level surface is ζ' throughout.

In equation (13) of *The Earth*, p. 246, I suppress the factor $0{\cdot}02$ $(=0{\cdot}14^2)$ and apply the factor $1/420$ to l, m. This divides the expression, for given ν, by about 3600. Thus to fit my estimate of the damping would make the thickness of the boundary layer about 1400 km and the kinematic viscosity about 10^{12} cm^2/sec. This viscosity is inconsistent not only with estimate (*b*), mentioned above, but with the purely geophysical estimate (*a*). Further, at such thickness, ordinary boundary layer theory would need a considerable correction, and the consideration of Bondi and Gold becomes relevant, that too high a viscosity would drag the core around with the shell and the dissipation would fall off again. It does however seem, apart from other considerations, that suitable viscosity could give damping of the right order of magnitude.

I think that some points of Bondi and Gold's discussion need further clarification, particularly in view of remarks made when the paper was read.* Their simplified model gives for the maximum damping a time factor

$$\exp\left(-\frac{\beta\varkappa\omega t}{2(1+\varkappa)}\right).$$

Here ω is the Earth's mean rotation speed, β the dynamical ellipticity of the shell (equal to that of the Earth, since ellipticity of the core is neglected) and $\varkappa$ is the ratio of the mean moments of inertia of the core and shell. Since the free period is $2\pi/\beta\omega$ and $\varkappa$ is about $0{\cdot}1$, this amounts in a period to about $\exp(-\frac{1}{11}\pi)$, and the time needed to reduce the amplitude to e^{-1} of its original value is about 3·5 periods. Thus the maximum damping, at first sight, would be consistent with my estimate of about 15 years, and even with Walker and Young's estimate of about 3 years.† The questions that remain are whether the supposed maximum

Observatory, **75**, 89–91, 1955.

†A. M. Walker and A. Young, *Observatory*, **75**, 1–4, 1955; *M.N.*, **115**, 443–459, 1955.

is actually a maximum, and if so, how far the actual value is likely to fall short of it. There are theorems of minimum rates of dissipation for steady motions in the theories of viscosity and electric currents, and since the period in this case is long they are presumably applicable in this case. I therefore see no reason to doubt that their maximum is an over-estimate. As Bondi and Gold say, however, the actual motion would be substantially different from theirs and the actual damping might need to be nearly the maximum consistent with the type of resistance assumed. Whether this is an argument against, for instance, electromagnetic damping, may be left to personal judgment. Without more detailed examination, however, it seems to be possible to say that the damping cannot be due to viscosity in the core but might just possibly be due to electromagnetic damping.

It has been suggested that the upper bound given by (*a*) might be irrelevant to the variation of latitude, for two reasons. First, the viscosity might depend greatly on the period. However, for normal liquids the viscosity can be determined either from steady motion in a tube or from torsional oscillations of a plate, and the two methods agree. Secondly, the discovery of the "second coefficient of viscosity" for liquids introduces a doubt as to whether an estimate of viscosity from longitudinal waves would be applicable to a mainly distortional movement. The second coefficient, however, expresses a resistance to expansion and will give extra damping of longitudinal waves without a corresponding addition for distortions. Thus, if it is important, the estimate of the ordinary viscosity given by longitudinal waves will be too high, and the argument is strengthened.

I did not give in *The Earth* an explicit estimate of the viscosity in the shell needed to account for the damping. This is easily found from (19) on p. 247. For elastico-viscosity τ' is infinite and the equation leads to a time of relaxation of rigidity

$$\tau = \frac{40}{\gamma} = 2600 \text{ days},$$

and the effective coefficient of viscosity would be of the order of 10^{20} gm/cm sec. This is not out of the question. The gravity anomalies would be consistent with absence of strength at depths over 700 km at the cost of a strength of about 3×10^8 dynes/cm^2 above that level. An infinite set of solutions attributing the damping to elastic afterworking would also be possible.

160 *Huntingdon Road,*
Cambridge :
1956 *February* 22.

OBSERVATIONS FROM AN AIRCRAFT OF THE ZODIACAL LIGHT AT SMALL ELONGATIONS

D. E. Blackwell

(Received 1956 April 30)

Summary

The need for polarization data for the zodiacal light between elongations 20° and 35° is discussed. It is shown that such data can be obtained by observations from high altitude, and especially from aircraft, under suitable conditions. Measurements of brightness in absolute units and of polarization obtained between elongations 21° and 31° along the ecliptic using a Sunderland aircraft at a height of 9000 ft over the South Pacific Ocean on 1955 May 24 are given. The zodiacal light axis was then vertical to within 0°·3. The average ecliptic latitude of the axis of symmetry on this occasion was only +0°·17. The data are interpreted in terms of electron densities in interplanetary space, and the effect on the computed electron densities of errors in the data and their interpretation are discussed. The angle between the axis of symmetry of the electron component and the ecliptic for this range of elongation is probably less than 1°.

---

1. *Introduction.*—During the last few years there has been a renewed interest in the zodiacal light phenomena, perhaps partly stimulated by a paper of Whipple (**1**) in which he discusses for the first time the possibility that the phenomena are due entirely to the scattering of solar radiation by free electrons. Since then it has been generally assumed that at least part of the zodiacal light is due to electron scattering, the remainder being due to scattering by dust. The reason for this assumption is that the observed polarization for all elongations smaller than 60° is probably too great to be attributable to dust scattering alone. It is not easy to make a definite decision about this, however, because our knowledge of the dust component is still very scanty, and will not be increased until more observational data are available. Briefly, we may reason as follows. The colour of the zodiacal light differs slightly from that of the average solar disk (**2, 3**). Hence, not all of the light is due to electron scattering. Further, as the colour is not greatly different from that of the Sun, Rayleigh scattering by dust cannot be the dominant process, and the effective particle size cannot be less than about 0·3 μ. This means that the high polarization associated with Rayleigh scattering need not be expected. Van de Hulst (**4**) has calculated the polarization to be expected from scattering by large particles, obtaining for water droplets scattering through an angle of 30° a value of 5 per cent. The average phase function of zodiacal light particles is not known, but this result makes it likely that the polarization of the dust component is not greater than 10 per cent at elongation 30°. On the other hand, the observed polarization of the zodiacal light at this elongation is of the order of 23 per cent.*

* See paras. 4 and 11 for a more complete discussion.

The important problem has therefore emerged of deducing from zodiacal light data the electron density as a function of distance from the Sun. The general principles involved are well known. The contributions from dust and electrons have first to be separated. The simplest kind of observation that can be used for this purpose is that of polarization. Denoting the brightness of the dust and electron components as F and K respectively, and their polarizations as p^F and p^K, we have for the total observed polarization

$$p_0 = \frac{F}{F+K} \cdot p^F + \frac{K}{F+K} \cdot p^K. \qquad (1)$$

If p^F is known, or can be assumed zero, this equation can be solved by successive approximation and both K and F calculated. For the solar corona, within the range of elongation 0°–5°, p^F can without much error be assumed zero (**7**). But reliable observations of the polarization of the zodiacal light have hitherto existed only for elongations greater than 35°, and for these elongations we have no knowledge whatsoever of the value of p^F. It is true that plausible predictions can be made using idealised models, but for a completely reliable prediction it would be necessary to know accurately the distribution of particles in size, their distribution in space, their shapes and orientations, their surface properties and composition. The supposition of Whipple (**6**) that the particles are highly porous and of low density complicates the problem even further. There are reasons, even, for supposing that the polarization of the dust component is negative (**5**). Faced with this problem there are only two courses open to us, if the polarization data are to be used to derive electron densities. We must either measure the polarization of the dust component, or confine work to those elongations where it can be safely neglected. In this paper we consider the second course.

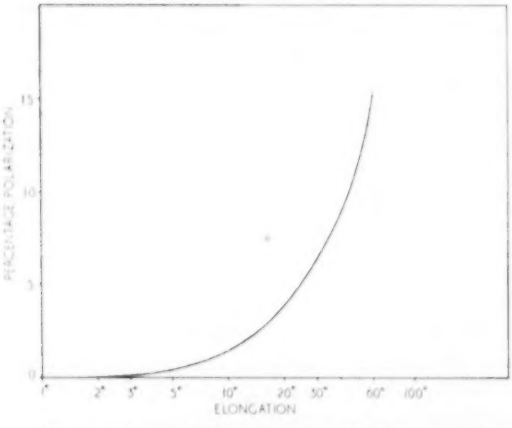

FIG. 1.—*Assumed polarization curve for dust component.*

2. *Need for observations at small elongations.*—In Fig. 1 is shown a curve which gives the maximum likely polarization of the dust component. It has been constructed by taking the kind of value suggested by Whipple (**1**) and van de Hulst (**4**) for elongation 60°, and the values expected for Rayleigh scattering for small elongations, and making a plausible interpolation. The reliability of an electron

density calculation which uses measured values of the polarization at a particular elongation, depends upon the ratio $R = p^{F+K}/p^F$, p^F now being the likely value of the dust polarization. The quantity $R-1$ has been plotted in Fig. 2, using the results for p^{F+K} deduced from observations described later in this paper, and those of Behr and Siedentopf (**2**), together with the plausible values for p^F just suggested. No reliance can be placed on electron density deductions at elongations for which $R-1 \leqslant 0$. This figure demonstrates that, for elongations in the range $36^\circ > \epsilon > 22^\circ$, this ratio is never less than 2·7, which means that the error of calculation of electron density, if p^F is assumed zero, is not likely to be more than 37 per cent. In particular, observations in the region $\epsilon < 7^\circ$ and around $\epsilon = 30^\circ$ can be interpreted with a maximum likely error of 30 per cent, while beyond elongation 60° interpretation in terms of electron densities becomes practically worthless (unless there is prior knowledge of p^F). The minimum elongation for which reliable data for the polarization of the zodiacal light have hitherto been obtained is $\epsilon = 35^\circ$. The corresponding maximum elongation in the solar corona is 5°. These elongations correspond to minimum distances from the Sun of $20R_\odot$ and $123R_\odot$, and between these distances there are no electron density values available. It is evidently very important that measures of the zodiacal light should be brought inwards at least to an elongation of about 20°, because this will lead to reliable electron density values being obtained within the distance range $123R_\odot$ to $74R_\odot$. In this paper we shall show that reliable measures can in fact be obtained at least as close to the Sun as elongation 22°.

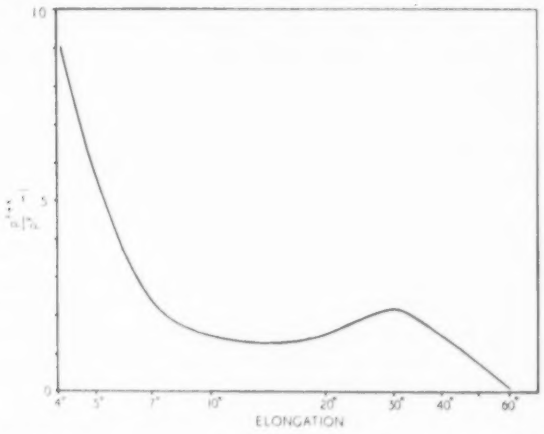

FIG. 2.—*Supposed variation of* $p^{F+K}/p^F - 1$ *with elongation* (p^{F+K} *is the observed or interpolated polarization of the zodiacal light and* p^F *the assumed polarization of the F component).*

3. *Kind of observations needed.*—The prime purpose of these measurements of the zodiacal light would be to obtain reasonably accurate values of electron density. For this, measurements of both total brightness and polarization are required. The more accurate measurements of the *brightness* of the zodiacal light, for example, those of Roach *et al.* (**3**), show that there is a relation of the form $I = k\epsilon^{-n}$ between the brightness and elongation which represents the observations to a high order of accuracy between elongations 30° and 70°. The aircraft observations of Blackwell (**7**), which link the solar corona and the zodiacal light,

show that this relation reproduces the observations with an accuracy of the order of 5 per cent at least over the range of elongation 6°–70°. As the error in the interpretation of the observations may be as high as 25 per cent there is therefore no need to measure the brightness of the zodiacal light in the very difficult region $20^\circ < \epsilon < 30^\circ$, but it is sufficient to measure it over the range $30^\circ < \epsilon < 50^\circ$ and extrapolate to smaller elongations. It will become apparent later that this simplifies the problem considerably. The *polarization*, however, presents a completely different problem. As the values which are plotted in Fig. 9 show, it is not possible to make a reliable interpolation between the solar corona and the zodiacal light in the region $20^\circ < \epsilon < 35^\circ$, and it is therefore essential to obtain accurate measurements.

4. *Previous observations.*—There have been many investigations of zodiacal light brightness. Among the earlier work the most extensive and reliable is that done photoelectrically by Elvey and Roach (**8**) between elongations 40° and 90°. In work of this kind the great difficulty is to decide upon the brightness of the background, and in a later paper by Roach *et al.* (**6**) this problem is discussed in detail. Here, values of zodiacal light brightness between elongations 30° and 100° are given. The difficulties of measurement are shown by a comparison with the results of Behr and Siedentopf (**2**); at the elongation of 35° the brightness given by Roach is twice that given by Behr and Siedentopf. This may be a real difference in brightness, but Regener (**9**) in some very careful measurements does not detect any systematic variation with time over a period of 15 months.

There have, unfortunately, been few quantitative investigations of polarization. The first was by Dufay (**10**) who used a photographic method between elongations 30° and 90°. The second was by Behr and Siedentopf (**2**) who used a photoelectric method between elongations 35° and 90°. The two sets of data agree as to order of magnitude, but whereas at 40° elongation Dufay obtains the value 12·5 per cent, Behr and Siedentopf derive 23 per cent. Take-uchi (**11**) has made measurements at elongation 60°. No observations exist for the important range of elongation $20^\circ < \epsilon < 35^\circ$.

5. *Conditions for observations in this region.*—To observe the zodiacal light at small elongations it is clearly necessary to observe as soon after sunset and as close to the horizon as possible. Suppose that under exceptional conditions it is possible to observe within 4° of the horizon. Fig. 3 shows the brightness of the zodiacal light and of the sky that may be expected at altitude 4° for different depressions of the Sun below the horizon. The zodiacal light curve shows the observed brightness uncorrected for atmospheric extinction. The data for the sky brightness in this figure, which are approximate only, have been obtained photographically from an aircraft by methods described later. Some ground observations at smaller depressions of the Sun below the horizon have also been used in constructing the diagram, all of which refers to an effective wave-length of 6300 A.

The diagram demonstrates that under these conditions the zodiacal light is equal in brightness to the sky background at an elongation of 23°. If the atmospheric conditions are satisfactory it should thus be possible to make observations to at least this elongation. However, the sky brightness increases very rapidly with decreasing depression of the Sun below the horizon and it is clear, first, that good timing of the observations is necessary, and secondly, that the smallest elongation at which observations can be made is sharply defined.

The second intersection of the two curves at elongation 29° is of no significance because there is no need to observe at this elongation so close to the horizon.

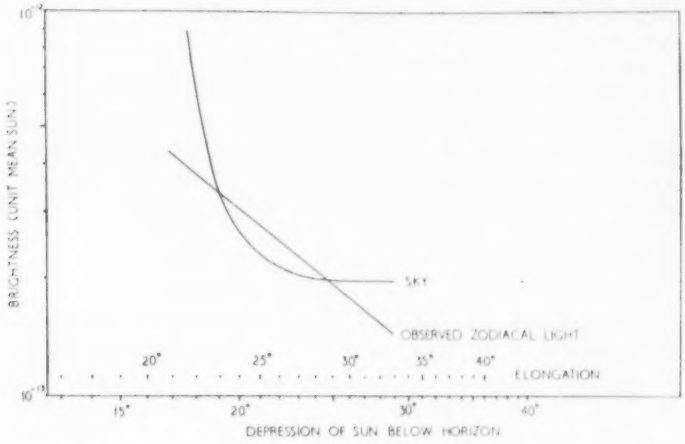

FIG. 3.—*Variation of sky brightness and zodiacal light brightness with depression of the Sun below the horizon. All measurements refer to an altitude of 4°.*

It is clearly essential to have exceptionally good observing conditions for quantitative observations of this nature. In particular, it is not easy to make such observations from the ground because the light path passes very close to the Earth's surface for a great distance, and is therefore much influenced by low lying dust and haze. To avoid this difficulty it is desirable to observe over a sea horizon either from an isolated mountain peak or from an aircraft. The great advantage of an aircraft is that it enables observation to be made over open ocean, far from large land masses, where the air is virtually free from dust and smoke. Under these conditions the atmospheric extinction is small (as is demonstrated later) and its variation with altitude regular. From an elevated position useful observations can be made down to an altitude ϕ above the depressed horizon, where ϕ is the depression of the horizon. In this problem there is little to be gained from observing at a height* greater than 10 000 ft; at this height the observer is already above most haze and dust, and observations can be made to within 2° of the horizon before the haze layer is penetrated by the light path.

To reduce as much as possible the effects of atmospheric extinction the ecliptic should be nearly vertical.

6. *Observations.*—The observations of the zodiacal light described here were made as part of the programme of an expedition to Fiji to observe the total solar eclipse of 1955 June 20. These observations were planned to be complementary to the eclipse observations, all being made at about the same time. They were made over sea in an open Sunderland aircraft of the Royal New Zealand Air Force at a height of 9000 ft and in the approximate position

Latitude 16°·3 S
Longitude 179°·5 W

* In this paper the following usage is adopted : height refers to elevation of aircraft above ground, altitude refers to angular elevation of line of sight above horizon.

Two flights were made for this purpose, both in excellent weather conditions. No photographs were taken near sunset because of the confusion at that season between the Milky Way and the zodiacal light.

TABLE I

Photographs of zodiacal light

Date	Photograph	Inclination of ecliptic to vertical	Mean depression of Sun below horizon	Mean galactic latitude
1955 May 24	I	0° 19′	19°·7	−50°
	II		18°·1	
1955 June 24	III	9° 32′	19°·3	−25°
	IV		17°·2	

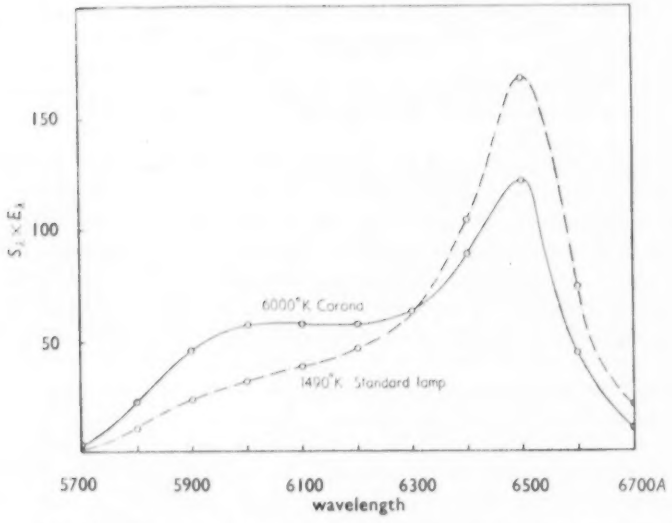

FIG. 4.—*Spectral sensitivity of camera for sources of colour temperature 6000 deg. K and 1490 deg. K.*

The camera was similar in design to that used to observe the total solar eclipse of 1954 June 30; a description of this camera has already been published (**7**). There is no need in work of this kind to use high quality lenses; we are simply measuring the brightness of a featureless surface, and in any case without elaborate apparatus the irregular motion of the aircraft during the relatively long exposures soon vitiates good definition. Three simple lenses of white glass were used, each of diameter 7·1 cm and focal length 12·9 cm, with relative aperture $f/1{\cdot}8$, giving a plate scale of 0°·44 per mm and a field of 60°. Each lens was used in conjunction with a Chance OY1 filter, giving the spectral sensitivity shown in Fig. 4 for a source at 6000 deg. K. The effective wave-length* is close

* The evaluation of the effective wave-length is described in detail in a previous paper (**5**).

to 6300 A. Two of the three lenses were also backed by suitably orientated sheets of HN22 Polaroid filter. The three lenses formed three separate images on to one Ilford HP3 plate. Under these conditions an exposure of 5 min gave an excellent direct photograph, but an underexposed polarization photograph. Photographs I and II were given exposures of 15 min and 5 min respectively, and III and IV were given 8 min and 4 min. Nos. I and II were taken while the zodiacal light was still almost uncontaminated by sunlit sky near the horizon, III and IV were taken later to obtain the polarization of the dawn sky.

Several hours later on the ground an absolute calibration from a sub-standard lamp was put on to another plate of the same batch through a quartz step wedge, and the zodiacal light plate and calibration plate developed together. The substandard lamp was later compared with a second standard which had been calibrated by the National Physical Laboratory. The brightness of the zodiacal light could thus be obtained in absolute units, and by using the value for the mean brightness of the Sun given by Minnaert (**12**) the zodiacal light could be related directly to the average brightness of the solar disk. Precautions mentioned in a previous paper (**7**) were taken to ensure photometric accuracy. Particular attention has been paid to the variation of camera sensitivity with distance from the optical axis.

The camera was mounted on a table behind an open hatch in the side of the aircraft. A crude attempt to guide was made, but much reliance was placed on the stability of the aircraft. It was found that in reasonably good flying conditions this results in nearly round star images rather more than 1° in diameter for an exposure time of 5 min. Such definition is amply good enough for this problem.

7. *Measurement of atmospheric transmission.*—The atmospheric transmission was measured on one occasion only from the aircraft at a height of 9000 ft, but as the sky was of excellent quality on this occasion, and on all other occasions when observations were made from the aircraft, the results can be assumed to be representative. The extinction was measured by taking calibrated photographs of the rising moon. In the reduction of the observations the extinction formula

$$I = I_0 e^{-km_0} \qquad (2)$$

was used, where I_0 is the intensity of radiation entering the Earth's atmosphere, I the observed intensity, k an absorption coefficient and m_0 the total mass of air along the line of sight. The unit of m_0 is the mass of air along a vertical line of sight starting from the Earth's surface. The quantity m_0 has been evaluated by numerical integration for an aircraft height of 9000 ft and for various altitudes above the horizon, using a standard atmosphere (**13**). A plot of $\log I$ against m_0 now gives the value of k. A good fit to a straight line was obtained for values of m_0 ranging from 9·5 air masses to 20·8 air masses, the gradient of which gives the value $k = 0{\cdot}080 \pm 0{\cdot}01$ *air mass*$^{-1}$.

A comparison of this value with those values given by Allen (**14**) for the various atmospheric constituents demonstrates the almost complete absence of atmospheric dust during the present series of observations. At this geographical position the contributions to k given by Allen are, excluding dust,

from molecular scattering	0·0558
1 cm precipitable water (p. 110, 111)	0·0018
2 mm ozone at N.T.P. (p. 120)	0·0193

making a total of $k=0{\cdot}077$. This means that the contribution from dust is between 0·003 and 0·013. For "fairly clear conditions" Allen gives the dust contributions as $k=0{\cdot}055$, which is about seven times greater than the value found in the present work.

We are forced by the nature of the problem to work as close to the horizon as possible, so that we should now ask the question—how accurately should the extinction be measured? It is seen from equation (2) that the error ΔI_0 in deriving the true intensity I_0 from a measured intensity I is related to the error Δk in measurement of k, by the relation

$$\frac{\Delta I_0}{I_0} = \frac{\Delta k}{k} . \log_e \frac{I_0}{I} . \tag{3}$$

The ratio $\left[\frac{\Delta I_0}{I_0}\right] \Big/ \left[\frac{\Delta k}{k}\right]$ is plotted against altitude in Fig. 5 for $k=0{\cdot}080$ air mass^{-1}, and a height of 9000 ft. The probable error in k is of the order of 10 per cent, and from the diagram we deduce that at all altitudes greater than 4° above the depressed horizon the error in derivation of I_0 from this cause is less than 10 per cent. At 10° above the horizon it is only 3 per cent. These errors are much smaller than those due to uncertainty in the sky background, and it is therefore sufficient to know k to within 10 per cent. We emphasize again at this stage, that it is possible to treat atmospheric absorption quantitatively at such low altitudes only because of the absence of dust or smoke haze along the line of sight, due partly to the geographical positions and partly to the use of an aircraft.

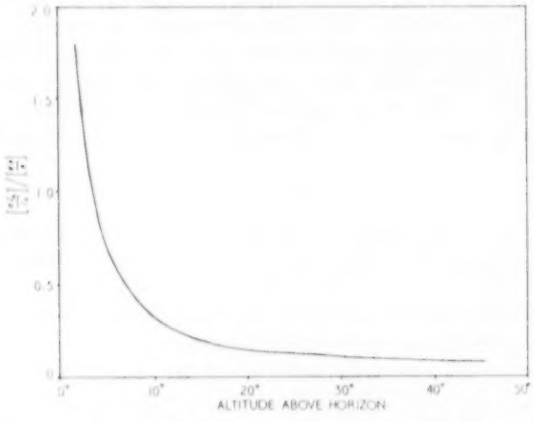

FIG. 5.—*Error in estimate of intensity caused by error in estimate of atmospheric extinction.*

These absorption coefficients refer to a point source outside the Earth's atmosphere. It is the usual practice in investigations of the night sky light to use a value for the extinction which is one half of this (**15, 16**). This procedure is used because the absorption is chiefly due to scattering and in any direction the observer sees light scattered from all parts of the night sky. In this case it is not justified because the solid angle subtended by the zodiacal light is comparatively small, and the point source extinction is used.

8. *Measurement of position on the photographs.*—As the photographs show stars to the fifth magnitude, there are sufficient data for a plate solution by a modification of Turner's method (**17**) in which the plate distortion of the optical system is first measured. The positions of the star images on the better plates can be measured with a ruler to within 0·2 mm or 0°·1, and the first plate solution reproduces their positions with this accuracy. The average position of the horizon is reasonably well defined and the altitude of any part of the sky above the horizon is taken directly from the photograph. There is thus no need to have any knowledge of the position or orientation of the aircraft, or of the precise time at which the photograph was taken.

9. *Axis of symmetry of zodiacal light.*—The first two plates are well suited to this measurement because when they were taken the ecliptic was vertical at the horizon to within a fraction of a degree. These photographs were taken with the Sun at the average distance of 19°·7 and 18°·1 below the horizon respectively. Table II gives the deviation of the axis of symmetry of the zodiacal light from the ecliptic, averaged from these two plates. All deviations are to the north of the ecliptic. The accuracy of measurement is of the order of 0°·1. The average

TABLE II

Deviation from ecliptic of axis of symmetry of zodiacal light 1955 *May* 24

elongation	25°	27°·5	30°	32°·5	35°	37°·5	40°	42°·5
deviation	−0°·22	0	0	−0°·18	−0°·20	−0°·13	0°·33	0°·33

deviation on this occasion was only +0°·17, which in circular measure about the Sun is 0°·28. These results support the view of Regener (**9**) that the zodiacal light is indeed highly symmetrical with respect to the ecliptic. Presumably the axis of symmetry tends towards the solar equator with decreasing distance from the Sun. However, the change from the ecliptic to the solar equator must occur comparatively close to the Sun because, on this occasion, the angle between the two was 7°·1.

10. *The brightness of the zodiacal light and of the sky background.*—Our task is to measure the brightness of the zodiacal light as a function of distance from the Sun as far as elongation 50°. For this purpose plate I has been used because this was the earliest photograph of the series and was taken when the Sun was so far below the horizon that, except for a band very close to the horizon, none of the sky background brightness is due to the scattering of sunlight in the Earth's atmosphere. Visual examination of the appearance of the dawn sky makes it clear that the scattering of sunlight is at first confined to a narrow band at the horizon, for it is here that the sky suddenly begins to brighten, the part above remaining dark for a longer time. The brightness has been measured by scanning the plates with the Cambridge Observatories microphotometer. The procedure outlined by Roach *et al.* (**3**) has been used to obtain the sky background down to elongation 28°. The resulting data obtained from plate I are shown in Fig. 6. It should be emphasised at this stage that aircraft observations are not necessarily more accurate than ground observations for elongations greater than 35°. The barrier to high accuracy in this region is the brightness of the inevitable background,

and if the Sun is 20° below the horizon this is not appreciably diminished by observing from an aircraft. These observations are not in good agreement with those of Roach *et al.* (**3**). For example, at elongation 35° we obtain a brightness of $3{\cdot}89 \times 10^{-13} \bar{B}_{\odot}$, where $\bar{B}_{\odot}$ is the average brightness of the solar disk at λ 6300 A. Roach* obtained the value, on 1952 November 18/19, of $5{\cdot}15 \times 10^{-13} \bar{B}_{\odot}$. Regener, in his careful work, obtained $7{\cdot}29 \times 10^{-13} \bar{B}_{\odot}$, using a photoelectric cell without a colour filter. Behr and Siedentopf (**2**), on the other hand, at wave-length 5400 A, obtained the value of $3{\cdot}46 \times 10^{-13} \bar{B}_{\odot}$. It is important to decide whether these discrepancies represent a real variation or are the result of errors of observation. The following points are relevant to this matter. First, it is most undesirable to use stars of known stellar magnitude as an intermediate standard of surface brightness. The surface brightness of the zodiacal light has eventually to be related to the surface brightness of the Sun, and the extinction produced by the Earth's atmosphere enters once into all reductions. A more direct and satisfactory procedure is therefore to measure the brightness of the

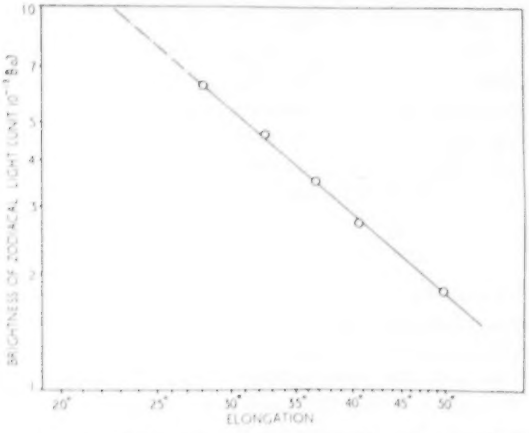

FIG. 6.—*Brightness of zodiacal light. Morning, 1955 May 24.*

zodiacal light in absolute units and to make a good estimate of the atmospheric extinction at the time of observation. The atmospheric absorption from a height of 9000 ft and at an altitude of 15° above the horizon (corresponding to an elongation of 35°) is of the order of 20 per cent at wave-length 6300 A under good conditions; it should be possible to determine the extinction coefficient with an error of less than 10 per cent, and hence the error in the extra-terrestrial flux from this cause should be less than 2 per cent. Second, the error in measurement of brightness at elongation 35° due to an error in the estimation of the background is small. At this elongation, according to these measurements, the contribution of the zodiacal light is about 67 per cent of the total, and even if the estimate of the background light is 50 per cent in error, the error in the zodiacal light measurement will be only 24 per cent. The discrepancies noted above are much larger than this; in the present work even the sum of zodiacal light and background is still not equal to the zodiacal light brightness observed by Roach; the extreme variation in the values given by Roach is 49 per cent. In spite of the comments

* The value for 6300 A is considerably lower than the mean value for all wave-lengths.

of Regener, it is difficult to believe that the observed variations are other than real. Thirdly, as the zodiacal light is due to the scattering of sunlight, its brightness should be referred to that of the average Sun and not that of the centre of the disk. In particular, the colour of the zodiacal light should be compared with the colour on the average solar disk.

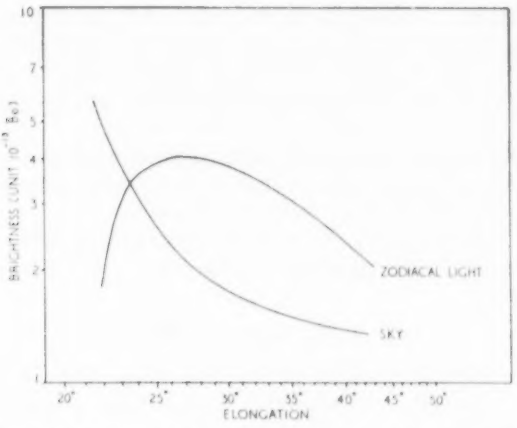

FIG. 7.—*Observed brightness of zodiacal light (uncorrected for extinction) and brightness of sky background for a depression of the Sun below the horizon of 19°·7.*

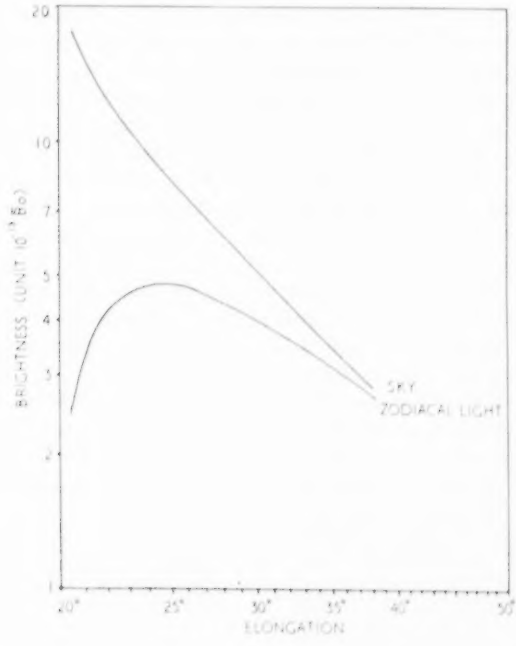

FIG. 8.—*Observed brightness of zodiacal light (uncorrected for extinction) and brightness of sky background for a depression of the Sun below the horizon of* 18°·1.

The data for the brightness of the zodiacal light obtained from plate I can now be applied to plate II, taken a few minutes afterwards, to find the increased contribution of the sky brightness from scattered sunlight. The results are shown in Figs. 7 and 8 for two depressions of the Sun below the horizon. Each of these diagrams gives data for various altitudes above the horizon for one position of the Sun below the horizon; in Fig. 3 the data relate to one altitude of observation and a range of positions of the Sun. All the diagrams show that observations of this nature near the horizon cannot be made with the Sun less than about 18° below the horizon. This is an absolute limit to observation by this method, which will not be appreciably improved upon by observing from a greater height.

11. *Measurement of polarization.*—The polarization photographs on plate II are of good quality and better exposed than those on other plates; only these photographs have therefore been used in the reductions.

The observed polarization is the sum of contributions from the zodiacal light, scattered sunlight and night sky background. If P_0 is the observed polarization, we have

$$(I_Z + I_S + I_N)P_0 = I_Z P_Z + I_S P_S + I_N P_N \qquad (4)$$

where I_Z, I_S and I_N are the intensities of the three components, and P_Z, P_S, P_N their polarizations. To obtain P_Z from the observed polarization it is necessary to know I_Z, I_S, I_N, P_S, P_N.

The separation of the observed intensity into the two parts I_Z and $I_S + I_N$ has already been discussed. A careful separation of I_S and I_N is not required because under these conditions the contribution from scattered sunlight, I_S, both in intensity and polarization, is far greater than that from the night sky. An approximate value for I_N has been taken from plate I.

Scattered sunlight predominates in the photographs on plate IV, and this plate has been used for the measurement of its polarization. At an altitude of 7°·5 above the depressed horizon the observed polarization is 10·0 per cent. Putting in a correction for the zodiacal light contribution, this gives the value of 9·2 per cent for the polarization of the sunlit background. This is close to the value of 9·6 per cent, which would be predicted by a simple application of Rayleigh scattering theory at this elongation. The values of P_S for various altitudes above the horizon have therefore been computed from this theory. This is preferable to a direct measurement because at higher altitudes there is an increasing confusion with the zodiacal light and at lower altitudes the photographic density becomes too high for accurate measurement.

The value chosen for P_N is not critical. Van de Hulst (**18**) has pointed out that the night sky background should be polarized very near the horizon because here it is chiefly scattered light that is seen. Following the computations of van de Hulst we have taken the polarization of the sky emission to be 6 per cent at the horizon, diminishing to 1 per cent 10° above the horizon.

The observed polarizations on plate II vary from 7 per cent at elongation 20° to 15 per cent at elongation 30°. The data resulting from the reduction of the smoothed observations are shown in Fig. 9. Also on Fig. 9 are plotted the data from the 1954 eclipse (**5, 7**) and those taken from the work of Behr and Siedentopf (**2**). The present results appear to confirm the high polarizations obtained by Behr and Siedentopf, but do not agree with the smaller polarizations found

by Dufay* (**10**). It is unfortunate that insufficient exposure prevents the present observations being continued beyond elongation 30°, because a combination of these data with those of Behr and Siedentopf makes it likely that there is a maximum of polarization near elongation 35°.

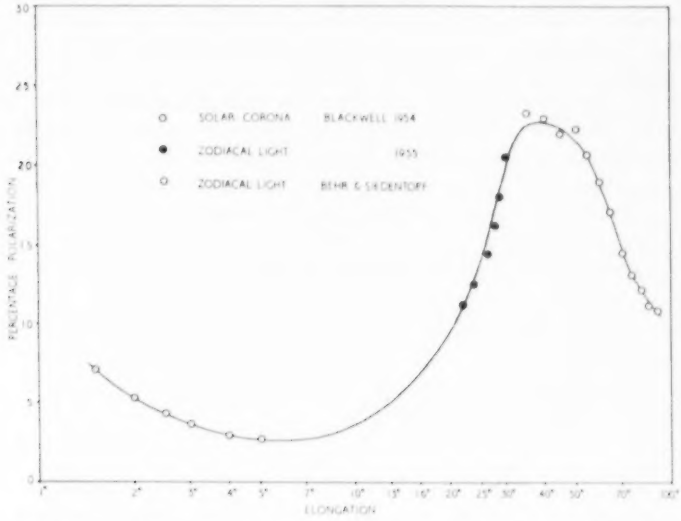

FIG. 9.—*Polarization of outer corona and zodiacal light. Data for the outer zodiacal light are from the work of Behr and Siedentopf.*

A potent source of error in all measurements near the horizon under these conditions can result from near specular reflection from the sea. At an angle of incidence of 84° the reflection coefficient is about 52 per cent and the degree of polarization of the reflected light is 18 per cent. Serious errors will result if

TABLE III

Elongation	Polarization
5°	2·8 per cent
10°	3·7
20°	9·5
25°	14·1
30°	19·2
35°	22·2
40°	22·6
50°	21·7

any of this light intrudes upon the zodiacal light. This will occur if the guiding (which results in sharp star images and a blurred horizon) or the lens aberrations cause some mixing. To avoid the effects of diurnal motion it is not sufficient to guide well; it is also necessary to use a short exposure to give a sharp horizon. The data presented here are probably not seriously affected by errors of this kind.

* Dufay makes no mention of his correction for the sky background; his observations may be undercorrected.

The error of these measurements is unlikely to be greater than ± 3 per cent in absolute measure, i.e., the maximum relative error varies from ± 30 per cent at 22° elongation to ± 15 per cent at 30° elongation.

It is now possible to interpolate the polarization measurements between the solar corona and the zodiacal light. Table III contains polarization data for a smoothed model between elongations 5° and 50°, which is based partly on Behr and Siedentopf's data, and is partly an interpolation between the outer corona and the inner zodiacal light.

The polarization data of Fig. 9 and the intensity data of Fig. 6 have been used to calculate electron densities in the zodiacal light region along the ecliptic assuming that the polarization of the F component is zero for the range of elongation 5° to 50°. The results are shown plotted in Fig. 10 (middle line) together with data previously obtained on the outer corona. These values are lower than those given in a previous publication (**2**) because the smaller values for the brightness of the zodiacal light found in the present paper have been used.

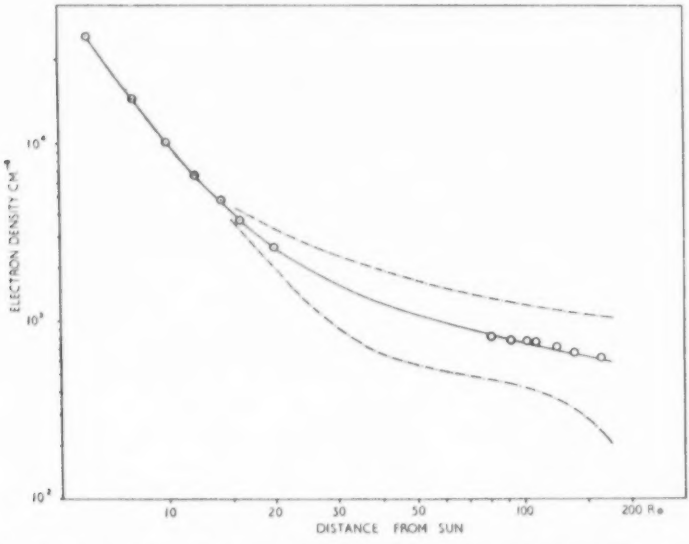

FIG. 10.—*Electron densities in the outer corona and inner zodiacal light regions. Middle curve —observed electron density. Outer curves—maximum errors resulting from uncertainties in observational data and in polarization of F component.*

At large elongations ($\epsilon > 50°$) considerable errors in electron density values can result from the assumption $p^F = 0$. Maximum and minimum values of electron density have been computed using the data of Fig. 1 for the maximum likely polarization of the F component (positive or negative). No account has been taken of the possibility of a sudden cut-off of electron density. The results are shown in Fig. 10 as the upper and lower curves. These curves also include the effects of an uncertainty in the brightness of the zodiacal light of 20 per cent, and an uncertainty in the polarization at elongation 30° of ± 2 per cent absolute.

It is important to know how symmetrical about the ecliptic is the electron component. The likely deviation from the ecliptic can be determined from these

observations only if the shape of the electron cloud is known. To form an order of magnitude of the quantities involved we assume that the electron cloud is an ellipsoid of revolution with major and minor axes in the ratio of 5 : 1—a not improbable value judging from the electron density data obtained at the 1954 eclipse (**5, 7**). Knowing, now, the contribution of the electrons to the total zodiacal light, and also the fact that the axis of the total light is within $0^{\circ}\cdot3$ of the ecliptic (in circular measure about the Sun), we can calculate the maximum likely deviation of the axis of the electron component from the ecliptic. The result is that the axis of symmetry of the electron component is probably not more than about 1° (in circular measure) from the ecliptic.

12. *Acknowledgments.*—This work was done during an expedition to Fiji to observe the total solar eclipse of 1955 June 20, and to make measurements of the zodiacal light. We acknowledge with gratitude the active cooperation of the Royal New Zealand Air Force who made available a Sunderland aircraft for this purpose. Great help was given at Lauthala Bay by the Commanding Officer, Wing Commander Le Pine, and his staff. The work could not have been carried through without the active encouragement and advice of Professor R. O. Redman. Funds for the expedition (other than the running costs of the aircraft) were provided by a grant from the Royal Society through the Joint Permanent Eclipse Committee. The apparatus was made in the Observatories' workshops by Mr J. Hignell.

The Observatories,
Cambridge:
1956 *April* 29.

References

(1) F. L. Whipple and J. L. Gossner, *Ap. J.*, **109,** 380, 1949.
(2) A. Behr and N. Siedentopf, *Zeits. f. Astrophys.*, **32,** 19, 1953.
(3) F. E. Roach, H. B. Petit, E. Sandberg-Hanssen and D. N. Davis, *Ap. J.*, **119,** 253, 1954.
(4) H. C. van de Hulst, *Les particles solides dans les Astres.* Institut d'Astrophysique Cointe-Liège (Belgique) 1955, p. 88.
(5) D. E. Blackwell, *M.N.*, **115,** 629, 1955.
(6) F. L. Whipple, *P.A.S.P.*, **67,** 367, 1955.
(7) D. E. Blackwell, *M.N.*, **116,** 56, 1956.
(8) C. L. Elvey and F. E. Roach, *Ap. J.*, **85,** 231, 1937.
(9) V. H. Regener, *Ap. J.*, **122,** 520, 1955.
(10) J. Dufay, *C.R. Acad. Sci. Paris,* **181,** 399, 1925.
(11) T. Take-uchi, *Trans. I.A.U.*, **6,** 173, 1938.
(12) M. Minnaert, *B.A.N.*, **2,** 75, 1924.
(13) C. W. Allen, *Astrophysical Quantities*, p. 113, Athlone Press, London, 1955.
(14) C. W. Allen, *loc. cit.*, p. 116.
(15) C. L. Elvey and A. H. Farnsworth, *Ap. J.*, **96,** 451, 1942.
(16) S. L. Piotrowski, *Ap. J.*, **106,** 466, 1947.
(17) H. H. Turner, *M.N.*, **54,** 13, 1893.
(18) G. P. Kuiper, *The Atmospheres of the Earth and Planets*, p. 89, University of Chicago Press, 1947.

RADIO OBSERVATIONS OF A LUNAR OCCULTATION OF THE CRAB NEBULA

C. H. Costain, B. Elsmore and G. R. Whitfield

(Communicated by M. Ryle)

(Received 1956 June 4)

Summary

Observations were made at wave-lengths of 3·7 m and 7·9 m of the lunar occultation of the Crab Nebula on 1956 January 24. At 3·7 m, observations were made throughout the occultation, and the distribution of radio brightness across the nebula was derived. The position of the radio source agrees closely with that of the optical nebula but its size is somewhat larger.

At 7·9 m, severe man-made interference occurred during the emersion but observation of the immersion suggested that at this wave-length the source was considerably more extended. Recent optical evidence has suggested that the emission from the Crab Nebula is due to the acceleration of high energy electrons in weak magnetic fields ; a variation of the spectral distribution of the radio emission from centre to limb may be associated with a radial variation in the energy spectrum of the high energy particles or of the magnetic field.

By comparing the time of obscuration at 3·7 m with the computed value, an estimate was made of the refraction occurring in the lunar atmosphere ; an electron density at the Moon's surface of 10^4 cm^{-3} was derived, a figure which corresponds to a surface density of the lunar atmosphere about 10^{-13} of that of the Earth's.

1. *Introduction.*—During the period 1955–1956, two occultations of the Crab Nebula by the Moon were visible from Cambridge. Observations of these were made to determine in greater detail the distribution of radio brightness across the source, previously derived by interferometric methods (Baldwin, 1954; Mills, 1953), and to determine with more certainty the density of the lunar atmosphere deduced from the occultation of the radio source in Gemini (Elsmore and Whitfield, 1955).

The first occultation occurred low in the sky on 1955 November 30, and the observations were seriously affected by man-made interference. Only the second occultation, that of 1956 January 24, will be discussed.

2. *Apparatus.*—Observations were made at wave-lengths of 3·7 m and 7·9 m. At both wave-lengths, phase-switching receivers (Ryle, 1952) were used in conjunction with fixed aerial systems. The positions of the source, as seen from Cambridge at times of immersion and emersion, are indicated in Fig. 1.

(*a*) *The 3·7 m wave-length aerial system.*—The aerial system was designed to fulfil two conflicting requirements : first to discriminate between the radiation from the source and that from the general galactic structure, and secondly to allow continuous observation of the source for several minutes on either side of the calculated times of immersion and emersion. These conditions were satisfied by using two widely-spaced aerials on an axis which produced interference maxima running tangentially to the path of the source, as indicated in Fig. 1.

The two aerials were separated by a distance of 213 m on a horizontal axis of azimuth 120° East of North, giving an effective aperture of 37 wave-lengths. Each of the two aerials consisted of a broadside array of eight half-wave dipoles.

(*b*) ***The 7·9 m wave-length aerial system.***—At 7·9 m wave-length, an existing aerial system was used which consisted of two groups of aerials mounted 56 wave-lengths apart on an East–West axis. One group contained 4, the other 16 Yagi aerials. The maxima of the reception pattern in the direction of the occultation were approximately horizontal and 2° apart. Two different phasing arrangements of the aerials in the larger group were necessary to observe both immersion and emersion.

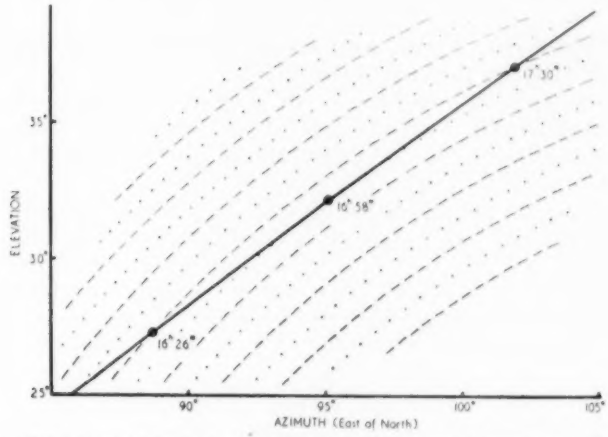

FIG. 1.—*The path of the source as seen from Cambridge on 1956 January 24. The axis of the 3·7 m aerial system has an azimuth of 120° E, and the position of the maxima and minima are indicated by - - - - - and . . . . . respectively.*

3. ***Observations:*** (*a*) ***3·7 m wave-length.***—The record of the occultation is shown in Fig. 2 together with a mean curve determined from records obtained on days before and after the occultation. Besides the deflection produced by the Crab Nebula, the records show minor contributions from other sources, the principal one being the nebulosity IC 443 in Gemini (maximum at $16^h\,52^m{\cdot}5$ U.T.). The effect of these sources may be completely removed by subtracting the two curves from one another. The difference, at any time, represents the radiation from the area occulted by the Moon. In order to express this difference as a fraction of the total intensity, it is necessary to know the deflection that would have been produced, at this time, by the whole source. This was computed from a knowledge of the position of the source and the geometry of the receiving system. The occultation curves obtained at immersion and emersion are shown in Fig. 3 (*a*).

The path of the Moon's centre, as viewed from Cambridge, passed very near to the position of the centre of the Crab Nebula. Thus at immersion and emersion two nearly identical scans across the source were obtained. The two curves were superposed for comparison in Fig. 3 (*a*); the time interval for the best fit was found to be 59·6 minutes. The calculated time interval between immersion and emersion was 59·2 minutes. The discrepancy of 0·4 minutes

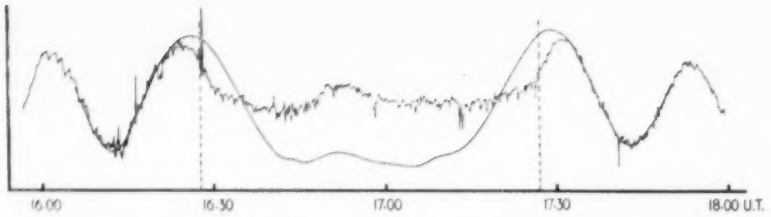

FIG. 2.—*The record of the occultation of 1956 January 24, obtained at 3·7 m. The smooth curve is the mean of records obtained on days before and after the occultation. The dashed lines show the calculated times of immersion and emersion of the optical centre of the Crab Nebula.*

may be due to refraction in the lunar atmosphere and the significance of this result will be discussed in Section 4(*c*).

(*b*) *7·9 m wave-length.*—The observations at 7·9 m were very seriously affected by man-made interference. This limited the accuracy of the measurements at immersion to 15–20 per cent and made observation of the emersion impossible. The immersion curve is shown in Fig. 3(*b*).

4. *Interpretation:* (*a*) *Distribution of brightness.*—During immersion, successive strips of the source are covered by the passage of the Moon from West to

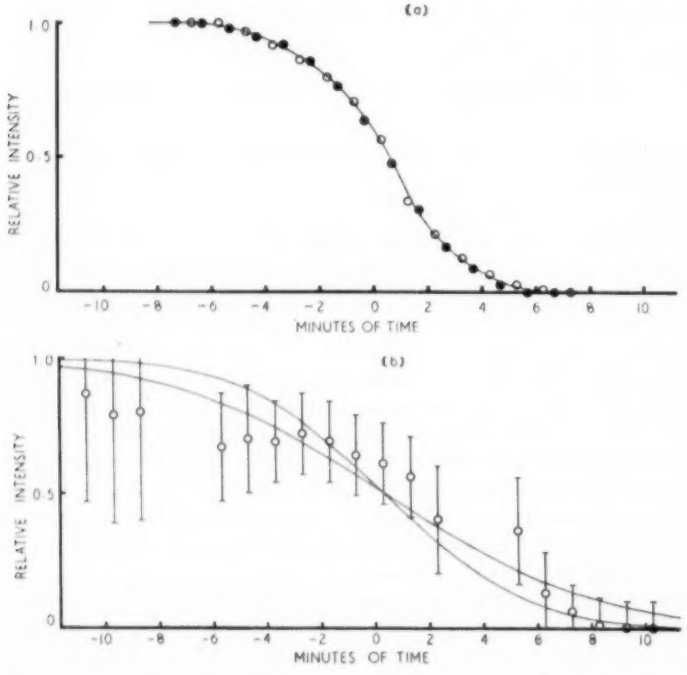

FIG. 3.—*Occultation curve of 1956 January 24 at (a) $\lambda = 3{\cdot}7$ m and (b) $\lambda = 7{\cdot}9$ m. Immersion and emersion are indicated by ○ and ● respectively. The times are relative to the calculated time of immersion of the optical centre of the Crab Nebula (emersion displaced 59·6 minutes).*

East. Therefore the curve shown in Fig. 3(*a*) represents the integral of the distribution of brightness projected on an East–West axis. This curve was differentiated to yield the distribution shown in Fig. 4. The shape of the outer limbs cannot be determined accurately, but the area beneath the curve for radial distances greater than 2·5 minutes of arc cannot be appreciably different from that shown.

The accuracy of the points in Fig. 3 (*b*) is not sufficient to give a reliable measure of the strip distribution of brightness at 7·9 m; it is, however, possible to find the approximate width of the source by determining the occultation curves for Gaussian models of brightness distribution. The curves for two such models, which correspond to probable error limits, are shown in Fig. 3(*b*), and the corresponding brightness distributions in Fig. 4.

The most important feature brought out in Fig. 4 is the difference in apparent size of the radio source at the two wave-lengths. Whilst the radiation at 3·7 m is confined to a region just slightly larger than the visible nebula, a considerable portion of the radiation at 7·9 m comes from beyond this region. This result suggests that the object extends to considerably greater radial distances than is revealed in photographs. Occultation measurements at a wave-length of 75 cm in Holland* have shown that, at this wave-length, the source is smaller than at 3·7 m. Possible explanations for this progressive increase in size with increasing wave-length will be discussed in Section 5.

(*b*) *Comparison with the optical Crab Nebula.*—The visible radiation from the Crab Nebula comes from a nearly elliptical region approximately centred on a double star. The coordinates of the North-following component of this central double star are

$$\text{R.A. } 05^{h}\,31^{m}\,31^{s}\cdot5, \qquad \text{Dec. } 21^{\circ}\,58'\,54''\ (1950).\dagger$$

Using Bessel's method, the times of immersion and emersion computed for this position were $16^{h}\,27^{m}\cdot7$ and $17^{h}\,26^{m}\cdot9$ U.T., respectively. These times were confirmed by interpolation of the Moon's topocentric coordinates provided by Mr Sadler of the Nautical Almanac Office.

Since the position of the Moon at any time is known with great precision, an occultation provides a more accurate measure of the position of a radio star than is possible with conventional methods. In this case, where the source is extended, the time of immersion of the centre of gravity of the East–West strip distribution determines the effective right ascension. This time was $16^{h}\,28^{m}\cdot0$ U.T. and corresponds to

$$\text{R.A. } 05^{h}\,31^{m}\,32^{s}\cdot2\ (1950).\ddagger$$

This coincides quite closely with the position of the centre of the optical nebula and with the most accurate position determined from interferometric observations by Baldwin (1954), R.A. $05^{h}\,31^{m}\,30^{s}\cdot5 \pm 1^{s}\cdot5$ (1950). A sketch of a photograph of the Crab Nebula, taken in red light (6300 A–6700 A), is included for comparison in Fig. 4.

Because the track of the Moon's centre passed close to the position of the radio source, it was not possible to measure its declination accurately.

* We are indebted to Dr C. Seeger for sending us these results prior to publication.

† We are indebted to Dr D. W. Dewhirst of the Cambridge Observatory for making a special determination of this position.

‡ This result is based on the assumption that refraction occurs on the sunlit limb of the Moon only. If this is not the case, the position is R.A. $05^{h}31^{m}32^{s}\cdot7$.

The high resolution of an observation of this kind makes it well suited to an investigation of fine structure in the brightness distribution. Unfortunately, the ultimate resolution, determined by Fresnel diffraction at the Moon's limb, was not realized in this case due to the smoothing of the original records. This was necessary because of interference which reduced the effective resolution to $\frac{1}{2}'$.

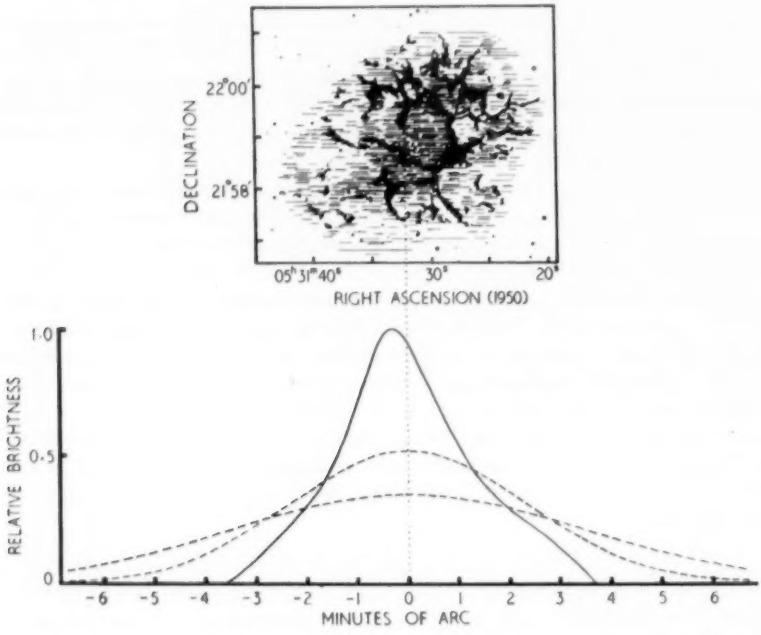

FIG. 4.—*The distribution of brightness across the Crab Nebula projected onto an East-West axis at* $\lambda = 3{\cdot}7$ *m (full line) and* $\lambda = 7{\cdot}9$ *m (dashed lines). The dotted line shows the position of the centre of gravity of the* $3{\cdot}7$ *m distribution (two solutions shown).*

The observed intensity, averaged in this way, showed no variations from a smooth curve greater than about 4 per cent of the total intensity. This result suggests that there are no localized regions larger than $\frac{1}{2}' \times \frac{1}{2}'$ having a surface brightness more than double the mean brightness near the centre of the source.

(*c*) *The lunar atmosphere.*—The difference between the calculated and observed time of obscuration of the source, $0^{m}{\cdot}4 \pm 0^{m}{\cdot}26$, may be attributed to refraction at the Moon's limb. If it is assumed that the refraction occurs only at the sunlit limb of the Moon, an angle of refraction of $13'' \pm 9''$ is obtained. Although this value is hardly significant, it is very probable that the angle of refraction is less than $22''$; this figure provides an upper limit for the electron density at the Moon's surface of 10^{3} to 10^{4} el. cm^{-3}. This derivation is discussed in a separate paper (Elsmore, in preparation), where it is shown that the density of the lunar atmosphere must be less than 10^{-13} of the density of the terrestrial atmosphere at sea-level.

5. *Discussion.*—Earlier observations at Cambridge by Adgie have provided information on the spectral variations of the total emission of several sources, including the Crab Nebula, over the range 3·7–7·9 m. These, together with the

present results, indicate that the emission from the central region of the nebula decreases with increasing wave-length, whilst in the outer regions the intensity increases rapidly with wave-length. The latter variation is in the same sense but appears considerably more marked than in the majority of radio sources. Such a variation might be due to: (*a*) re-absorption in the outer shell, (*b*) scattering by irregularities in the electron density in the outer regions; since scattering increases as the square of the wave-length, an appreciable broadening of the source might occur at longer wave-lengths, (*c*) a real variation of the emitted spectrum in different parts of the source.

Early models for the Crab Nebula (Greenstein and Minkowski 1953) proposed non-thermal sources embedded in ionized hydrogen, in order to account for the flat spectrum in the range 30–1200 Mc/s. The electron densities assumed were based on the supposition that the optical radiation was due to "free–free" transitions.

The work of Oort and Walraven (1956) has shown clearly that both the optical and radio emission may be explained in terms of the acceleration of fast electrons in weak magnetic fields, as originally proposed by Shklovsky (1953).

The electron density of any re-absorbing shell is now quite inadequate to explain the observed spectrum. If, on the other hand, the observed distributions were due to scattering, it would be necessary to postulate a scale for the irregular structure of a few km only.

It therefore seems more probable that the variation in the spectrum across the source is due to a real change in the emitted spectrum, such as might arise from radial variations in the magnetic field or in the energy spectrum of the fast electrons.

We are indebted to Mr M. Ryle and Dr A. Hewish for their helpful criticism. This work was carried out as part of a programme of research at the Cavendish Laboratory, supported by a grant from the Department of Scientific and Industrial Research. One of us (C. H. C.) is indebted to the National Research Council of Canada for a Special Scholarship, and another (G. R. W.) to Trinity College, Cambridge, for a Coutts Trotter Studentship.

Cavendish Laboratory,
Cambridge:
1956 *May* 3.

References

Baldwin, J. E., 1954, *Observatory*, **74**, 120.
Elsmore, B. and Whitfield, G. R., 1955, *Nature*, **176**, 457.
Elsmore, B., in preparation.
Greenstein, J. L. and Minkowski, R., 1953, *Ap. J.*, **118**, 1.
Mills, B. Y., 1953, *Aust. J. Phys.*, **6**, 452.
Oort, J. H. and Walraven, Th., 1956, *B.A.N.*, **12**, 285.
Ryle, M., 1952, *Proc. Roy. Soc.* A, **211**, 351.
Shklovsky, I. S., 1953, *Doklady Akad. Nauk. USSR*, **90**, 983.

THE DISTRIBUTION OF BRIGHTNESS AT METRE WAVE-LENGTHS ACROSS THE SUN'S DISK

R. G. Conway and P. A. O'Brien

(Communicated by M. Ryle)

(Received 1956 June 5)

Summary

A set of interferometer observations has been made near sunspot minimum to determine the distribution of brightness across the Sun at wave-lengths of 60 cm, 1·4 m, 3·7 m and 7·9 m. At λ 60 cm, the distribution is completely determined, but at the longer wave-lengths the interferometer observations do not determine the distribution in the polar regions. Measurements of the eclipse of 1954 June 30 confirm the distribution at λ 60 cm, and lead to estimates of the poleward extension at the longer wave-lengths. An appendix considers the effect of the limited resolving power of the observations, and shows that no error should result except in any small-scale features of distributions.

1. *Introduction.*—Several attempts have been made to obtain radio observations of the Sun which may be used to derive a model of the Sun's atmosphere. Owing to the effects of refraction at the longer wave-lengths which originate in the corona and upper chromosphere, these regions may only be investigated if measurements are made of the distribution of brightness across the disk, as well as of the total emission. Observations at metre and decimetre wave-lengths have been made of solar eclipses by Christiansen, Yabsley and Mills (1949), Laffineur *et al.* (1950), Blum, Denisse and Steinberg (1952), Laffineur, Michard *et al.* (1954), but none of these observations has led to a unique solution to the brightness distribution. Interferometer observations have been made by Stanier (1950) and O'Brien (1953). The latter's observations were used by O'Brien and Bell (1954) to derive a preliminary model of the corona.

In this paper a new set of interferometer observations are described which were made during a long period of exceptionally low sunspot activity. During the same period, observations were also made of a solar eclipse, and the two sets have been combined to give distributions of brightness which are believed to be more reliable than any previously published at these wave-lengths. It is hoped that these distributions may be used to derive a model of the Sun's atmosphere.

2. *The interferometer observations.*—During the periods 1953 November 1–30 and 1954 April–June (in neither of which was any appreciable solar activity reported), a series of observations was made with interferometers of variable spacing connected to phase-switching receivers, as described by O'Brien (1953). The wave-lengths used were 60 cm, 1·4 m, 3·7 m and 7·9 m.

At λ 60 cm the amplitude of the record was measured as a function both of the aerial spacing and of the interferometer position angle.* In addition, the

* The interferometer position angle is defined as the angle between the interferometer plane of symmetry and the rotation axis of the Sun.

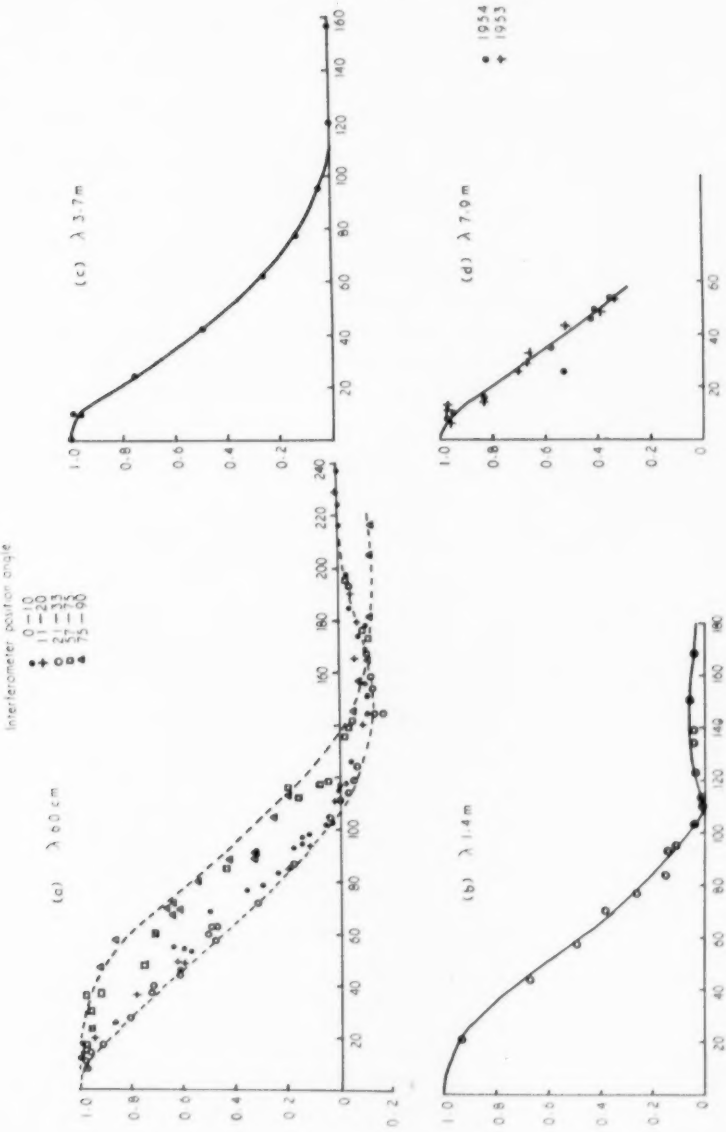

FIG. 1.—*Interferometer observations.*
Ordinates: relative amplitude.
Abscissae: aerial separation in wave-lengths.

phase of the records was measured for some of the larger spacings and was found to be negative. These results, which have been reported by O'Brien and Tandberg-Hanssen (1955), are shown in Fig. 1*a*.

At λ 1·4 m, 3·7 m and 7·9 m, the amplitudes but not the phases of the records were measured, and only one interferometer azimuth was available, in an approximately East–West direction. The results of these observations are shown in Figs. 1*b*, *c*, *d*. The phase of the subsidiary maximum at λ 1·4 m was not measured, but is assumed to be negative, as was found at λ 60 cm. This agrees with measurements by Firor (1956), at λ 1·45 m.

The absolute scale of brightness temperature is derived from the total emission of the Sun at each wave-length. At λ 60 cm and 1·4 m the aerial temperatures were calibrated against a noise signal generator, and the flux densities were derived from the calculated forward gain of the aerials. At λ 3·7 m and 7·9 m the record amplitudes were compared with those of the radio star in Taurus (the Crab Nebula). At each of the four wave-lengths a primary calibration has been made against a thermal noise source (Adgie and Smith, 1956). The values of flux density so found are given in Table I. The accuracy of each figure is estimated at 20 per cent.

TABLE I

Wave-length	60 cm	1·4 m	3·7 m	7·9 m
Flux Density in units 10^{-23} mks.	200	89	14	2·5

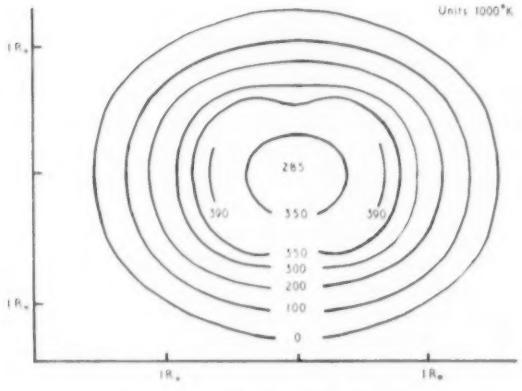

FIG. 2.—*Brightness distributions at* λ 60 *cm.*

The observations were converted to brightness distributions by the method of O'Brien (1953). The observations at λ 60 cm lead unambiguously to a brightness distribution (O'Brien and Tandberg-Hanssen, 1955) which is shown in Fig. 2. At λ 1·4 m, 3·7 m and 7·9 m the complete distribution cannot be obtained without a further assumption of symmetry, since the observations were made with a single value of the interferometer position angle, and hence lead only to a projected distribution.

Previously it has been usual to assume that the distribution is circularly symmetrical; in this case, the radial profile of the distribution is given by the

Fourier–Bessel transform of the observations (Machin, 1951). Alternatively, it is possible to interpret the observations in terms of a family of elliptical distributions. The contours of brightness of each member of the family are assumed to be concentric ellipses with major axes in the Sun's equatorial plane, and with the same axial ratio $\beta = \frac{\text{minor axis}}{\text{major axis}}$. Different members of the same family are distinguished by different values of β. The equatorial section of the brightness distribution of each member of the same family is made the Fourier–Bessel transform of the observations; the circular distribution is therefore included in the family as the member with $\beta = 1$.

Since the projection of a circle on to an arbitrary plane is an ellipse, all members of the same family have the same projection on to their major axis (apart from a scale factor of brightness equal to $1/\beta$), and are therefore equivalent to the same set of interferometer observations.

Brightness distributions at λ 1·4 m, 3·7 m and 7·9 m have been derived upon this assumption of elliptical symmetry, and the equatorial sections at each wave-length are shown in Fig. 3. The values of β, which determine both the scale of brightness and the polar section, are discussed below in Section 4.

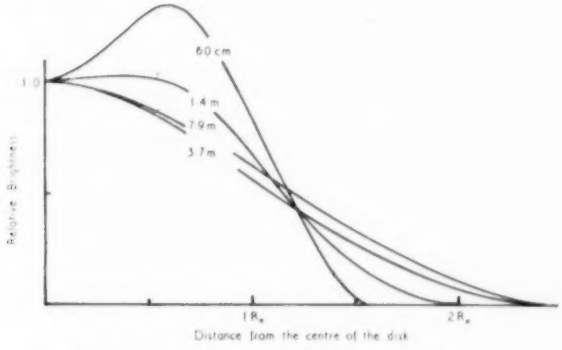

FIG. 3.—*Relative brightness in the equatorial plane.*

It is important to consider the effect on the derived distributions of the limited resolving power of the observations. A detailed analysis has been made, which follows the same methods as those of Bracewell and Roberts (1954), but which considers in particular the case of an isolated source, such as the Sun. This analysis, which is contained in the Appendix, shows that small-scale structure is lost, but that no error should occur in the average value of brightness over a finite interval of radius across the disk. Minimum values of this interval are given in the Appendix.

3. *The eclipse observations.*—A partial eclipse of the Sun was visible at Cambridge on 1954 June 30. First contact was at $11^h\,15^m$ U.T., and last contact at $13^h\,50^m$ U.T. At the maximum phase, at $12^h\,34^m$ U.T., 78 per cent of the Sun's diameter was obscured.

The eclipse was observed at wave-lengths of 60 cm, 1·4 m and 3·7 m, using phase-switching interferometers of small spacing, which recorded the Sun's radiation throughout the period of the eclipse. A measurement of total power

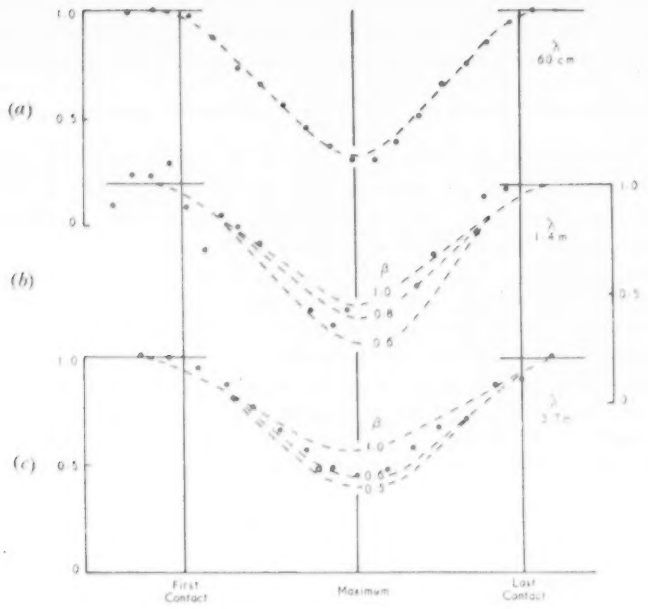

FIG. 4.—*Eclipse curves for Cambridge. The observations throughout the eclipse are represented by circles and the observation at transit by the square. The dashed lines show the expected curves for different values of β.*

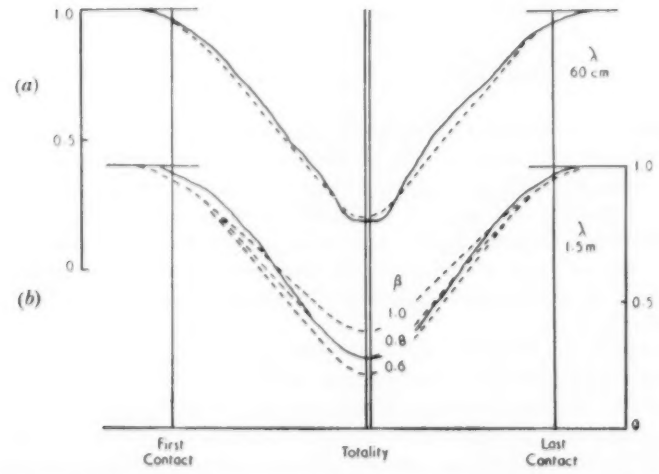

FIG. 5.—*Eclipse curves for Norway. The full lines show the observed intensities and the dashed lines show the expected intensities for different values of β.*

was also made at $\lambda 3{\cdot}7$ m using a single large fixed aerial which observed the Sun in transit. The time of transit was $12^{h}\,17^{m}$ U.T., close to the maximum phase of the eclipse.

The intensity of the Sun at each wave-length was measured on the day of eclipse and on control days before and after. The variation of intensity during the eclipse, expressed as a fraction of the average intensity of the controls, is shown in Figs. 4*a*, *b*, *c*. At $\lambda 3{\cdot}7$ m it was necessary to correct for the radiation from the radio-star in Taurus (the Crab Nebula). The correction was calculated from the known intensity and position of this source (Shakeshaft, Ryle, Baldwin, Elsmore and Thomson, 1955) and is included in Fig. 4*c*.

Observations were also made at $\lambda 60$ cm and $1{\cdot}5$ m by Eriksen, Hauge and Tandberg-Hanssen (1955) in Norway, from a point where the eclipse was total. The results of these observations are shown in Figs. 5*a*, *b*.

4. *The combination of the eclipse and interferometer results.*—At $\lambda 60$ cm, where the distribution was completely derived from the interferometer results, the eclipse measurements were used to check the interferometer measurements. The expected eclipse curves were derived for the partial eclipse at Cambridge and the total eclipse in Norway. They are shown in Figs. 4*a* and 5*a*, and are in good agreement with the observed curves.

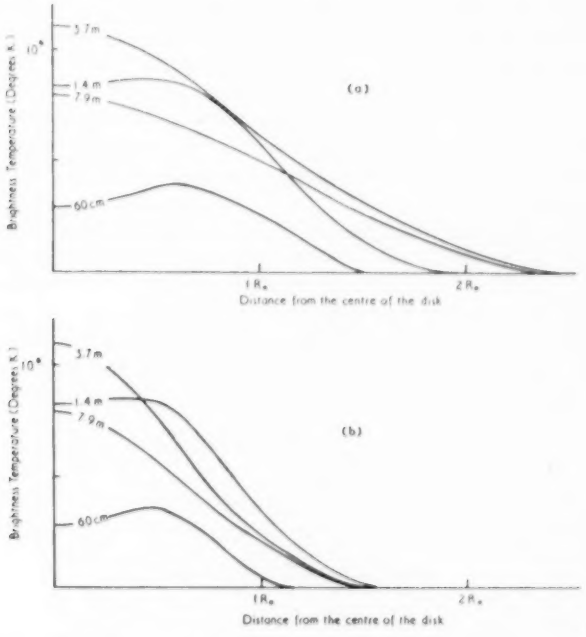

FIG. 6.—*Brightness distributions* (*a*) *at the equator,* (*b*) *towards the pole.*

At $\lambda 1{\cdot}4$ m and $3{\cdot}7$ m the eclipse observations may be used to distinguish between different elliptical models derived interferometrically. At each wave-length expected eclipse curves have been constructed for different values of β. These are shown in Figs. 4*b*, *c* and 5*b*. The observed curves do not fit the

curves for $\beta = 1$, showing that the distributions are not circularly symmetrical. The best fit is obtained at λ 1·4 m with $\beta = 0{\cdot}8$, and at λ 3·7 m with $\beta = 0{\cdot}6$. These values agree with previous estimates: O'Brien (1953) obtained $\beta = 0{\cdot}8$ at λ 1·4 m, and Blum, Denisse and Steinberg (1952) obtained $\beta = 0{\cdot}6$ at λ 1·75 m. The value of β at λ 7·9 m has not been determined, but the values at other wave-lengths suggest that an upper limit is 0·6. On the other hand, a value less than 0·6 would imply very severe limb-darkening at the pole. In order to fix the scale of brightness at λ 7·9 m the value of β will be taken as 0·6.

The brightness distributions, in the form of polar and equatorial profiles, derived using these values of β are shown in Fig. 6. These curves are suggested as the basis for an investigation of the structure of the corona. There is little doubt that they refer to the "quiet Sun" corona, since they were obtained in a period when for many months there was no appreciable activity. Reliable values of absolute brightness have been obtained by calibrating against thermal standards. The limited resolving power will cause no error except in any small-scale features of the distributions. The assumption of elliptical symmetry means that the polar profiles at the longer wave-lengths are less certainly known than the equatorial profiles. The equatorial profiles are almost independent of this assumption, since the interferometer observations lead to the equatorial projection of each distribution, which virtually determines the equatorial profile. For this reason, the most reliable deductions about the variation of the electron density and temperature with height in the corona may be made for the equatorial regions, based on the profiles for the equatorial plane.

Appendix.—This Appendix considers what distortion of the brightness distribution may result from the limited resolving power determined by the maximum aerial spacing used. The treatment is based on that of Bracewell and Roberts (1954), and extends the analysis for the special case of a single isolated source, such as the Sun.

Let $P(r)$ be the principal solution for the brightness distribution, i.e. the Fourier transform of the interferometer observations $A(s)$, which are made in the range $s \leqslant s_0$. (For simplicity, the Fourier transform is considered, so that $P(r)$ is strictly the projected distribution. The arguments are not materially altered if $P(r)$ is a radial profile, obtained by a Fourier–Bessel transform). Let the unknown difference between $P(r)$ and the true distribution $T(r)$ be an "invisible" distribution $I(r)$:

$$P(r) = 2\int_0^{s_0} A(s)\cos(2\pi sr)\,ds$$

$$T(r) = 2\int_0^{\infty} A(s)\cos(2\pi sr)\,ds$$

$$I(r) = 2\int_0^{\infty} i(s)\cos(2\pi sr)\,ds$$

where $i(s)$ is unknown for $s > s_0$, identically zero for $s \leqslant s_0$.

In the distribution considered, that of a single isolated source, $T(r)$ is limited to small values of r, and is of course never negative. It will now be shown that these restrictions increase the effective resolving power.

It may be seen by inspection of Fig. 6, that the $P(r)$ is negligible for r greater than a certain value r_0 at each wave-length. Since $I(r)$ contains no Fourier components with $s \leqslant s_0$, it is either zero, or an oscillating function, changing

sign twice in an interval not greater than $1/s_0$. $T(r)$ is always positive; hence $I(r)$ must be zero when $r>r_0$. If a function $f(x)$ is limited to a range $\pm x$, an extension of the Convolution Theorem shows that its Fourier transform is "smooth", i.e. does not change appreciably in an interval less than $1/x$. $I(r)$ is limited to the range $\pm r_0$, and hence $i(s)$ is smooth within an interval of $1/r_0$. Since $i(s)$ is by definition zero for $s \leqslant s_0$, it cannot have an appreciable value for $s<s_1$, where $s_1=s_0+1/r_0$.

This result indicates that $I(r)$, if it is not zero, is oscillatory, changing sign on the average at least twice in an interval of $1/s_1$. The effective resolving power corresponds to s_1, not s_0, an improvement of about twice. Although the limited resolution may cause an error in the value of $P(r)$ at a single point, there will be no error in the average value of $P(r)$ in an interval greater than $1/s_1$, since this is

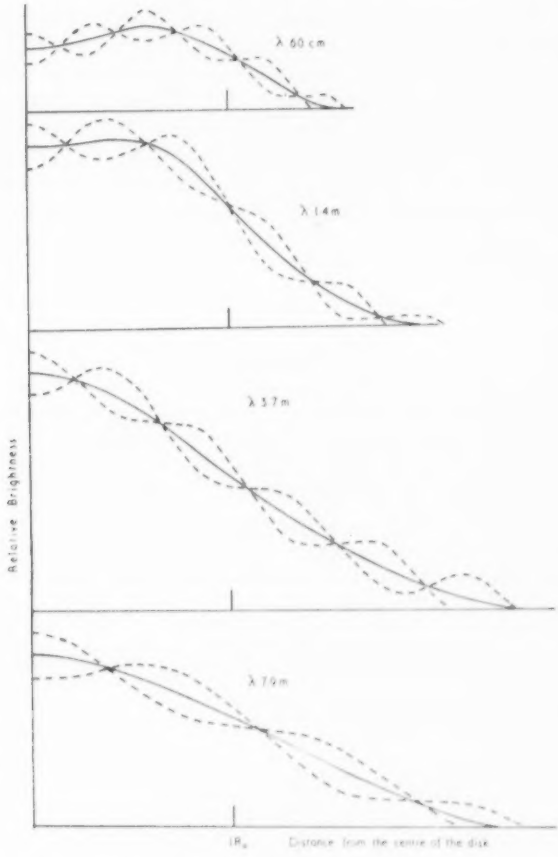

FIG. 7.—*Principal distributions with examples of possible even distributions.*

the same as that of $T(r)$. In other words, structure in $T(r)$ whose scale is less than $1/s_1$ is lost, but all structure whose scale is greater than $1/s_1$ is retained. The quantities s_0, r_0 and $1/s_1$ at each of the four wave-lengths are given in Table II,

and in Fig. 7 the principal distributions $P(r)$ are shown with possible error distributions $I(r)$ having periods $1/s_1$.

TABLE II

Wave-length	60 cm	1·4 m	3·7 m	7·9 m	
s_0	250	168	157	54	Wave-lengths
r_0	1·5	2·0	2·5	2·5	Sol. Radii
$1/s_1$	0·6	0·8	0·9	1·5	Sol. Radii

Maximum values of $i(s)$ and $I(r)$ may be estimated if the assumption is made that $T(r)$ is not an oscillating function with many subsidiary maxima. This condition obtains if the maximum gradient of $I(r)$ is less than the maximum gradient of $P(r)$. The functions $I(r)$ shown in Fig. 7 are the maximum subject to this condition.

Even with the somewhat implausible "ripples" which the distributions $I(r)$ introduce, it can be seen that the large-scale features of the distributions remain unaltered. "Limb-brightening" is certainly present at λ60 cm, and is certainly absent at λ3·7 m. Furthermore, the region of maximum brightness at λ60 cm certainly occurs within the limb, most probably at $r < 0{\cdot}8$ solar radii.

Acknowledgments.—This work was carried out at the Cavendish Laboratory, Cambridge, as part of a programme of radio research supported by the Department of Scientific and Industrial Research.

Cavendish Laboratory,
Cambridge :
1956 *June* 4.

References

Adgie, R. and Smith, F. G., *Obs.*, **76,** 181, 1956.
Blum, E. J., Denisse, J. F. and Steinberg, J. L., *Ann. d'Astroph.*, **15,** 184, 1952.
Bracewell, R. N. and Roberts, J. A., *Aus. J. Phys.*, **7,** 615, 1954.
Christiansen, W. N., Yabsley, D. E. and Mills, B. Y., *Aus. J. Sci. Res.*, **2A,** 506, 1949.
Eriksen, G., Hauge, O. and Tandberg-Hanssen, E., *Astrophysica Norvegica*, **5,** 131, 1955.
Firor, J., *Ap. J.*, **123,** 320, 1956.
Laffineur, M. *et al.*, *Ann d'Astroph.*, **13,** 337, 1950.
Machin, K. E., *Nature*, **167,** 889, 1951.
Michard, R. and Laffineur, M. *et al.*, *Ann. d'Astroph.*, **17,** 358, 1954.
O'Brien, P. A., *M.N.*, **113,** 597, 1953.
O'Brien, P. A. and Bell, C. J., *Nature*, **173,** 219, 1954.
O'Brien, P. A. and Tandberg-Hanssen, E., *Obs.*, **75,** 11, 1955.
Shakeshaft, J. R., Ryle, M., Baldwin, J. E., Elsmore, B. and Thomson, J. H., *Mem. R.A.S.*, LXVII, 106, 1955.
Stanier, H. M., *Nature*, **165,** 354, 1950.

THE CENTRE-LIMB VARIATION OF THE SODIUM D LINE INTENSITIES

R. J. Bray

(Communicated by the Director of the University Observatory, Oxford)

(Received 1956 April 26)

Summary

New observations of the centre-limb variation of the Na *D* lines are compared with the earlier observations of Shane, Allen, Houtgast, Priester and Shcherbina-Samoilova. Central intensities found by the different observers agree within the experimental error. The new measurements provide no evidence for any centre-limb variation exceeding 1 per cent for points whose residual intensity is greater than 75 per cent, a result which agrees with Allen's conclusions but disagrees with those of Priester and the other workers.

The line cores are formed by coherent scattering, the central intensities being formally accounted for by a value of ϵ of $0{\cdot}0038 \pm 0{\cdot}0012$. Various mechanisms for producing non-zero central intensities are considered.

Introduction.—The recent observations of the centre-limb variation of the Na *D* lines published by Priester (**25**) and Shcherbina-Samoilova (**32**) have failed to resolve the discrepancies in the earlier observations of Shane (**31**), Allen (**2**) and Houtgast (**10**) pointed out by Spitzer (**33**). A new investigation of these lines was undertaken at Oxford in 1952 and is described in Section 1 of this paper. The results of all six investigations are compared in Section 2, and an attempt is made to determine the origin of the discrepancies. Finally, a brief theoretical discussion of the line cores, with particular reference to the central intensities, is given in Section 3.

1. *Observational method and results*

1.1. *Observations.*—Spectra of the *D* lines were obtained at seven points of the solar disk using the Oxford solar equipment (**21**, **22**, **23**). Each plate contains five spectra of equal exposure time; the exposure time for different plates varies from four to nine seconds. Of the five spectra on each plate, three are either exposures of the East or West limb (taken with a radial slit) or of the centre plus two intermediate points, and the remaining two are calibration exposures. The calibration was performed by a Hilger rhodium-on-glass step wedge placed over the slit; the construction and calibration of the wedge have been described (**4**). Calibration exposures were made at the centre of the disk; an additional exposure at the centre of the disk, with the wedge slightly displaced, allows one to correct for non-uniformity of slit illumination (**4**). A slit-width of 0·036 mm was used for all but the calibration exposures; this is the value for which the spectroscope apparatus function has been determined. An orange filter (Ilford

Micro 5) was placed before the slit to reduce scattered light in the spectroscope. The plates were brush developed in Parkhurst two-solution developer, which produces very little background fog. An interval of twenty-four hours or more was allowed to elapse between exposure and development in order to permit any initial fading of the latent image to occur. No experiments were performed on Eberhard effect; Redman's experience (**28**), however, suggests that the effect is negligible when brush development is used.

Of the twenty-two plates obtained, ten were selected for microphotometry—five limb plates and five centre-plus-intermediate plates. Only one of the three limb spectra on each plate was microphotometered; each of the final profiles for each position on the Sun is therefore the mean of five independent determinations from five different plates, each possessing its own characteristic curve.

1.2. *Microphotometry and reduction.*—Microphotometry was performed with the Observatory microphotometer (**20**) using an effective slit width of 0·033 mm. This corresponds to about one-eight the half-width of D_1; tests made on a number of narrow lines using both this slit and one having an effective width of 0·010 mm showed that no resolution was lost by using the wider of the two. The "profile" tracings were made with a magnification of 48·2, both D_1 and D_2 being recorded on a single tracing. With this magnification the tracing is insufficiently long to record more than 4A on either side of the line pair, so in order to make sure of reaching the true continuum (in terms of which the profiles must be expressed) an additional tracing with a magnification of 6·89 was made for every "profile" tracing. These "continuum" tracings were measured at eighteen wave-lengths extending 22A to the violet of D_2 and a similar distance to the red of D_1. The wings of the D lines can be detected out to 13A on these tracings. The estimated error in the level of the continuum derived from each tracing is 0·5 per cent. Thirty-five "profile" tracings (corresponding to five profiles for each of seven positions on the disk) and an equal number of "continuum" tracings were measured. The "profile" tracings were measured at eighty-two wave-lengths.

The limb spectra were microphotometered at values of $\cos\theta$ (θ = angle of emergence) of 0·199, 0·239, 0·299 and 0·380 with a scatter of 0·002. Prior to microphotometry the plates were marked at the corresponding calculated distances from the apparent limb by a dividing machine attached to a Cambridge micrometer. An independent check of these positions was made by microphotometry *across* the marks and the limb (i.e. perpendicular to the dispersion), the "true" limb being defined as the point of inflexion of the resulting curve. No systematic difference between these two methods of determining distances from the limb could be detected. The centre and intermediate spectra were microphotometered at their centres, which correspond to values of $\cos\theta$ of 1·000, 0·800 and 0·554 respectively.

Microphotometry of the calibration and uniformity spectra was performed in a direction perpendicular to the dispersion in two regions free from all but very faint lines. These regions are λ5877·8–λ5879·2 and λ5913·0–λ5914·1; according to the "Rowland Revision" (**30**) they each only contain three lines of Rowland intensity -3 and one of -2. The resulting characteristic curves, corrected for non-uniformity of slit illumination, were combined to give a mean curve for each plate.

To form a mean profile the five individual profiles for each of the seven positions on the disk were averaged logarithmically (at the same wave-lengths); this

has the effect of averaging errors in the continuum as well as errors at points in the profile. The r.m.s. error of each of the mean curves is 0·8 per cent (continuum = 100 per cent); this figure remains more or less constant over the profile, though there is usually an increase in the neighbourhood of blends.

1.3. *Correction for spectroscopic distortion.*—Correction of the observed profiles for spectroscopic distortion involves the solution of the well-known equation of obliteration

$$O(\lambda) = \int_{-\infty}^{+\infty} T(\lambda')\, A(\lambda - \lambda')\, d\lambda',$$

where $O(\lambda)$ is the observed profile, $T(\lambda)$ the true profile, and $A(\lambda)$ the spectroscope apparatus-function. The experimental determination of $A(\lambda)$ has been fully described elsewhere (**4**); because of the importance of the far wings of $A(\lambda)$ in fixing the observed central intensities, a fact originally pointed out by Allen and Redman (**27, 29**), the determination was carried down to 9×10^{-5} of the peak intensity. The wings of the apparatus-function were smoothed and the outer portions were approximated by an inverse square law, which, in agreement with Redman's results (**27**), fits the observed wings fairly well. The advantage of obtaining an analytical formula for the outer parts is that $A(\lambda)$ can be extrapolated to infinity, which in principle is necessary for the solution of the above equation.

It is also necessary to know $O(\lambda)$ to infinity in order to obtain an exact solution, though errors in the far distant parts naturally have little effect on the solution. Account must therefore be taken of the numerous weak disturbing lines (mostly of atmospheric origin) whose effect is equivalent to a general reduction of the continuum (cf. Redman (**28**)). Beyond 6A from the centres of each of the *D* lines the average level of the continuum was taken to be 96·8 per cent, a figure arrived at by considering the total amount of light removed by disturbing lines in a certain region in the neighbourhood of the *D* lines. Within 6A, however, the effect was allowed for by superimposing on the measured wings of the *D* lines rectangular profiles to represent the disturbing lines. The equivalent widths of these lines were obtained from the "Utrecht Atlas" (**15**); the Atlas values were multiplied by 2·1 to take account of the greater water vapour content at Oxford compared with that at Mt. Wilson. The multiplying factor was derived by measuring the equivalent widths of one or two selected atmospheric lines on each of the ten Oxford plates and comparing with the Atlas value. The profiles of disturbing lines near the cores of the *D* lines were measured along with the *D* line profiles, since these can have a large effect on the solution.

The solution of the integral equation was carried out by Burger and van Cittert's method (**5, 6**), which has the advantage over other methods in that exact account can be taken of sharp irregularities in $O(\lambda)$ and $A(\lambda)$. The progress of the solution gives automatically the residuals $O - \int T_n . A$, where T_n is the nth approximation to T; this not only provides a useful check on the occurrence of errors in computation but also gives a fairly precise indication of when the iteration should be stopped. The calculations reduce essentially to the obliteration of a succession of curves, the first of which is the original observed curve. The solution was first obtained for the profiles at the centre of the disk; convergence was reasonably rapid, four iterations being necessary to reduce the residuals to less than the random photometric error 0·8 per cent. The final true profiles at the centre of the disk, together with the observed profiles, are shown in Fig. 1; also shown are observed points.

An examination of the wings of the profiles obtained at the different values of $\cos\theta$ shows that for r (residual intensity) greater than about 75 per cent any variation with $\cos\theta$ is less than the random photometric error 0·8 per cent. This surprising result is discussed in connection with the observations of the other five workers in Section 2. The work in solving the integral equation is thereby

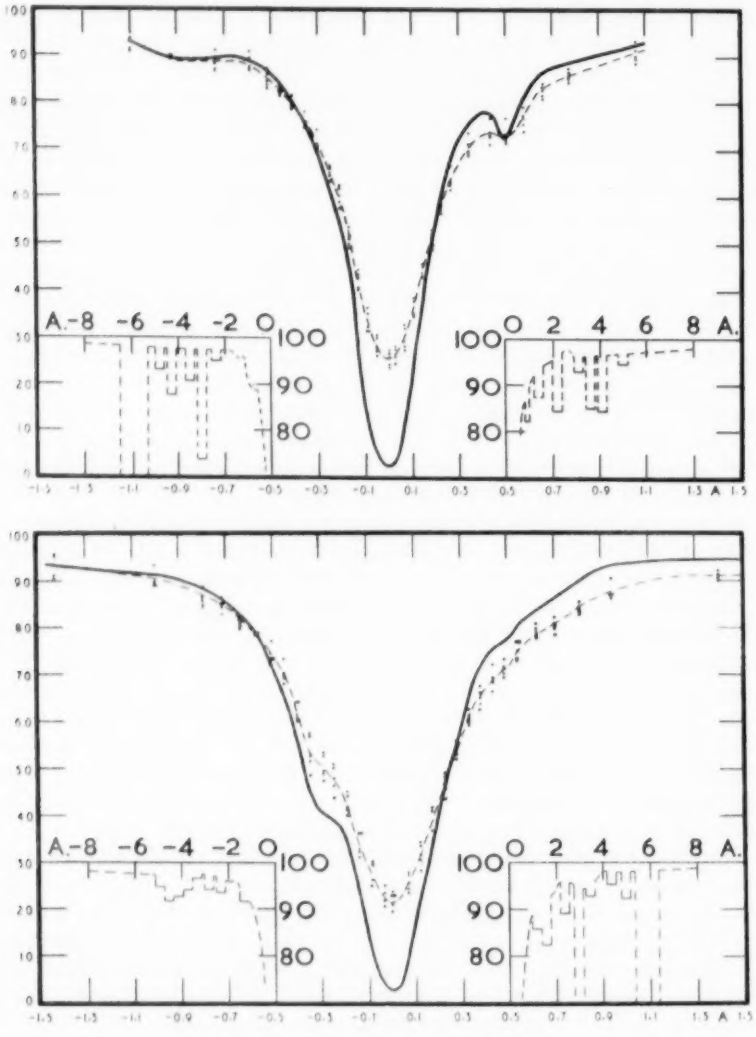

FIG. 1.—*True and observed profiles.*
Abscissae : Angstroms.
Ordinates : intensity (continuum = 100 per cent).

The dashed curves are the observed profiles at the centre of the disk, the dots being observed points. The continuous curves show the effect of correcting for spectroscopic distortion. The insets show the far wings together with the rectangular profiles used to represent disturbing lines. The upper diagram refers to D_1, the lower to D_2.

TABLE IA

True profiles of D_1

I = intensity in per cent of continuum

cos θ	0·20	0·24	0·30	0·38	0·55	0·80	1·00
Δλ (A)							
−0·400	79·4	79·4	79·4	79·7	79·7	79·9	79·4
−0·350	74·8	74·8	74·8	74·5	74·5	75·7	74·8
−0·300	70·5	69·3	67·9	68·1	67·6	69·8	68·8
−0·250	64·8	63·1	60·9	60·4	59·8	62·4	61·4
−0·200	55·8	55·5	53·1	51·1	51·2	51·4	52·9
−0·175	49·8	50·5	47·7	45·7	45·5	44·9	47·1
−0·150	42·3	42·3	39·9	38·6	38·0	37·3	38·8
−0·125	33·0	29·3	29·0	27·0	28·5	26·8	24·7
−0·100	20·5	18·4	17·7	16·6	20·2	16·9	14·1
−0·075	13·4	11·8	11·8	9·7	13·6	10·3	8·8
−0·050	8·8	7·5	7·9	6·4	7·7	6·0	5·0
−0·025	6·6	5·1	5·8	5·2	4·7	3·6	2·9
0·000	6·3	4·4	5·4	4·9	4·0	3·1	2·5
0·025	6·6	5·2	5·8	5·3	4·5	4·1	3·6
0·050	9·2	9·4	9·0	8·8	7·5	7·8	7·2
0·075	16·6	17·5	16·5	15·2	15·5	14·6	13·5
0·100	28·2	26·6	24·7	23·9	26·3	23·2	22·2
0·125	36·1	35·2	32·8	32·7	33·9	32·2	31·2
0·150	43·2	43·5	41·1	41·8	40·5	40·5	39·4
0·175	50·2	50·2	49·8	50·3	46·9	48·4	47·1
0·200	56·9	56·3	57·1	57·2	52·9	55·2	54·3
0·250	67·5	65·3	65·8	66·0	62·5	65·7	65·6
0·300	73·8	71·4	71·7	71·8	69·7	74·6	72·2
0·350	76·0	74·5	75·9	76·3	74·7	78·9	75·9
0·400	77·0	76·5	77·9	77·6	77·6	78·6	77·9
0·450	77·2	77·2	77·2	77·2	77·2	76·5	77·2

For all values of cos θ:—

Δλ (A)	*I*	Δλ (A)	*I*	Δλ (A)	*I*
−1·700	97·0	−0·800	89·2	0·600	82·8
−1·600	96·6	−0·750	89·4	0·650	86·3
−1·500	95·8	−0·700	89·7	0·700	87·6
−1·400	95·5	−0·650	89·9	0·750	88·5
−1·300	95·6	−0·600	89·4	1·100	93·3
−1·200	95·7	−0·550	87·9	1·700	95·0
−1·100	93·0	−0·500	86·1	1·800	95·1
−1·000	90·7	−0·450	83·4	1·900	95·3
−0·950	89·8	...	...	2·500	97·3
−0·900	89·3	0·500	72·8	2·600	97·4
−0·850	89·0	0·550	77·7	2·700	97·3
				2·800	96·3

TABLE Ib

True profiles of D_2

I = intensity in per cent of continuum

cos θ	0·20	0·24	0·30	0·38	0·55	0·80	1·00
Δλ (A)							
−0·550	77·9	77·5	76·7	77·6	78·4	77·9	76·7
−0·500	72·1	72·4	71·1	72·5	73·0	73·2	70·9
−0·450	64·8	65·4	63·3	65·3	61·4	64·8	65·0
−0·400	58·0	58·1	57·1	57·0	52·2	53·5	55·6
−0·350	52·4	51·9	51·9	49·1	45·8	45·2	45·2
−0·300	48·7	47·3	46·6	43·2	41·3	41·8	40·6
−0·250	48·7	46·9	47·2	45·3	40·2	40·6	39·0
−0·200	47·1	44·6	42·6	40·8	38·5	36·3	35·6
−0·175	43·9	41·2	38·5	36·7	35·9	32·5	32·1
−0·150	35·0	34·8	33·5	30·6	32·2	27·6	25·8
−0·125	24·0	25·9	26·7	22·9	23·3	21·2	19·5
−0·100	16·5	17·0	20·0	17·1	14·4	15·3	13·6
−0·075	11·8	10·5	13·8	12·4	9·7	9·5	9·0
−0·050	8·1	6·6	8·2	7·6	6·6	6·4	5·2
−0·025	7·0	6·1	3·6	3·9	6·0	3·8	3·1
0·000	6·8	6·1	2·8	3·4	5·8	3·5	2·5
0·025	7·0	6·2	3·2	3·8	6·0	3·8	2·9
0·050	8·2	7·0	6·3	6·7	7·3	6·4	5·5
0·075	13·4	11·8	13·5	12·7	12·5	12·3	10·9
0·100	22·2	20·1	23·3	20·3	19·6	18·9	16·9
0·125	29·7	29·8	29·8	26·9	26·8	24·8	22·7
0·150	37·0	37·8	35·6	33·3	32·9	30·3	28·0
0·175	42·8	44·2	40·8	39·6	38·0	35·9	33·6
0·200	47·3	48·4	45·3	44·0	41·4	40·7	39·4
0·250	54·6	54·1	51·3	49·8	46·9	48·2	49·3
0·300	61·7	59·4	58·3	56·4	54·9	56·0	58·3
0·350	67·3	64·3	65·2	65·5	63·5	64·8	67·3
0·400	71·2	69·5	70·9	70·1	69·0	71·6	72·8
0·450	74·7	73·9	74·7	73·5	73·8	77·4	75·5
0·500	76·8	77·2	77·7	76·9	78·2	80·3	77·1
0·550	77·2	77·3	77·3	79·0	78·1	80·9	80·5
0·600	81·7	82·1	82·6	82·7	82·4	82·6	82·6

For all values of cos θ:—

Δλ (A)	*I*	Δλ (A)	*I*	Δλ (A)	*I*
−4·300	96·8	−0·900	90·1	0·850	91·3
−3·100	97·3	−0·850	89·3	0·900	92·4
−2·000	95·8	−0·800	88·2	0·950	93·4
−1·900	95·7	−0·750	87·0	1·400	94·5
−1·800	95·9	−0·700	85·3	2·000	94·2
−1·700	95·8	−0·650	83·1	2·100	95·8
−1·600	95·4	−0·600	80·6	2·200	95·8
−1·500	94·3	...	...	3·300	94·4
−1·400	93·0	0·650	84·3	3·800	97·2
−1·100	91·5	0·700	85·9	3·900	97·7
−1·000	91·2	0·750	87·7	4·000	97·9
−0·950	90·7	0·800	89·4	4·100	98·0

shortened, since having solved the equation for the profiles at the centre of the disk, we can then apply it to the *difference* between the profile at the centre and the profiles at the other six positions. This procedure shortens the labour since the range of integration is then finite. The true profiles of the *D* lines for each of the seven positions are given in Table I.

1.4. *Experimental error.*—Following Redman (**28**) it is convenient to divide the sources of error into two classes, namely those present in the observed profiles before correction for spectroscopic distortion and those introduced by the process of correction. In the first class we must consider random photometric error, error due to inaccuracy in the wedge calibration, and error due to scattered light in the spectroscope, telescope and atmosphere.

The random photometric error is 0·8 per cent (continuum = 100 per cent) except in the wings, where it is reduced to $0{\cdot}8/\sqrt{7}=0{\cdot}3$ per cent by averaging the results obtained at the seven positions (see above). The r.m.s. errors of the wedge calibration have been given elsewhere (**4**). The maximum error in the line profiles due to this cause is 0·3 per cent in the region of the line "flank" ($r\sim 50$ per cent), decreasing to 0·2 per cent in the wings; at the line centre the error is negligible.

Scattered light in the spectroscope can be an important source of error in profile determination. However, Plaskett (**22**) finds that for a slit height of 19 mm the scattered light in the Oxford spectroscope is only 1·5 per cent of the total flux at a wave-length of $\lambda 4320$. At longer wave-lengths the amount is smaller, and can be further reduced by using a smaller slit height and a colour filter. In the present work an orange filter (Ilford Micro 5) was used for all exposures. The slit height for the "profile" exposures was about 8 mm; since this is nearly the same as the height of the wedge, the small remaining amount of scattered light is nearly the same for the calibration as for the profile exposures, and cannot therefore be a source of error.

Scatter in the telescope and atmosphere has the effect that at each point in the image a certain percentage of the light comes from points where the profile may differ from that appropriate to the point under consideration. The possible error reaches its greatest magnitude at the limb. Short-range scatter can be ignored owing to the slowly-varying nature of the profiles and to the compensatory effect of light scattered from both sides of the point in question. The extreme point in the present work ($\cos\theta = 0{\cdot}2$) corresponds to a distance of 1·86 mm, i.e. about 20″, from the limb. If we assume complete compensation for a region of radius 20″ surrounding the point then we need only consider scatter from distances greater than 20″, which according to Kinman (**11**) is 0·0504 (surface brightness = 1·00) under normal conditions. At the limb we must take one-half this value, namely 0·025. Consequently at a point for which $\cos\theta = 0{\cdot}2$, 97·5 per cent of the light originates at this point while the remaining 2·5 per cent comes from distances greater than 20″, where the intensity at a given point in the profile may differ by, say, 10 per cent. Hence if r is the true intensity at some point in the limb profile (continuum = 100 per cent) the measured intensity is

$$r' = \frac{r\times 97{\cdot}5 + (r-10)\times 2{\cdot}5}{100} = r - 0{\cdot}25,$$

the error therefore being 0·25 per cent. (Limb darkening increases this figure slightly). At points in the profile where the centre-limb variation is only a few per cent the error due to this cause can be ignored.

Errors arising from the process of correcting for spectroscopic distortion are of two kinds, namely errors caused by the actual process of solving the integral equation and errors due to apparatus-function errors. The errors due to the process of solution arise out of a magnification of the random errors present in the original observed profiles. The factor in the present work is estimated to be 1·8; magnification of random error does not affect the far wings of the profiles.

Apparatus-function errors exert their greatest effect at the centre of the profile where the difference between observed and true intensity is greatest. It is rather difficult to perform exact calculations, but by considering the core and the wings of the apparatus-function separately it is possible to obtain an approximate value for the effect of such errors, at any rate on the central intensities. R.m.s. errors for the apparatus-function core have been given elsewhere (**4**). If we take 3 per cent (in units of the peak intensity) as being a representative figure for the error in the region −0·075A to 0·075A then we find the resulting error in the central intensities is 0·6 per cent. Similarly, the wings of the apparatus-function, which may be in error by 8·5 per cent of the stated intensity for points beyond 1·8A, lead to an error in the central intensities of 0·25 per cent. The effect of errors in intermediate regions of the apparatus-function is difficult to assess. However, if we take a figure intermediate to those obtained for the core and wings, we obtain the result that the total error in the central intensities caused by apparatus-function errors is 0·6 + 0·25 + 0·4 = 1·3 per cent. The effect of these errors on points in the profile other than the central intensity is probably very small.

Collecting the various sources of error and assuming Gaussian distributions we obtain the following figures for the possible errors of the true profiles: central intensity, 1·9 per cent; flanks, 1·5 per cent; wings, 0·4 per cent.

TABLE II

Modern observations of the D lines

Observer	*Place*	*Date*	*Instrument*	*d*	*Size of image*	*Exposure time*	cos θ
Houtgast	Utrecht	Sept., 1935; May, Aug., 1936	Grating	...	12 cm	30s–90s	1·00, 0·80 0·60, 0·44 0·31, 0·20 0·14, 0·10
Houtgast	Potsdam	Aug., 1938	Grating	0·047 A	13 cm	5s–70s	,,
Allen	Mt. Stromlo	Late 1937	Prism	...	13 cm	...	1·00, 0·26
Shane	Berkeley	...	F.-P. and grating	·029 A	11 cm	...	1·00, 0·26
Priester	Göttingen	Sept., 1950	Lummer plate and grating	·020 A	22 cm	45s–18m	1·00, 0·80 0·60, 0·44 0·31, 0·20 0·14
S.-Samoilova	Moscow	Aug., 1951	Grating	·088 A	14 cm	45s–50s	1·00, 0·17
Bray	Oxford	Sept., 1953	Prism	·112 A	18 cm	4s–9s	1·00, 0·80 0·55, 0·38 0·30, 0·24 0·20

(*d* = apparatus-function half-width.)

2. *Comparison with previous observations.*—Table II gives a summary of modern investigations of the *D* lines. It will be seen that of the six observers, only Houtgast, Priester and the present author observed at points other than the centre and limb. A general idea of the agreement among the various workers can be obtained from Fig. 2, which shows the limb profiles of D_1 and D_2. It

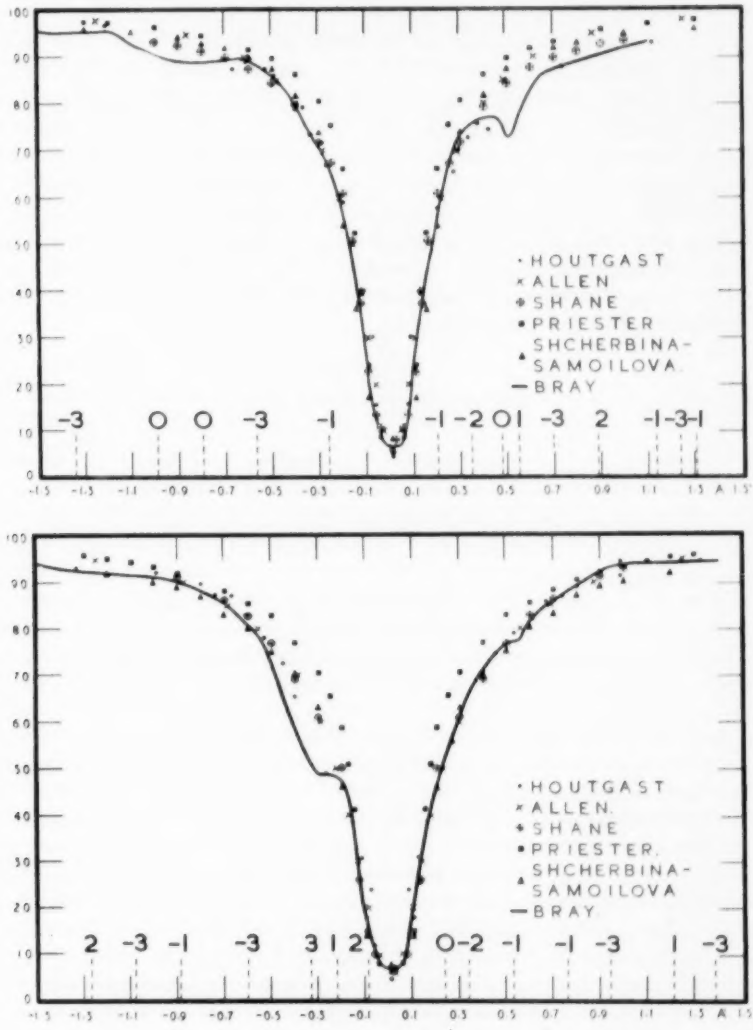

FIG. 2.—*Limb profiles of D lines.*

Abscissae : Angstroms.
Ordinates : intensity (continuum = 100 per cent).

The cos θ values for the various observers are as follows : Houtgast, Priester and the present author, 0·199 ; *Shane,* 0·262 ; *Allen,* 0·259 ; *Shcherbina-Samoilova,* 0·173. *The positions and Rowland intensities of disturbing lines are also shown. The upper diagram refers to* D_1, *the lower to* D_2.

should be noted that the values of $\cos\theta$ are not the same for all observers, the values being 0·199 for Houtgast, Priester and the present author, 0·262 for Shane, 0·259 for Allen, and 0·173 for Shcherbina-Samoilova. The positions and Rowland intensities of disturbing lines are also shown. The most noteworthy discrepancy, which is immediately apparent from the figure, is that Priester's limb observations lie considerably higher than those of the other workers. The discrepancies are discussed in detail below.

2.1. *Central intensities.*—Central intensities at centre and limb only found by the different observers are given in Table III. At first sight it may seem that there are rather large discrepancies, but if we calculate the r.m.s. deviation $s=\sqrt{\Sigma(\text{residual})^2/5}$ we obtain the following values: D_1–centre, 1·6 per cent; limb, 1·6 per cent; D_2–centre, 1·7 per cent; limb, 0·9 per cent. Since the estimated error in the present work is 1·9 per cent (and the values for the other workers are likely to be similar) we can conclude that the observations of the central intensities agree within the experimental error. There is some evidence that the central intensity of D_1 is greater than that of D_2; the difference is comparable with the r.m.s. error of the mean, however, and may be due to the presence of the heavy blend on the violet side of D_2.

TABLE III

Central intensities of the D lines

	D_1		D_2	
Observer	*Centre*	*Limb*	*Centre*	*Limb*
Shane	5·8%	8·0%	5·2%	7·0%
Allen	7·2	6·0	6·6	6·0
Houtgast	5·3	4·4	2·8	4·6
Priester	5·4	5·1	3·9	6·1
S.-Samoilova	6·4	8·3	6·2	7·0
Bray	**2·5**	**6·3**	**2·5**	**6·8**
Mean	5·4	(6·4)	4·5	(6·3)

(The cos θ values for the limb are as follows: Houtgast, Priester and Bray, 0·199; Shane, 0·262; Allen, 0·259; Shcherbina-Samoilova, 0·173. Continuum intensity = 100%).

2.2. *Flanks and wings.*—The most striking discrepancies among the various workers lie in the centre-limb variation of the wings. Allen and the present author agree in finding little or no variation, Priester finds a very large variation, and the other observers find a variation lying between these extremes. At points where the present observations show a difference between limb and centre profiles of 3 per cent, Priester nevertheless finds a difference of 14 per cent, while at points where the present observations show no difference at all Priester finds a difference of 5 per cent to 8 per cent. Shane and Shcherbina-Samoilova also find a large centre-limb variation, though not as large as Priester's. These discrepancies are shown in Table IV, which gives the difference between the intensity at the limb and the intensity at the centre for a number of selected points in the violet side of D_1 and the red side of D_2. The last line gives the r.m.s. deviation from the mean $s=\sqrt{\Sigma(\text{residuals})^2/5}$, which varies from about $1\frac{1}{2}$ per cent to $4\frac{1}{2}$ per cent. The corresponding r.m.s. deviations for the actual intensities in the profiles, as opposed to the centre-limb differences, are similar, being about 1 per cent to 5 per cent. The latter figures are rather large in view of the error estimate in the present work ($1\frac{1}{2}$ per cent for the line flank) but this

estimate takes no account of possible systematic error, such as systematic error in the wedge calibration. It is difficult to account for the discrepancies in the centre-limb differences on this basis, however, since such systematic errors would presumably affect centre and limb profiles equally, leaving their difference unaltered.

TABLE IV

Discrepancies in limb-centre differences

	D_1					D_2					
$\Delta\lambda$ (A)	−0·20	−0·30	−0·40	−0·50	−0·60	0·20	0·30	0·40	0·60	0·70	0·90
Shane	11·6%	8·4%	5·7%	3·8%	2·9%	11·4%	10·1%	8·3%	6·6%	4·8%	4·1%
Allen	4·9	2·4	1·0	0·3	0·1	6·3	5·2	3·1	0·5	0·0	−0·8
Houtgast	8·8	4·2	2·0	1·1	0·0	9·0	10·0	6·9	2·4	2·2	1·4
Priester	14·0	12·6	8·3	4·7	2·6	18·2	14·0	10·0	5·6	4·1	2·4
S.-Samoilova	6·5	5·0	3·0	4·0	3·0	14·0	11·0	8·0	4·0	3·0	2·0
Bray	2·9	1·7	0·0	0·0	0·0	7·9	3·4	−1·6	−0·9	0·0	0·0
R.m.s. deviation	4·2	4·1	3·1	2·1	1·5	4·4	3·9	4·3	2·9	2·0	1·8

(The quantity tabulated is limb intensity minus centre intensity for various points in the violet side of D_1 and the red side of D_2. The last line gives the quantity $s = \sqrt{\Sigma(\text{residuals})^2/5}$).

While on the subject of systematic errors, it may not be out of place to emphasize that in line profile work an accurate determination of the nearby continuum is as important as an accurate determination of the actual profile, since ultimately the profile must be expressed in terms of the continuum intensity. The precautions taken in the present work to achieve this end have been described in Section 1.2, but it is not certain that the other observers exercised the same care. Shane, for example, seems to have measured the continuum at a distance of only 4A from the line, which according to the present observations lies well within the wing. This could lead to an error of 2 per cent or 3 per cent in the wings. The use by Houtgast and Priester of Minnaert's method of locating the continuum is also open to criticism. In this method it is assumed that the profile wings follow an inverse square law, but a test of the method applied to the present observations of the violet wing of D_1 (which is relatively free from blends) shows that the wing is incapable of being represented by such a law. It is estimated that the use of the method may lead to errors of the order of 2 per cent or 3 per cent in the profile wings. A further objection to the use of Minnaert's method is that application *before* correction for spectroscopic distortion is invalid, because the portions of the wings and flanks used may be altered by the correction process; on the other hand the true level of the continuum must be known before correction for spectroscopic distortion is carried out. There seems no way out of this vicious circle. The use of the method is in any case unnecessary when we are dealing with relatively narrow lines in a region fairly free from disturbing lines.

However, it seems unlikely that this and other sources of systematic error can wholly account for the discrepancies in the centre-limb variation. Spitzer (**33**) mentions the possibility that the solar line profiles undergo an actual variation

with time: Minnaert (**13**) has also discussed this question and he and van der Meer (**14, 12**) have made attempts to detect such a variation. In the case of the *D* lines we can assert that *if* the discrepancies are due to a real variation with time, then the variation is uncorrelated with the solar cycle. This is shown by the dates at which the various investigations were carried out (cf. Table II). Allen's observations, which agree with the present observations in showing a very small centre-limb variation, were made at the solar maximum of 1937, while the present observations were made in 1953 near a minimum of solar activity. Priester's observations, which show a large centre-limb variation, were made three years past the maximum of 1947. Clearly there is no correlation with the solar cycle. The possibility of a connection with active regions of the Sun cannot be ruled out, however.

The possibility of a *latitude effect* must also be considered, though here we have insufficient data to come to any definite conclusions. In the present work the limb exposures were made in the neighbourhood of the equator. Those of Priester and Shcherbina-Samoilova were made in the region of the poles of the Sun. Shane and Allen do not state the latitude of their limb observations, and Houtgast, after finding the deviation with latitude negligible, paid no further attention to the question of latitude. As far as the data go, the observations are consistent with a bigger centre-limb variation for the polar limb than for the equatorial limb—i.e. a weaker polar limb profile than equatorial limb profile.

3. *A theoretical discussion of the line cores.*—The physical mechanism responsible for the formation of resonance lines is scattering rather than absorption. An atom in the ground state absorbs a quantum which raises it to a higher state. After a time of the order of 10^{-8} seconds the atom returns to the ground state, emitting a quantum of the same frequency. The whole process is therefore equivalent to scattering. A small fraction ϵ of the excited atoms are de-excited by superelastic collisions with electrons, photo-ionization, or induced transitions to higher excited states rather than by spontaneous transitions to the ground state. The value of ϵ can be determined from the measured central intensity, as we shall show below.

For the moment we assume that the scattering is coherent; the question of non-coherent scattering is considered later. The discussion is confined to the line cores and it is assumed that η_ν (the ratio of the line to the continuous absorption coefficient) is independent of τ, the optical depth in the continuous spectrum, and that $B(\tau)$, the continuous emission per unit mass, is a linear function of τ, so that

$$B(\tau) = B(0)(1 + \beta\tau). \tag{1}$$

In the line core these are likely to be reasonably good approximations, since the core is formed in a thin layer at the top of the atmosphere throughout which the physical conditions remain fairly constant. β is proportional to the gradient of $B(\tau)$ in this layer, and does not necessarily have the same value as the value given by limb darkening, since the continuous spectrum (observed between $\cos\theta = 1$ and $\cos\theta = 0{\cdot}2$) originates much deeper down in the atmosphere. For this reason, it is probably preferable to regard β as an unknown parameter, at any rate until we have a more certain knowledge of the temperature distribution in the higher layers. On the other hand, should our analysis of the *D* lines lead to a value

very different from the limb darkening value, we should rightly regard the result with suspicion. In actual practice we find that when the analysis is made on the basis of coherent scattering the two values are very similar.

3.1. *Comparison of theory and observation.*—The equation of transfer for coherent scattering in the Eddington–Strömgren notation is

$$\mu \frac{dI_\nu(\tau,\mu)}{d\tau} = (1+\eta_\nu)I_\nu(\tau,\mu) - (1-\epsilon)\eta_\nu J_\nu - (1+\epsilon\eta_\nu)B(\tau), \tag{2}$$

where $\mu = \cos\theta$. When η_ν is independent of τ, and $B(\tau)$ is given by (1) the solution (Eddington approximation) for the emergent radiation is

$$\frac{I_\nu(0,\mu)}{B(0)} = 1 + \frac{\beta\mu}{1+\eta_\nu} - \frac{1+\eta_\nu - \frac{2}{3}\beta}{1+\eta_\nu+\frac{2}{3}q_\nu}\cdot\frac{\eta_\nu(1-\epsilon)}{1+\eta_\nu+\mu q_\nu}\ ;\ q_\nu = \sqrt{3(1+\eta_\nu)(1+\epsilon\eta_\nu)}. \tag{3}$$

A similar formula has been used by Plaskett (**19**); Woolley and Stibbs (**40**) have compared (3) with Chandrasekhar's exact solution. The difference is very small except at the extreme limb ($\mu = 0$), particularly for large η_ν.

In order to substitute for $I_\nu(0,\mu)$ the actually observed quantity $r_\nu(0,\mu) = I_\nu(0,\mu)/I_0(0,\mu)$, we require the limb darkening in the continuous spectrum $I_0(0,\mu)$. It is preferable to use the *observed* limb darkening for this purpose, rather than the limb darkening given by (3) with $\eta_\nu = 0$, thus confining the assumption of linearity of $B(\tau)$ to the high-lying layers in which the line cores are formed. Observations of limb darkening have been made by Abbot (**1**), Moll, Burger and van der Bilt (**16**), Raudenbusch (**26**), Canavaggia and Chalonge (**7**), Pierce, McMath, Goldberg and Mohler (**18**), and Peyturaux (**17**). By interpolation from graphs the limb darkening at λ 5893 was obtained for each of the observers and a mean was taken. The mean limb darkening is represented within 0·5 per cent by the formula

$$I_0(0,\mu) = B(0)(1+\beta'\mu+\gamma'\mu^2), \tag{4}$$

with $B(0) = 0{\cdot}340$, $\beta' = 2{\cdot}60$, $\gamma' = -0{\cdot}676$. The quantity $I_\nu(0,\mu)$ appearing in (3) is obtained by combining (4) with the measured $r_\nu(0,\mu)$.

In comparing theory and observation we make use of the observations of Houtgast, Priester and the present author, since each of these observed at several intermediate points of the disk in addition to the centre and limb. Initially we shall consider D_1, which is less influenced by blends than D_2. We first determine an upper limit to ϵ:—

At the line centre $\eta_\nu = \eta_0$, say, and since $\eta_0 \gg 1$ we have

$$q_0 = \sqrt{(3)}\eta_0\sqrt{\left(\frac{1}{\eta_0}+\epsilon\right)}.$$

Hence (3) becomes

$$\frac{I_{\nu 0}(0,\mu)}{B(0)} = 1 - \frac{1}{1+\frac{2}{\sqrt{3}}\sqrt{\left(\frac{1}{\eta_0}+\epsilon\right)}}\cdot\frac{1-\epsilon}{1+\mu\sqrt{3}\sqrt{\left(\frac{1}{\eta_0}+\epsilon\right)}} \tag{5}$$

approximately, since $1+\eta_0 \gg \beta\mu$. It is clear from (5) that the central intensity depends substantially on $\sqrt{(1/\eta_0+\epsilon)}$, and therefore does not allow us to determine

η_0 and ϵ separately.* However, we can find an upper limit to ϵ, say ϵ_{max}, by letting $\eta_0 \to \infty$. Using the mean central intensity of D_1 at $\mu = 1$ obtained by Houtgast, Priester and the present author ($r = 4{\cdot}4$ per cent) we obtain $\epsilon_{max} = 0{\cdot}0024$. (When we use the mean of all six observers, $r = 5{\cdot}4 \pm 0{\cdot}7$ per cent, we obtain $\epsilon_{max} = 0{\cdot}0038 \pm 0{\cdot}0012$). The actual value of ϵ is probably fairly close to this upper limit, owing to the high value of η_0 ($\sim 10^4$ according to Harris (**8**)).

We can now proceed to the solution of (3), letting $\epsilon = 0$ and $\epsilon = 0{\cdot}0024$ in turn. At each point in the profile we have two unknowns, namely η_ν and β, so by using observed values of r (the mean of the values obtained by Houtgast, Priester and the present author) for two values of μ(1·0 and 0·2) we can obtain a pair of values (η_ν, β) which exactly reproduce the measured r at both centre and limb at this point in the profile. Ideally, values of β obtained in this way from different points in the profile should be identical. However, the profile is very insensitive to the value of β, particularly in the inner core; this has the effect that small variations in the profile give rise to quite large fluctuations in β. The best fit with observation occurs for $\beta = 3{\cdot}7 \pm 1{\cdot}0$. The values of η_ν, which, with this value of β, produce *exact* agreement with observation at $\mu = 1$ are given (both for $\epsilon = 0$ and $\epsilon = 0{\cdot}0024$) in Table V. (It will be noticed that for $\Delta\lambda \geqslant 0{\cdot}125$A the value of η_ν is not affected by ϵ).

TABLE V

Values of η_ν

$\Delta\lambda$ (A)	$\epsilon = 0$	$\epsilon = 0{\cdot}0024$	$\Delta\lambda$ (A)	$\epsilon = 0$	$\epsilon = 0{\cdot}0024$
0	516	∞	0·175	5·40	5·40
0·025	402	1810	0·200	4·41	4·41
0·050	155	212	0·250	3·20	3·20
0·075	52·4	56·2	0·300	2·55	2·55
0·100	22·0	22·4	0·350	2·12	2·12
0·125	11·3	11·3	0·400	1·82	1·82
0·150	7·05	7·05			

Using the values of η_ν given in Table V we can now calculate the profiles at other points of the disk. Theory and observation are compared in Fig. 3. The agreement is good, the theoretical curves lying well within the observational scatter, so we can conclude the observations are well represented by coherent scattering.

The value of β found above is in fair agreement with the value given by extrapolating the limb darkening formula (4) to the extreme limb, which gives $\beta = 2{\cdot}6$ for $0 \leqslant \tau \leqslant 0{\cdot}1$†; the value given by radiative equilibrium is also 2·6 according to Sykes' calculations (**35**). Had we decided to select the latter value right from the start, instead of following the procedure described, our results would scarcely have been different, owing to the insensitivity of the core to the precise value of β.

* In theory, by using the central intensity of D_2 as well as that of D_1, η_0 and ϵ can both be determined—cf. Shane (**31**). In practice, however, the difference in the central intensities of the two lines is comparable with the r.m.s. error, making this a very unsafe procedure. This difference is only 0.9 per cent, and in any case may be due to the heavy blend with water vapour lines on the violet side of D_2 (cf. Fig. 2).

† Sykes' analysis of limb darkening observations (**35**) gives the value 10, however.

The values of η_ν given in Table V, when doubled, ought to reproduce correctly the measured profiles of D_2, since η_ν is proportional to the oscillator strength, which is twice as big for D_2 as for D_1. When the computed and observed profiles of D_2 are compared we find quite good agreement over the inner core, but beyond $\Delta\lambda = 0{\cdot}20$A the computed profiles fall below the observed profiles, the difference amounting to about 10 per cent at $\Delta\lambda = 0{\cdot}40$A. This disagreement may be a consequence of our assumption that η_ν is independent of τ. This assumption

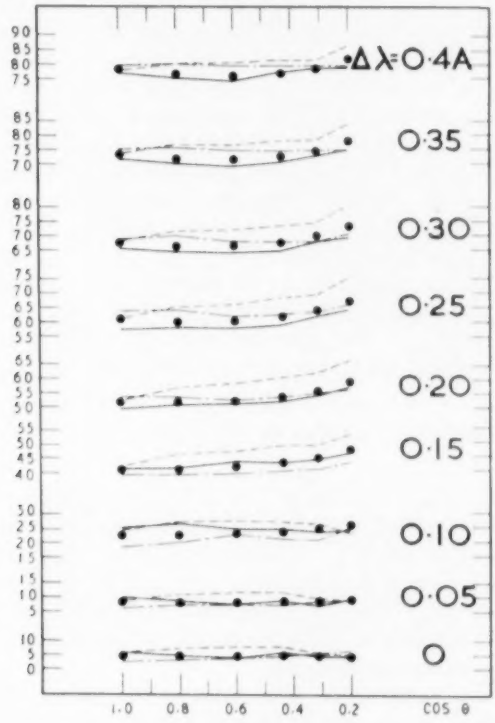

FIG. 3.—*Observed and computed centre-limb variation of D_1.*
Abscissae : cos θ.
Ordinates : intensity (continuum = 100 per cent).

————*Hougast* ; – – – – – – – – – – *Priester* ; — — — — — — — — *Bray.*
Filled circles represent values computed from (3) *with* $\epsilon = 0$, $\beta = 3{\cdot}7$, *using values of* η_ν *given in the second column of Table V. Similar results are obtained with* $\epsilon = 0{\cdot}0024$, *using values of* η_ν *given in the third column of Table V.*

becomes progressively less and less valid as we proceed outward from the core to the wings, owing to the fact that the change in effective optical depth $\bar{\tau}(\simeq\mu/(1+\eta_\nu))$ in going from centre to limb becomes greater. For example, at $\Delta\lambda = 0{\cdot}30$A, $\eta_\nu = 2{\cdot}55$, and $\bar{\tau}$ changes from $1/3{\cdot}55 = 0{\cdot}28$ at the centre to $0{\cdot}2/3{\cdot}55 = 0{\cdot}06$ at the limb, a change which may be sufficient to invalidate our assumption of constant η_ν. At $\Delta\lambda = 0{\cdot}10$A, where η_ν rises to 22, $\bar{\tau}$ only changes from 0·04 to 0·01 and the error involved in assuming η_ν to be constant is correspondingly less. The

disagreement of D_2 with theory indicates that the assumption is only valid for $\Delta\lambda \leqslant 0{\cdot}20$A.

The above results show that it is unnecessary to invoke non-coherent scattering to account for the cores of the D lines. How far is this conclusion consistent with our knowledge of the physical mechanisms responsible for non-coherent scattering? With regard to Zanstra's mechanism (**41**) we may remark that in the higher layers of the atmosphere the collisional broadening of the ground state is small owing to the low gas pressure, so that non-coherency due to this cause probably does not appreciably affect the line core. Deeper down collisional broadening becomes important and the wings may be formed non-coherently, as Houtgast (**10**) has attempted to show. (The mode of formation of the wings is still rather obscure, however, for Harris (**8**) finds that the wings can be represented by coherent scattering, a result confirmed by Hitotuyanagi and Inaba (**9**). There seems no justification for assuming *pure absorption*, as Priester (**25**) and other Göttingen workers have done). An additional source of non-coherency is re-distribution due to Doppler effect (see Unsöld (**36**)). In so far as this process affects the Doppler core, our conclusion that the cores are formed by coherent scattering is perhaps surprising.

Confirmation for our conclusion can be obtained by carrying out an analysis of the observations on the basis of the non-coherent equation of transfer similar to that described above for the coherent equation. When the scattering is completely non-coherent J_ν in (2) must be replaced by $\bar{J}$ where

$$\bar{J} = \frac{\int J_{\nu'} l_{\nu'} \, d\nu'}{\int l_{\nu'} \, d\nu'} .$$

Owing to the highly peaked nature of l_ν, it is a good approximation to replace $\bar{J}$ by $J_{\nu 0}$. The solution of the resulting equation of transfer is readily performed by the method used in deriving (3). When an attempt was made to fit this solution to the observations a value of β of the order of 30 was required when η_0 was put equal to 10^4 (Harris (**8**)). Unless independent evidence should favour such a high value, this can be taken as confirmation for our conclusion that the D line cores are formed by coherent scattering.

3.2. *The numerical value of* ϵ.—The mean of the values obtained for the central intensity of D_1 at $\mu = 1$ by all six observers is $5{\cdot}4 \pm 0{\cdot}7$ per cent; in the absence of any mechanisms for producing non-zero central intensities other than de-excitation of the upper state of the transition, this leads to a value of ϵ of $0{\cdot}0038 \pm 0{\cdot}0012$ ($0{\cdot}0024$ when we use the results of Houtgast, Priester and the present author only). One such mechanism is chromospheric emission: the presence of chromospheric detail on D line spectroheliograms (**3**) shows that some such emission undoubtedly occurs. An additional mechanism for raising the central intensity is the superposition (by poor seeing or other causes) of granular elements having different line-of-sight velocities; the addition of several slightly displaced profiles raises the central intensity (**27**, **28**, **29**). Such smearing is a complex effect depending on seeing, vertical apparatus-function half-width and microphotometer-slit height. The dominating factor in the present work is the seeing, the seeing disk at Oxford being about 3″ under the best conditions. This figure may be compared with a vertical apparatus-function half-width of 1″·7 and a microphotometer-slit height of 1″. Under

these conditions granular elements 1″ in diameter are completely smeared, and the central intensities correspondingly raised.

Since part of the central intensity must be due to these two processes, it is clear that the above value of ϵ, derived from the measured central intensity, is only an upper limit, and a direct comparison between the "observed" value and a value computed from theory is not possible. Nevertheless, it is interesting to calculate from theory the contribution made to ϵ by various de-exciting processes. It is only possible to perform this calculation for the photo-ionization and collisional mechanisms; induced transitions have been qualitatively considered by Unsöld (**37**), but with present theory it does not seem possible to give a quantitative result. The contribution to ϵ made by photo-ionization can be calculated with the aid of the formula quoted by Strömgren (**34**) for the photo-ionization transition probability of a hydrogen-like atom. If we substitute a colour temperature of 6500 deg. K and a dilution factor of 0·3, following Woolley (**38**), we obtain a contribution to ϵ of 0·0009—i.e. about one-quarter the observed value.

The contribution made by superelastic collisions with electrons, say ϵ_e, depends on the electron pressure p_e and the kinetic temperature of the electrons. The latter we can take to be 4650 deg. K, the boundary temperature of the Sun according to Plaskett (**24**). Making use of formulae given by Woolley and Stibbs (**39**), we obtain $\epsilon_e = 1{\cdot}1 \times 10^{-2} p_e$. The latter calculation is of some interest because it gives us an upper limit to the electron pressure of $0{\cdot}26 \pm 0{\cdot}11$ dynes/cm². Whatever the contribution to the central intensity made by chromospheric emission or granular motion, p_e cannot exceed this value or the central intensity would be higher than the measured value.

I should like to thank Professor H. H. Plaskett for his continuous guidance and generous assistance during all phases of the work. I am indebted to Dr D. W. N. Stibbs for a number of helpful discussions on the topics discussed in Section 3. I should also like to thank the Master and Fellows of Balliol College for the award of the Skynner Senior Studentship in Astronomy and the Department of Scientific and Industrial Research for a maintenance grant.

University Observatory,
Oxford:
1956 *March* 31.

References

(1) C. G. Abbot, *Ann. Smithsonian Inst.*, **4**, 221, 1922.
(2) C. W. Allen, *M.N.*, **100**, 10, 1939.
(3) L. d'Azambuja, *Ann. Obs. Paris-Meudon*, **8**, II, 1930.
(4) R. J. Bray, *M.N.*, **114**, 540, 1954; *Comm. Univ. Obs., Oxford*, No. 45, 1954.
(5) H. C. Burger and P. H. van Cittert, *Zs. f. Phys.*, **79**, 722, 1932.
(6) H. C. Burger and P. H. van Cittert, *Zs. f. Phys.*, **81**, 428, 1933.
(7) R. Canavaggia, D. Chalonge, *Ann. d'Ap.*, **9**, 143, 1946.
(8) D. L. Harris, *Ap. J.*, **109**, 53, 1949.
(9) Z. Hitotuyanagi and H. Inaba, *Sci. Rep. Tôhoku Univ.*, Ser. I, **38**, 209, 1954.
(10) J. Houtgast, "The Variations in the Profiles of Strong Fraunhofer Lines Along a Radius of the Solar Disk", Utrecht, 1942.
(11) T. D. Kinman, *M.N.*, **113**, 613, 1953; *Comm. Univ. Obs., Oxford*, No. 41, 1953.
(12) A. P. H. van der Meer, *Zs. f. Ap.*, **13**, 157, 1937.
(13) M. Minnaert, *M.N.*, **107**, 274, 1947.

(14) M. Minnaert, W. Bleeker and A. P. H. van der Meer, *Zs. f. Ap.*, **8**, 59, 1934.
(15) M. Minnaert, G. F. W. Mulders and J. Houtgast, " Photometric Atlas of the Solar Spectrum ", Amsterdam, 1940.
(16) W. J. H. Moll, H. C. Burger and J. van der Bilt, *B.A.N.*, **3**, 83, 1925.
(17) R. Peyturaux, *Ann. d'Ap.*, **18**, 34, 1955.
(18) A. K. Pierce, R. R. McMath, L. Goldberg and O. C. Mohler, *Ap. J.*, **112**, 289, 1950.
(19) H. H. Plaskett, *M.N.*, **91**, 870, 1931.
(20) H. H. Plaskett, *M.N.*, **95**, 160, 1934; *Comm. Univ. Obs., Oxford*, No. 4, 1934.
(21) H. H. Plaskett, *M.N.*, **99**, 219, 1939; *Comm. Univ. Obs., Oxford*, No. 14, 1939.
(22) H. H. Plaskett, *M.N.*, **112**, 177, 1952; *Comm. Univ. Obs., Oxford*, No. 33, 1952.
(23) H. H. Plaskett, *M.N.*, **112**, 414, 1952; *Comm. Univ. Obs., Oxford*, No. 34, 1952.
(24) H. H. Plaskett, " Vistas in Astronomy ", ed. A. Beer, Vol. I, p. 640, London, 1955.
(25) W. Priester, *Zs. f. Ap.*, **32**, 200, 1953.
(26) H. Raudenbusch, *A.N.*, **266**, 301, 1938.
(27) R. O. Redman, *M.N.*, **95**, 742, 1935.
(28) R. O. Redman, *M.N.*, **97**, 552, 1937.
(29) R. O. Redman, *M.N.*, **98**, 311, 1938.
(30) C. E. St. John, C. E. Moore. L. M. Ware, E. F. Adams and H. D. Babcock, " Revision of Rowland's Preliminary Table of Solar Spectrum Wave-lengths ", Washington, 1928.
(31) C. D. Shane, *Lick Observatory Bulletin*, **19**, 119, 1941.
(32) I. S. Shcherbina-Samoilova, *R.A.J.*, **30**, 414, 1953.
(33) L. Spitzer, *Ap. J.*, **99**, 107, 1944.
(34) B. Strömgren, *Zs. f. Ap.*, **10**, 237, 1935.
(35) J. B. Sykes, *M.N.*, **113**, 198, 1953; *Comm. Univ. Obs., Oxford*, No. 38, 1953.
(36) A. Unsöld, " Physik der Sternatmosphären ", 2nd edn., p. 293, Berlin, 1955.
(37) A. Unsöld, *Ibid.*, p. 497.
(38) R. v. d. R. Woolley, *M.N.*, **94**, 631, 1934.
(39) R. v. d. R. Woolley, D. W. N. Stibbs, " The Outer Layers of a Star ", p. 121, Oxford, 1953.
(40) R. v. d. R. Woolley and D. W. N. Stibbs, *Ibid.*, p. 138.
(41) H. Zanstra, *M.N.*, **101**, 273, 1941.

SPECTROPHOTOMETRY OF THE OUTER CORONA

C. W. Allen

(Received 1956 April 26)

Summary

A low dispersion spectrograph with an occulting bar was used at the solar eclipse of 1954 June 30 to obtain three coronal spectra extending to six solar radii. Photometric measurements show a slight increase of reddening with radial distance. The Fraunhofer lines of the outer corona are faint and an interpretation of their measured intensities leads to a rather high coronal electron density.

---

1. *Observations.*—The prime purpose of the University of London Observatory Eclipse Expedition to Syd Koster, Sweden in June 1954 was to make photometric measurements of the corona using an occulting principle to reduce the great difference of brightness between the inner and outer corona. For the direct coronal photographs this required the use of an occulting *disk* already described in (**1**), and for spectra the same principle calls for an occulting *bar*. It is important to notice that the bar does not affect the colour characteristics of the radiation.

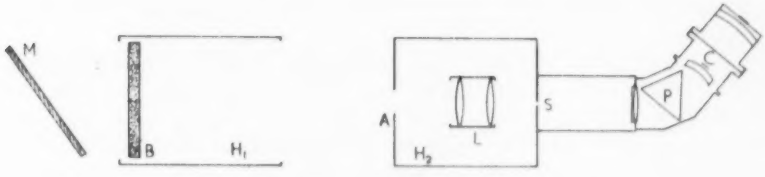

FIG. 1.—*Optical system for spectrograph—not to scale.*

The optical system for the spectrograph is shown in Fig. 1. An image of the Sun reflected from the coelostat mirror M is formed by the telescope lens L on the centre of the slit S which was in the equatorial direction. The hood H_2 contains an aperture A focussed by L onto the prism P. The image of A was a little smaller than the aperture of the collimator-prism-camera system and therefore A defines the effective aperture of the spectrograph. The occulting bar B was shaded from stray light by the hood H_1. B was oriented at right angles to the slit S, and the width of B was such that the light from the Sun's disk was just excluded from A; i.e. width B = width $A + \overline{BA} \times$ Sun's diameter (in radians). Hence during the eclipse the extreme inner corona was just excluded but the rest of the corona was admitted with aperture variation partially compensating for brightness variation. For the corona beyond 2·3 solar radii the effective aperture was complete.

The camera had an $f/1{\cdot}0$ Maksutov optical system of 9·2 cm focal length and aperture. Unfortunately there was no opportunity of testing the camera before departure of the expedition and considerable spherical aberration was found to exist (The Maksutov corrector has since been replaced by a Schmidt plate). With the wide angle camera it was possible to obtain spectra of the eclipse sky in less than a minute. In an effort to reduce the aberrations the camera aperture in the dispersion direction was reduced to 3·7 cm by means of A. The speed of the camera was reduced by this aperture together with the film holder obstruction to 37 per cent of the full ($f/1$) power. The focal length of the telescope lens L was 47·0 cm, the collimator focal length 124 cm, the slit width 0·25 mm, the spectrographic dispersion 240 A/mm at $H\gamma$, and the whole spectrum length 7 mm. Ilford HP3 film was used cut to 2 cm diameter disks.

For the standardization of brightness and colour, test spectra were obtained of Sun-illuminated white blotting paper (see **1**), using a greatly reduced camera aperture. Photographic density calibration was obtained by means of a step wedge. Standardized Fraunhofer line intensities spectra were obtained by making exposures during twilight. A wave-length comparison was provided from a mercury-helium discharge tube. The various test films and the eclipse films were developed separately but with similar conditions.

Three coronal spectra were obtained, the exposure times being 8 sec, 24 sec, and 72 sec. In each case the spectra could be detected to the limit of the field, i.e. 6·4 solar radii in both equatorial directions. The eclipse was observed through variable cloud which was thickest for the shorter exposures. The resulting images revealed a continuous spectrum with Fraunhofer absorption lines in the outer corona and some of the strongest Flash lines at the limb. The coronal emission line $\lambda 5303$ could be detected with difficulty close to the limb on the short exposure and not at all on the longer exposures. Without doubt this was due to the smallness of the dispersion and the faintness of the line in the outer corona.

The occulting bar was useful in reducing the brightness near the limb, but the scale of the image (solar radius = 0·16 mm) was too small in relation to the aberrations to allow an investigation of any steep radial photometric changes. The only measurements that could be attempted were (*a*) the coronal spectral intensity distribution in relation to radial distance, and (*b*) Fraunhofer line equivalent widths in relation to radial distance. The justification for presenting the results is that they extend further into the outer corona than those previously available.

2. *Spectral intensity distribution.*—In order to determine the intensity distribution as a function of r, the projected distance from the Sun's centre in terms of the solar radius, the spectra were examined with a Hilger Recording Microphotometer. Runs were made both along and across the spectra.

Density calibration curves were prepared in the usual way from the step wedge spectra. It was found that the (Ilford HP3) film contrast was greater in the green-yellow than the violet–blue regions but that the band of red sensitivity near $H\alpha$ had less contrast than all the rest of the spectrum. This made an apparent change of distribution with film density which required correction.

The most critical correction to be made was that for sky illumination. At the limiting distance of $r = 6{\cdot}4$ the radiation was predominantly, but not entirely, from the sky. The only way to determine the proportion of sky light at the

limiting distance was to use the information from the direct photographs (**1**), (which went to $r = 12$ where the radiation was almost entirely sky light). A sky correction was deduced which left the remaining coronal spectrum a little redder than at the Sun's limb. For the smaller radii the influence of the sky correction is much reduced but we find the resulting spectral distribution still varies rather slowly and consistently with the radial distance. This suggests that the correction has not introduced any considerable errors although of course it would have been preferable to have made the correction entirely independently of (**1**).

After correction the various runs were smoothed in regard to wave-length and r. No steep colour effects were noted, nor was there any evidence that the radial intensity gradient was steeper in the red and violet than in the green as reported by Sokolova (**2**). In Table I the results are expressed as coronal brightness I_c at 4000 A and 6000 A relative to sunlit blotting paper brightness I_s when both corona and paper are reduced to the same value at 5000 A. There is a slight redness of the corona relative to the paper throughout. Probably

TABLE I

Log (I_c/I_s) *where* I_c = *coronal brightness,* I_s = *sunlit blotting paper brightness (reduced to equality at* 5000 A)

r	4000 A	5000 A	6000 A	Index of colour
1·5	−0·06	0·00	+0·03	0·09
2·0	−0·04	0·00	+0·01	0·05
3·0	−0·06	0·00	+0·02	0·08
4·0	−0·09	0·00	+0·04	0·13
5·0	−0·07	0·00	+0·04	0·11
6·0	−0·08	0·00	+0·06	0·14

some of this can be explained by colouring of the paper and general reddening of the corona on passing through thin cloud. Of more interest is the apparent slight increase of reddening as r increases.

In order to compare the observations with theoretical values we define an index of colour as the logarithmic excess of brightness at 6000 A over that at 4000 A when compared with the distribution of the mean Sun (for theory) or of the sunlit blotting paper (for observations). The measured values taken from Table I are shown in Fig. 2. The calculated index of colour is zero for the K corona (component due to electron scatter). The index is 0·176 for the F corona (diffracted component) in the outer regions (where scattering coefficient is proportional to wave-length), but in the inner corona it is rather dependent on the size of the diffracting particles (see Blackwell **3**). In Fig. 2 we differentiate between (*a*) large diffracting particles ($> 2 \times 10^{-3}$ cm radius) and (*b*) particles of 10^{-3} cm radius. The final colour depends on K/F the brightness ratio of the K to the F corona. For K/F we use (*i*) the van de Hulst equatorial sunspot minimum model (**4**) and (*ii*) the higher K/F values derived in Section 3 below. The change of observed colour with r tends to favour a large particle size ($> 2 \times 10^{-3}$ cm radius). Either proposed value of K/F gives agreement within the experimental error which might be as much as 0·05, but the results are slightly in favour of the higher K/F.

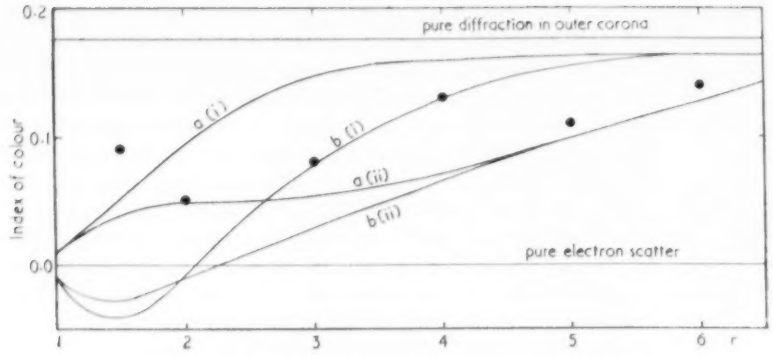

FIG. 2.—*Relation between coronal colour and radial distance.*
• *Observed (relative to sunlit blotting paper)*
——— *Calculated (relative to mean Sun)*
a = large particles *b = particle radius* 10^{-3} *cm*
(i) = van de Hulst model *(ii) = Section 3 data.*

3. *Fraunhofer line intensities.*—Fraunhofer lines were visible in the outer regions of the 24 sec and 72 sec exposure spectra, but they appeared to be fainter and more diffuse than in the test spectra taken at twilight. There does not appear to be any noticeable breadth difference in the emission lines of the corresponding comparison spectra, and the natural conclusion would be that the Fraunhofer lines in the outer corona had suffered an extra broadening effect (of about 5 or 10 A). However this conclusion should be viewed with caution since it disagrees with that reached earlier by Ludendorff (**5**) and Allen (**6**) who used a much higher spectroscopic resolution. The weakness of the lines and the effect of film grain prevent any reliable photometric test of this point.

Line weakness and grain also prevent accurate measures of the Fraunhofer line intensities. Only the G-band near 4300 A was strong enough to be detected

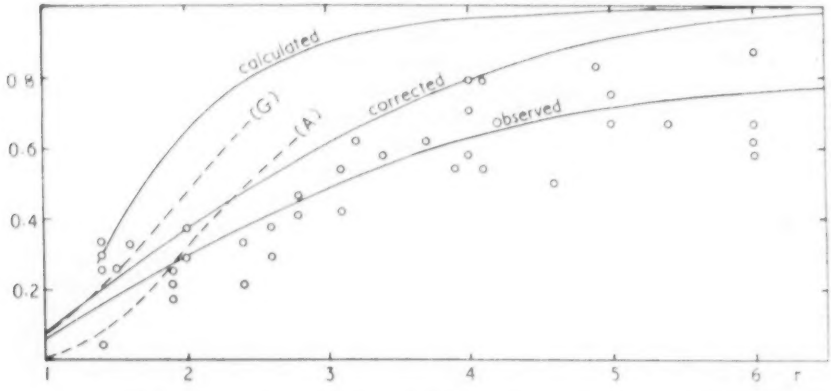

FIG. 3.—*Ordinates : Coronal line depth or equivalent breadth relative to corresponding solar Fraunhofer Line.*
Abscissae : Solar radial distance.
corrected = observed + 26 per cent.
calculated is from van de Hulst data.
— — — — — *earlier observations by Grotrian (G) and Allen (A).*

consistently on the microphotograms. In Fig. 3 we have plotted measurements of the ratio of the depth of the G-band in the corona to the depth in the twilight test spectra. It will be remembered that this ratio should equal $(F+S)/(K+F+S)$ where S represents the sky brightness. Some allowance has been made for the diffusion of bright inner coronal light onto the outer regions. It is noticed that even at $r=6$, where K is negligible, the G-band depths are less in the corona than in the test spectra. Probably this is related to the quality of the eclipse spectra (associated with the extra broadening mentioned above) and the measured ratios have therefore been increased by 26 per cent to give the corrected curve of Fig. 3. for which the outer corona G-band has its full depth. It is found that even when corrected in this way the coronal line intensities are less than expected. The calculated curve in Fig. 3 is from the van de Hulst model (**4**) for the equator at spot-minimum when superimposed on the sky intensity found at this eclipse. Fig. 3 also shows earlier eclipse measurements for relatively small r made by Grotrian (**7**) and Allen (**6**).

The difference between the corrected and calculated curves of Fig. 3 is too large to ascribe to experimental error and the measurements suggest that the ratio K/F used by van de Hulst is too low. From the corrected curve of Fig. 3, and the coronal brightness measurements of (**1**), one may derive values for K and F for the coronal equator at the 1954 eclipse. Values obtained are compared with those from the van de Hulst model and from Blackwell's polarization measurements (**8**) in Table II. We find that the new value of K, and therefore the electron density, in the outer corona is about 4 times greater than the model, while Blackwell's K is about 2 times greater. The new estimate of F in the inner corona represents a significant reduction.

TABLE II

r	1954 eclipse		v. d. Hulst model		Blackwell	
	K	F	K	F	K	F
	10^{-10} mean solar brightness					
1·5	780	195	620	268		
2·0	190	71	85	100		
2·5	69	27	21	52		
3·0	33	13	7·1	33		
4·0	12·6	7·5	1·9	15·7		
5·0	4·5	5·5	0·8	8·9		
6·0	1·8	4·0	0·5	5·6	1·0	6·0

(In order to bring Blackwell's F Brightness to our wave-length it has been reduced by 20 per cent.)

There have been many indications from radio astronomy and solar-terrestrial physics which suggest that the electron density estimates of Baumbach (**9**) should not have been reduced so substantially by the K and F segregation as originally thought (**10**). It was from absorption line intensities and polarization that the original segregation was made and we now find that both of these lead, in reasonable agreement, to higher electron densities.

4. 1955 *June* 20 *eclipse.*—An attempt was made to repeat the observations at the eclipse of 1955 June 20 observed from Ceylon. In this case the spectrograph dispersion and sky acceptance area were both considerably greater. However the corona was obscured by thick cloud.

Grants for the two eclipse expeditions mentioned were made by the Joint Permanent Eclipse Committee, Mr J. Miller, and the University College London. In Sweden the spectrograph was operated by Mr A. S. Asaad, and in Ceylon by Mr E. W. Foster. For preliminary arrangements relating to the selection of both eclipse sites I have much to thank Dr H. von Klüber. Much help is acknowledged from local authorities and residents in both Sweden and Ceylon.

University of London Observatory,
Mill Hill Park, London, N.W.7:
1956 *April.*

References

(1) C. W. Allen, *M.N.*, **116,** 69, 1956.
(2) V. S. Sokolova, *Pub. Ac. Sc. Kasakhstan*, **1,** 49, 1953; *Astron. News Letter*, No. 76, 27, 1955.
(3) D. E. Blackwell, *M.N.*, **112,** 652, 1952.
(4) H. C. van de Hulst, *B.A.N.*, **11,** 135, 1950.
(5) H. Ludendorff, *Sitz. Preuss. Akad. Wiss.*, **5,** 83, 1925.
(6) C. W. Allen, *M.N.*, **106,** 137, 1946.
(7) W. Grotrian, *Z. f. Ap.*, **8,** 124, 1934.
(8) D. E. Blackwell, *M.N.*, **116,** 56, 1956.
(9) S. Baumbach, *Astr. Nach.*, **263,** 121, 1937.
(10) C. W. Allen, *M.N.*, **107,** 426, 1947.

EXCITATION OF CHROMOSPHERIC EMISSION

H. H. Plaskett

(Received 1956 April 26)

Summary

The presence of the Lyman-alpha line in emission across the whole disk of the Sun suggests that the chromosphere is excited by a mechanism additional to that given by the absorption of photospheric radiation. To find some of the properties of this additional excitation the observed intensity of a chromospheric line, as observed at the limb of the Sun outside an eclipse, is derived as an integral containing the source function. A numerical method of solving this integral equation is outlined, and from the solution the excitation temperature and the density can be found as functions of radial height in the chromosphere. Other applications of the integral equation are briefly discussed.

Introduction.—The construction of biaxial Sun-followers, notably at the University of Colorado, has allowed long-exposure spectra of the Sun to be taken from rockets. On a flight to an altitude of 81 km made in an Aerobee Rocket on 1952 December 12, an exposure of 28 sec showed the hydrogen Lyman-alpha line (Lα) in emission (**3**). This result has been confirmed by R. Tousey, and in a spectrum exhibited at the Dublin meeting of the I.A.U. a strong emission Lα could be seen stretched more or less uniformly across the whole disk of the Sun. It seems probable that this is a characteristic of the normal chromosphere rather than the result of a fortuitous flare which would, presumably, have given a sharply localized emission.

Photospheric radiation by itself appears to be incapable of producing Lα emission in the integrated spectrum of chromosphere and photosphere. Excitation of chromospheric hydrogen by photospheric radiation can occur in two ways—on the one hand by the absorption of Lα quanta from the photospheric continuum giving excited atoms, and on the other by the absorption of quanta from the continuum to the violet of the Lyman limit giving ionized atoms. In so far as the first process gives detailed balancing it will never result in an emission line appearing in the integrated spectrum of the chromosphere and photosphere. For consider a chromosphere surrounding a spherical black body and containing atoms capable of absorbing and emitting a single line. Then from the conservation of energy, as Professor Zanstra has pointed out,* since the emission in the single line is obtained solely at the expense of the energy from that frequency in the continuum of the radiator, the total emission in the line integrated over the whole chromosphere is exactly equal to the total amount of energy integrated over the whole surface of the radiator which has been lost in that frequency from the continuum. The chromospheric line-emission, however, is very nearly isotropically distributed and that fraction, approximately

* Private communication in 1927.

one half, which lies within the solid angle subtended by the radiator will be effectively lost to the frequency concerned, its only effect being slightly to warm the radiator. Hence if we consider radiation in the frequency of the line which escapes outside a sphere drawn about the chromosphere there will be a net loss of energy, and the spectrum will show a continuum crossed by an absorption line at this frequency.

The second process, that of photo-ionization and recombination, at first sight looks more promising. In particular the photospheric radiation which is absorbed occurs beyond the limit of the Lyman series so that the chromospheric Lα resulting from recombination will not, in the integrated spectrum of photosphere and chromosphere, be superposed on a continuum crossed by a chromospherically produced absorption line at the same frequency. On the other hand the geometrical dilution of photospheric radiation is only one half so that the cyclic process of ionization and recombination is but little favoured in the chromosphere (**4**). Moreover it is difficult to see how the photosphere beyond the Lyman limit can have sufficient energy to produce by this process an Lα-line of the observed intensity. The radiation which escapes from the photosphere in the far ultra-violet, as the observations of Tousey and others show (**5**), is effectively black-body radiation corresponding to the boundary temperature of the photosphere. If we take this to be 4650 deg. K, then the total flux available beyond the Lyman limit, received outside the Earth's atmosphere in the absence of a chromosphere, amounts only to 7×10^{-7} microwatts cm^{-2}, —a negligible fraction of the 5×10^{-2} microwatts cm^{-2} received, according to Rense (**3**), from Lα itself*.

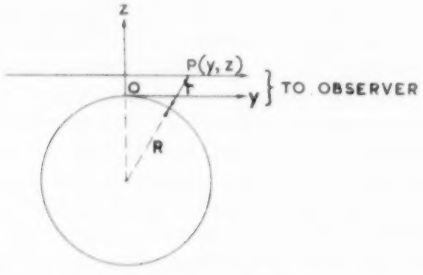

Since the absorption neither of Lα nor of Lyman-continuum quanta from the photosphere can account for the observed Lα emission, we conclude that there must be some additional mechanism of chromospheric excitation. The nature of this excitation is the fundamental problem posed by the chromosphere. It is the purpose of the present paper to show how observations of chromospheric lines without an eclipse, such as those of Unsöld (**7**), Keenan (**1**) and notably the interferometer observations of Treanor (**6**), can be used to find the excitation temperature of the chromosphere as a function of radial height. A knowledge of this temperature is clearly the first step towards finding the nature of the additional mode of excitation.

1. *The integral equation.*—The geometrical circumstances of an observation of the chromosphere are shown in the figure. Consider a rectangular yz-coordinate system with origin on the limb of the Sun and the positive y-axis

* Only for boundary temperature of 6800 deg. K would the two amounts of energy be comparable.

pointing to the observer. Then at a point P(y, z) in the chromosphere, radially distant r km from the boundary of the photosphere and on a sight-line which passes z km above the origin, we shall have

$$y^2 \simeq 2R(r-z). \tag{1.1}$$

This follows since $z \leqslant r \ll R$, where R is the radius of the photosphere. Then if $I(\nu)$ is the specific intensity at P of a chromospheric line, the equation of radiative transfer in the direction of y increasing will be given by

$$\frac{dI(\nu)}{dy} = -\kappa_\nu I(\nu) + j_\nu,$$

where κ_ν is the linear coefficient of absorption at the frequency ν in the line, and j_ν is the volume coefficient of emission. Defining the tangential optical depth by

$$t = -\int_\infty^y \kappa_\nu \, dy, \tag{1.2}$$

the equation of transfer takes the form

$$\frac{dI(\nu)}{dt} = I(\nu) - \frac{j_\nu}{\kappa_\nu}.$$

The observed intensity, $I_z(\nu)$, in the frequency ν of the chromospheric line at a height z km above the limb is then given by

$$I_z(\nu) = \int_0^{t_1} \frac{j_\nu}{\kappa_\nu} \exp(-t)\, dt, \tag{1.3}$$

where

$$t_1 = \int_{-\infty}^{\infty} \kappa_\nu \, dy.$$

is the total tangential optical depth in the frequency ν of the line at a height z km above the limb.

If the broadened state, originating from radiative and collisional damping, is "naturally excited" (as may be reasonably assumed), and the atom has a Maxwellian velocity distribution, the linear absorption coefficient is given by

$$\kappa_\nu = \frac{h\nu_{12}^0}{c} n_1(r) B_{12} \frac{1}{b\sqrt{\pi}} H(\alpha, v). \tag{1.4}$$

Here $n_1(r)$ is the number of atoms in the lower of the two states of the line per unit volume at a radial height r in the chromosphere, B_{12} is the Einstein transition coefficient, and

$$b = \frac{\nu_{12}^0}{c} \sqrt{\frac{2kT_k}{m}}$$

where T_k is the kinetic temperature and m is the mass of the atom. Following Unsöld (**8**)

$$H(\alpha, v) = \exp(-v^2) - \frac{2\alpha}{\sqrt{\pi}} [1 - 2vF(v)] \tag{1.5}$$

where $\alpha = (\delta_1 + \delta_2)/b$, δ_1 and δ_2 being the half-widths of the two broadened states,

$$v = \frac{\Delta\nu}{b} = \frac{\nu - \nu_{12}^0}{b}$$

and where $F(v)$ is a tabulated function. Similarly it may be shown*, neglecting radiatively stimulated downward transitions, that the volume coefficient of emission is given by

$$j_\nu = \frac{h\nu_{12}^0}{c} n_2(r) A_{21} \frac{1}{b\sqrt{\pi}} H(\alpha, v) \tag{1.6}$$

where $n_2(r)$ is the number of atoms in the upper of the two states for the line per unit volume at height r, and A_{21} is the Einstein transition coefficient for spontaneous emission. Hence the source function which appears in equation (1.3) is given by

$$\frac{j_\nu}{\kappa_\nu} = \frac{c}{4\pi} \frac{n_2(r)}{n_1(r)} \frac{A_{21}}{B_{12}} = \frac{2h(\nu_{12}^0)^3}{c^2} \exp(-h\nu_{12}^0/kT_e) \tag{1.7}$$

since $A_{21}/B_{12} = g_1 \cdot 8\pi h(\nu_{12}^0)^3/g_2 \cdot c^3$. T_e is the required excitation temperature at the height r in the chromosphere. It should be noted that over the width of the chromospheric line the source function, j_ν/κ_ν, is independent of frequency.

Now re-write equation (1.3) in the form

$$I_z(\nu_{12}^0 + bv) = \int_0^{t_1'} \frac{j_\nu}{\kappa_\nu} \exp(-t)\, dt + \int_{t_1'}^{t_1} \frac{j_\nu}{\kappa_\nu} \exp(-t)\, dt, \tag{1.8}$$

where the first integral applies to a range of y given by $0 \leqslant y < \infty$ and the second to a range $-\infty < y \leqslant 0$, and where

$$t_1' = \int_0^\infty \kappa_\nu\, dy = \tfrac{1}{2} t_1, \tag{1.9}$$

since the chromosphere may be assumed to be spherically symmetrical. Now change the variable of integration from t to r. In both integrals of equation (1.8) we have from (1.2) and (1.4)

$$t = \frac{h\nu_{12}^0}{c} B_{12} \frac{1}{b\sqrt{\pi}} H(\alpha, v) \int_y^\infty n_1(r)\, dy, \tag{1.10}$$

where we have assumed that b, that is the kinetic temperature, is independent of radial height in the chromosphere. We have also assumed that α is independent of height, but since under chromospheric conditions $H(\alpha, v) \simeq \exp(-v^2)$ this latter assumption is not so serious. For simplicity we further assume that

$$n_1(r) = n_1(0) \exp(-\beta r), \tag{1.11}$$

where β, the reciprocal of the scale height, is determined by the kinetic temperature, the turbulent velocity, and the changing excitation and ionization. A more general density distribution is considered in Section 3.3. With the value for $n_1(r)$ given in (1.11) and from (1.1), equation (1.10) takes the form

$$t = \frac{h\nu_{12}^0}{c} n_1(0) \exp(-\beta z) \sqrt{\frac{2R}{\beta}} B_{12} \frac{1}{b\sqrt{\pi}} H(\alpha, v) \int_{v\sqrt{\frac{\beta}{2R}}}^\infty \exp(-\xi^2)\, d\xi.$$

---

* This derivation of the emission coefficient, as well as of the absorption coefficient, is based on transitions between broadened energy levels. It is assumed, and this is statistically correct for an assemblage of atoms, that the probability of an atom finding itself at a distance between s and $s + ds$ (measured in frequency units) from the centre of the level is given by $(\delta/\pi)\, ds/(s^2 + \delta^2)$ where δ is the half half-width of the broadened energy level (cf. L. Spitzer, *M.N.*, **96**, 794, 1936; H. H. Plaskett, *M.N.*, **115**, 256, 1955). Another way of looking at this problem has been suggested by Professor Zanstra to whom I am indebted for reading and commenting on this paper. He points out that the expression (1.4) for the absorption coefficient is always correct and that the expression (1.6) for the volume coefficient of emission can be derived on the assumption that the emission from level 2 takes place with complete redistribution in frequency with relative weight proportional to $H(\alpha, v)$.

For the range of values of y covered by the first integral of (1.8) we have $y = +\sqrt{2R(r-z)}$, and consequently for this integral

$$t = \frac{1}{2}\frac{h\nu_{12}^0}{c} n_1(0)\exp(-\beta z)\sqrt{\frac{2\pi R}{\beta}}\, B_{12}\frac{1}{b\sqrt{\pi}} H(\alpha, v)[1 - \operatorname{erf}\sqrt{\beta(r-z)}].$$

Following Pannekoek and Unsöld (**9**) we put

$$C(z) = \frac{h\nu_{12}^0}{c} n_1(0)\exp(-\beta z)\sqrt{\frac{2\pi R}{\beta}}\, B_{12}\frac{1}{b\sqrt{\pi}}, \tag{1.12}$$

where $C(z)$ is the total tangential optical depth at height z km above the limb for the centre of the line, that is when $v = 0$ and $H(\alpha, v) \simeq 1$. With this notation the variable t in the first integral of equation (1.8) is given by

$$t = \tfrac{1}{2}C(z)H(\alpha, v)[1 - \operatorname{erf}\sqrt{\beta(r-z)}], \tag{1.13}$$

and where consequently

$$\frac{dt}{dr} = -\tfrac{1}{2}C(z)H(\alpha, v)\frac{\beta}{\sqrt{\pi}}\{\beta(r-z)\}^{-1/2}\exp\{-\beta(r-z)\}.$$

Similarly for the second integral of (1.8) where $y = -\sqrt{2R(r-z)}$ we find

$$t = \tfrac{1}{2}C(z)H(\alpha, v)[1 + \operatorname{erf}\sqrt{\beta(r-z)}]. \tag{1.14}$$

Changing the variable of integration in both integrals of (1.8) from t to r, and noting that the limits of integration in the two integrals are respectively ∞ and z, and z and ∞, we find after a little algebra that

$$I_z(\nu_{12}^0 + bv) = C(z)H(\alpha, v)\exp\{-\tfrac{1}{2}C(z)H(\alpha, v)\}$$
$$\times \frac{\beta}{\sqrt{\pi}}\int_z^\infty \frac{j_\nu}{\kappa_\nu}\cosh\{\tfrac{1}{2}C(z)H(\alpha, v)\operatorname{erf}\sqrt{\beta(r-z)}\}\{\beta(r-z)\}^{-1/2}\exp\{-\beta(r-z)\}\,dr. \tag{1.15}$$

This is the integral equation required in order to find the source function, j_ν/κ_ν, as a function of r from the observed intensity of the chromospheric line. It takes an apparently simpler form if we change the variable of integration to

$$\zeta = \tfrac{1}{2}C(z)H(\alpha, v)\operatorname{erf}\sqrt{\beta(r-z)}, \tag{1.16}$$

when

$$I_z(\nu_{12}^0 + bv) = 2\exp\{-\tfrac{1}{2}C(z)H(\alpha, v)\}\int_0^{\frac{1}{2}C(z)H(\alpha, v)} \frac{j_\nu}{\kappa_\nu}\cosh\zeta\, d\zeta. \tag{1.17}$$

If, following Pannekoek and Unsöld (**9**), we assume j_ν/κ_ν independent of r, that is of ζ, the integral in (1.17) can be explicitly evaluated and we immediately reproduce their result.

$$I_z(\nu_{12}^0 + bv) = \frac{j_\nu}{\kappa_\nu}[1 - \exp\{-C(z)H(\alpha, v)\}].$$

2. *Numerical solution of the integral equation.*—Our integral equation (1.15) or (1.17), contains as unknowns the constants b, $n_1(0)$ and β, as well as j_ν/κ_ν as a function of r. A somewhat inelegant numerical solution can be found in the following way.

Divide the chromosphere up into four spherical shells

$$\begin{aligned} 0 \leqslant r \leqslant r_1 \quad \text{in which} \quad \frac{j_\nu}{\kappa_\nu} &= B_0 \\ r_1 \leqslant r \leqslant r_2 \qquad\qquad &= B_1 \\ r_2 \leqslant r \leqslant r_3 \qquad\qquad &= B_2 \\ r_3 \leqslant r < \infty \qquad\qquad &= B_2 + B_3\beta(r - r_3) \end{aligned}$$

where the B_i are unknown constants. Then our integral equation (1.15) takes the form

$$\left.\begin{aligned} I_z(\nu_{12}{}^0 + bv) = C(z)H(\alpha, v) \exp\{-\tfrac{1}{2}C(z)H(\alpha, v)\} \\ \times \frac{\beta}{\sqrt{\pi}}\left[\int_z^{r_1} B_0 \ldots + \int_{r_1}^{r_2} B_1 \ldots + \int_{r_2}^{r_3} B_2 \ldots \right. \\ \left. + \int_{r_3}^{\infty} \{B_2 + B_3\beta(r - r_3)\} \ldots \right]. \end{aligned}\right\} \qquad (2.1)$$

The first three integrals (with the finite limits) in this expression can be explicitly evaluated by changing to the variable ζ defined in equation (1.16).

The fourth integral needs more consideration. In full it is

$$\int_{r_3}^{\infty} \{B_2 + B_3\beta(r - r_3)\} \cosh\{\tfrac{1}{2}C(z)H(\alpha, v) \operatorname{erf}\sqrt{\beta(r - z)}\} \times \{\beta(r - z)\}^{-1/2} \exp\{-\beta(r - z)\}\, dr. \qquad (2.2)$$

Consider first the error function in the argument of the hyperbolic cosine. If we choose r_3, which is at our disposal, so that $\sqrt{\beta(r_3 - z_m)} = 2{\cdot}24$, where z_m is the maximum distance in km above the limb at which observations are made, then over the range of integration

$$0{\cdot}9985 \leqslant \operatorname{erf}\sqrt{\beta(r - z)} \leqslant 1{\cdot}0000$$

so that with an error of less than 0·2 per cent we can write

$$\cosh\{\tfrac{1}{2}C(z)H(\alpha, v) \operatorname{erf}\sqrt{\beta(r - z)}\} = \cosh\{\tfrac{1}{2}C(z)H(\alpha, v)\},$$

a constant. For example if $z_m = 7250$ km, corresponding to 10 seconds of arc above the limb, and if we take $\beta^{-1} \simeq 150$ km, a value of $r_3 = 8000$ km will satisfy these conditions. Finally changing the variable of integration from r to

$$\eta = \beta(r - z) \qquad (2.3)$$

our integral (2.2) takes the form

$$\frac{1}{\beta}\cosh\{\tfrac{1}{2}C(z)H(\alpha, v)\} \left[\{B_2 - B_3\beta(r_3 - z)\}\int_{\beta(r_3 - z)}^{\infty} \eta^{-1/2}\exp(-\eta)\, d\eta + B_3\int_{\beta(r_3 - z)}^{\infty} \eta^{1/2}\exp(-\eta)\, d\eta\right].$$

In terms of the incomplete Γ-function defined as

$$I^*(x, p) = \int_0^x \eta^p \exp(-\eta)\, d\eta \Big/ \int_0^\infty \eta^p \exp(-\eta)\, d\eta$$

and tabulated by Karl Pearson (**2**), this may be written

$$\frac{\sqrt{\pi}}{\beta}\cosh\{\tfrac{1}{2}C(z)H(\alpha, v)\} \times [\{B_2 - B_3\beta(r_3 - z)\}\{1 - I^*(\beta\overline{r_3 - z}, -\tfrac{1}{2})\} + \tfrac{1}{2}B_3\{1 - I^*(\beta\overline{r_3 - z}, +\tfrac{1}{2})\}].$$

Hence our integral equation (2.1) may be written as a linear equation in the unknowns, B_i, namely

$$I_z(\nu_{12}^0 + bv) = G_0B_0 + G_1B_1 + G_2B_2 + G_3B_3. \tag{2.4}$$

From the preceding discussion the dimensionless coefficients, G_i, are readily found to be

$$\left.\begin{aligned}
G_0 &= 2\exp\{-\tfrac{1}{2}C(z)H(\alpha,v)\}\sinh\{\tfrac{1}{2}C(z)H(\alpha,v)\operatorname{erf}\sqrt{\beta(r_1-z)}\}\\
G_1 &= 2\exp\{-\tfrac{1}{2}C(z)H(\alpha,v)\}[\sinh\{\tfrac{1}{2}C(z)H(\alpha,v)\operatorname{erf}\sqrt{\beta(r_2-z)}\}\\
&\quad -\sinh\{\tfrac{1}{2}C(z)H(\alpha,v)\operatorname{erf}\sqrt{\beta(r_1-z)}\}]\\
G_2 &= 2\exp\{-\tfrac{1}{2}C(z)H(\alpha,v)\}[\sinh\{\tfrac{1}{2}C(z)H(\alpha,v)\operatorname{erf}\sqrt{\beta(r_3-z)}\}\\
&\quad -\sinh\{\tfrac{1}{2}C(z)H(\alpha,v)\operatorname{erf}\sqrt{\beta(r_2-z)}\}]\\
&\quad +\tfrac{1}{2}C(z)H(\alpha,v)[1+\exp\{-C(z)H(\alpha,v)\}][1-I^*(\beta\overline{r_3-z},-\tfrac{1}{2})]\\
G_3 &= \tfrac{1}{2}C(z)H(\alpha,v)[1+\exp\{-C(z)H(\alpha,v)\}]\\
&\quad \times[\tfrac{1}{2}\{1-I^*(\beta\overline{r_3-z},+\tfrac{1}{2})\}-\beta(r_3-z)\{1-I^*(\beta\overline{r_3-z},-\tfrac{1}{2})\}].
\end{aligned}\right\} \tag{2.5}$$

If $H(\alpha,v)=\exp(-v^2)$, as is normally the case for chromospheric lines, then each of these coefficients, G_i, may be evaluated for any z and v, provided that β and the ratio $n_1(0)/b$ are given. In effect, therefore, the equation (2.4), linear in the unknowns, B_i, also contains in the coefficients, G_i, the unknowns β and $n_1(0)/b$.

The solution of (2.4) to find these various unknowns depends essentially on the fact that over the width of the emission line the source function is independent of frequency, and so consequently are its specific values, B_i. Consider for example the observed profile at two heights such that $r_2 < z \leqslant z_m$. As a result of this height restriction equation (2.4) reduces to

$$I_z(\nu_{12}^0 + bv) = G_2B_2 + G_3B_3.$$

At $v=0$ solve the resulting pair of simultaneous equations at these two heights for B_2 and B_3 for each of a number of pairs of arbitrary values of β and $n_1(0)/b$. From these solutions construct double-entry tables B_2-Table O and B_3-Table O giving respectively B_2 and B_3 each as a function of the arguments β and $n_1(0)/b$. Now for the same two heights and a frequency $\Delta\nu_1=(bv)_1$ similarly solve the pair of simultaneous equations and construct a number of double-entry tables B_2-Table I(b) and B_3-Table I(b) for the same arguments β and $n_1(0)/b$, but for a number of assumed values of b. Note that for constant $\Delta\nu_1$ any assumed value of b corresponds to a new value of v. Repeat this procedure for a third frequency $\Delta\nu_2$, obtaining tables B_2-Table II(b) and B_3-Table II(b) for the same values of the three arguments. For each value of b compare, say, B_2-Table I(b) and B_2-Table II(b), and choose that pair of arguments β and $n_1(0)/b$ which give identical values of B_2 in the two tables. Designate the resulting values of B_2 by $B_2\{b,\beta,n_1(0)/b\}$. Finally go back to B_2-Table O giving values of B_2 for the arguments β and $n_1(0)/b$, and choose that pair of arguments which gives a value of B_2 in this table identical with one of the $B_2\{b,\beta,n_1(0)/b\}$. We thus have found the values of b, β and $n_1(0)/b$ which give the required identical values of B_2 for the three different frequencies $\Delta\nu=0$, $\Delta\nu_1$, $\Delta\nu_2$.

The same three values of b, β and $n_1(0)/b$ should also give identical values of B_3 in the tables B_3-Table O, B_3-Table I(b) and B_3-Table II(b). Any marked failure to do so would be attributable either to inadequacy of the assumed density distribution (1.11), or to departure from the assumed constancy of kinetic

temperature, or finally to the crude representation of the chromosphere by spherical shells. Assuming that no such failure occurs we now have B_2, B_3, b, β, and $n_1(0)/b$. To find the remaining unknowns B_0 and B_1 select two observed profiles $I_z(\nu_{12}{}^0+bv)$ in the height range $0 \leq z < r_1$, and immediatelv solve the resulting two simultaneous equations for these unknowns.

3. *Applications and another form of integral equation*

3.1. *Optically thin chromosphere.*—If $C(z)$, the total tangential optical depth of the chromosphere at the centre of the line, is so small that its square and higher powers may be neglected, our integral equation (1.17) takes the form

$$I_z(\nu_{12}{}^0+bv) = 2[1-\tfrac{1}{2}C(z)H(\alpha,v)]\int_0^{\frac{1}{2}C(z)H(\alpha,v)} \frac{j_\nu}{\kappa_\nu}\,d\zeta$$

$$= C(z)H(\alpha,v)[1-\tfrac{1}{2}C(z)H(\alpha,v)]\frac{1}{\sqrt{\pi}}\int_0^\infty \frac{j_\nu}{\kappa_\nu}\eta^{-1/2}\exp(-\eta)\,d\eta. \qquad (3.1)$$

The second step follows as a consequence of changing the variable of integration, ζ, defined in (1.16), to η defined in (2.3). If now we represent the source function by a polynomial in r, namely

$$\frac{j_\nu}{\kappa_\nu} = g_0 + g_1 r + g_2 r^2, \qquad (3.2)$$

we find

$$I_z(\nu_{12}{}^0+bv) = C(z)H(\alpha,v)[1-\tfrac{1}{2}C(z)H(\alpha,v)]$$
$$\times\left[\left(g_0+\frac{g_1}{2\beta}+\frac{3g_2}{4\beta^2}\right)+\left(g_1+\frac{g_2}{\beta}\right)z+g_2z^2\right]. \qquad (3.3)$$

Since the g_i are independent of v, a procedure similar to that outlined in the previous section will give the values of the six unknowns. It is possible that equation (3.3) may be applicable to chromospheric helium which shows little evidence of self-reversal.

3.2. *Interpretation of spectroheliograms.*—Once the integral equation (1.15) has been solved for the unknowns b, $n_1(0)$ and β, and for j_ν/κ_ν as a function of r, we can readily predict the profile of a line at the centre of the disk. The radial optical depth, τ, in the chromosphere at the frequency $\nu_{12}{}^0+bv$ will be given by

$$\tau = -\int_\infty^r \kappa_\nu\,dr = \frac{h\nu_{12}{}^0}{c}B_{12}\frac{1}{b\sqrt{\pi}}H(\alpha,v)\int_r^\infty n_1(r)\,dr$$

$$= \frac{h\nu_{12}{}^0}{c}B_{12}\frac{1}{b\sqrt{\pi}}H(\alpha,v)\frac{n_1(0)}{\beta}\exp(-\beta r), \qquad (3.4)$$

the last step following from equation (1.11). The total tangential optical depth at the same frequency and at height $z=0$ above the limb will from (1.12) be given by

$$C(0)H(\alpha,v) = \frac{h\nu_{12}{}^0}{c}B_{12}\frac{1}{b\sqrt{\pi}}H(\alpha,v)n_1(0)\sqrt{\frac{2\pi R}{\beta}},$$

or from (3.4) the radial optical depth will be

$$\tau = \frac{C(0)H(\alpha,v)}{\sqrt{2\pi R\beta}}\exp(-\beta r). \qquad (3.5)$$

Knowing b, $n_1(0)$ and β this equation immediately gives us the radial optical depth for any r. When $r=0$ it gives τ_1, the total radial optical depth of the chromosphere.

With this definition the equation of radiative transfer in the direction of τ is,

$$\frac{dI_\nu}{d\tau} = I_\nu - \frac{j_\nu}{\kappa_\nu}.$$

Hence the observed intensity of a line at the centre of the disk is

$$I_\nu(\text{obs}) = I_\nu(\text{phot}) \exp(-\tau_1) + \int_0^{\tau_1} \frac{j_\nu}{\kappa_\nu} \exp(-\tau)\, d\tau. \tag{3.6}$$

Knowing I_ν(obs) and j_ν/κ_ν as a function of r for the undisturbed chromosphere, we can immediately find I_ν(phot), that is the profile of the photospheric absorption line as it would appear in the absence of a chromosphere. Spectroheliograms give evidence of disturbed chromospheric conditions, and having found I_ν(phot) we can use equation (3.6) to make an intelligent guess as to the origin and nature of these disturbances.

3.3. *Integral equation for another density law.*—Our integral equation has been derived on the assumption that the density in the chromosphere can be represented by

$$n_1(r) = n_1(0) \exp(-\beta r).$$

If this should prove inadequate, consider a law of the form

$$n_1(r) = c_0 \exp(-\beta_0 r) + c_1 \exp(-\beta_1 r). \tag{3.7}$$

Proceeding as in Section 1 and defining

$$C_0(z) = \frac{h\nu_{12}{}^0}{c} c_0 \exp(-\beta_0 z) \sqrt{\frac{2\pi R}{\beta_0}}\, B_{12} \frac{1}{b\sqrt{\pi}},$$

$$C_1(z) = \frac{h\nu_{12}{}^0}{c} c_1 \exp(-\beta_1 z) \sqrt{\frac{2\pi R}{\beta_1}}\, B_{12} \frac{1}{b\sqrt{\pi}},$$

where $C_0(z) + C_1(z)$ is the total tangential optical depth in the centre of the line at height z above the limb, we readily find that

$$I_z(\nu_{12}{}^0 + b\nu) = 2 \exp[-\tfrac{1}{2}\{C_0(z) + C_1(z)\}H(\alpha, v)] \int_0^{\frac{1}{2}\{C_0(z)+C_1(z)\}H(\alpha,v)} \frac{j_\nu}{\kappa_\nu} \cosh\zeta\, d\zeta\,. \tag{3.8}$$

As in Section 2 this may be written as a linear equation in the unknowns, B_i, and once again the coefficients, though more complex than those in (2.5), may be written down and evaluated. The solution of these new linear equations is likewise possible, though clearly it will present more difficulty than the simple case treated in Section 2.

To those colleagues who have patiently listened to lectures on this topic, and especially to Dr P. J. Treanor whose pertinent questions have greatly clarified its exposition, I wish to express my thanks.

University Observatory,
Oxford:
1956 *April* 20.

References

(1) P. C. Keenan, *Ap. J.*, **75,** 277, 1932.
(2) K. Pearson, *Tables of Incomplete Γ-Function*, London (H.M.S.O.), 1922.
(3) W. A. Rense, *Phys. Rev.*, **91,** 299, 1953.
(4) S. Rosseland, *Ap. J.*, **67,** 218, 1926.
(5) R. Tousey, *The Sun* (ed. G. P. Kuiper), p. 665, Chicago, 1953.
(6) P. J. Treanor, *Nature*, **176,** 1166, 1955.
(7) A. Unsöld, *Zs. f. Phys.*, **59,** 372, 1929; *Ap. J.*, **69,** 209, 1929.
(8) A. Unsöld, *Physik der Sternatmosphären* (2nd edn.), p. 262, Berlin, 1955.
(9) A. Unsöld, *Ibid.*, p. 627.

DETAILED STUDY OF THE DEVELOPMENT OF AN ACTIVE SOLAR REGION, 1954 AUGUST 20–27

Helen W. Dodson and E. Ruth Hedeman

(Communicated by R. R. McMath)

(Received 1956 April 5)

Summary

The week of 1954 August 20–27 provided an opportunity to study the development of an active solar region under circumstances of unusual simplicity. The calcium plage formed near the central meridian of the solar disk between 15^h00^m and 15^h10^m U.T. on August 20. In the week following its formation, the calcium plage grew to at least 3500 millionths of the solar hemisphere and became 2·4 times as bright as the dark portions of the mottled background of the K_{2s2} spectroheliograms.

Isophotometric studies of the calcium plage provide quantitative data for comparison with sunspot, magnetic, geomagnetic, radio flux, and coronal data made available by astronomers in all parts of the world. At least five flares or subflares were observed in the region before it traversed the west limb.

The study presents a comprehensive and partially quantitative account of of the formation, growth and decline of an isolated centre of solar activity. The problems encountered are illustrative of those that will be met on a grander scale in the solar studies of the International Geophysical Year.

It is possible to study the development of active solar regions under circumstances of unusual simplicity during the time when the Sun is just emerging from minimum in the 11-year solar cycle. The late summer of 1954, and especially the week of August 20–27 provided exactly this opportunity.

Between 15^h00^m and 15^h10^m on August 20 a small calcium plage formed very close to the central meridian, at about 30° south latitude. By 18^h00^m U.T. a spot was visible within the plage. There were no other disturbed regions on the entire visible solar hemisphere, and this fortunate circumstance continued through August 25 (Plate 3). In the week following its formation, the active centre was rotated from central meridian to solar limb. During this period it grew rapidly in size and intensity. It was the site of at least five flares and of enhanced radiation at radio frequencies. During its passage across the west limb, distinct maxima in both the red and green coronal lines were observed. The region was centred at $L = 175°$, $B = -30°$.

Study of this region is based on photometric measures of calcium spectroheliograms taken at the McMath–Hulbert Observatory and on data relating to the region, most kindly provided by the directors or members of the staff of the following observatories and establishments in many parts of the world:

Special Data

Cavendish Laboratory, Cambridge, England
Cornell University, U.S.A.
Hale Laboratory, U.S.A.
Mount Wilson Observatory, U.S.A.
Nagoya University, Japan

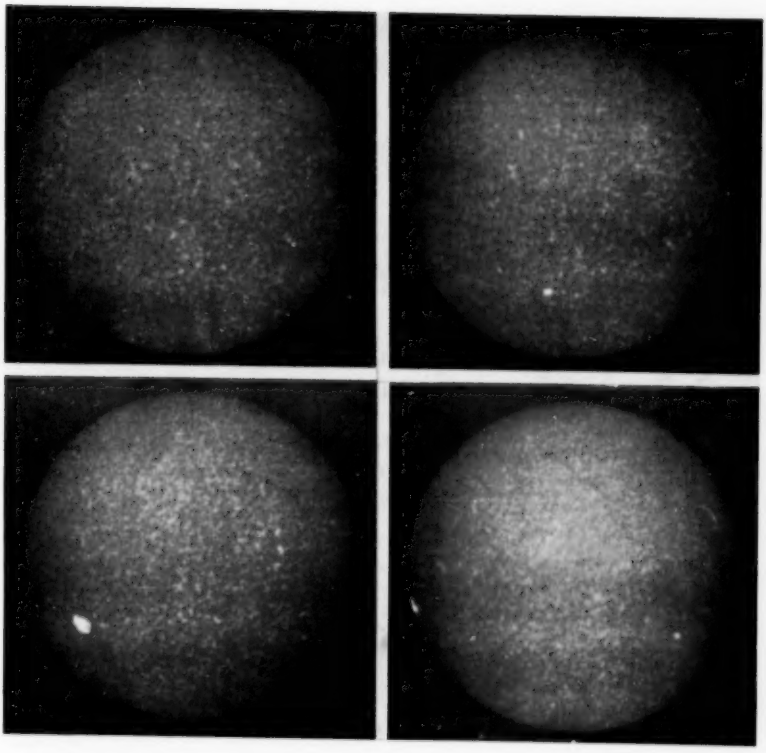

PLATE 1.—*Calcium spectroheliograms showing formation and development of plage. 1954 Aug. 20–27.*

(*a*) *Aug.* $20^d15^h00^m$ *U.T.* (*b*) *Aug.* $20^d20^h00^m$ *U.T.*
(*c*) *Aug.* $23^d16^h53^m$ *U.T.* (*d*) *Aug.* $26^d16^h50^m$ *U.T.*

Spectroheliograms are oriented with north at top and east at right. Note small additional plage in southeast on Aug. 26. This small region was detected by the high resolution instruments recording at 7, 10, and 60 cm.

National Research Council of Canada
Nederhorst Den Berg (NERA), Netherlands
Observatoire du Pic-du-Midi, France
Radiophysics Laboratory, Sydney, Australia
Royal Greenwich Observatory, Herstmonceux, England
Tokyo Observatory, Japan

Published Data

High Altitude Observatory, Climax, U.S.A.
Journal of Geophysical Research
Quarterly Bulletin of Solar Activity
U.S. Naval Observatory

Calcium plage.—The photometric study of the calcium plage consists of a series of isophotes made for ten-minute intervals during the early development of the region, then at half-hourly, hourly, and longer intervals as the region changed more slowly (Table I and Fig. 1). Intensities are expressed in units of the dark portions of the mottled background of the K_{232} spectroheliograms. Maximum intensity attained by the plage was 2·4 or an increase of about one magnitude. The maximum area of the plage as outlined by the 1·2 isophote was of the order of 3500 millionths of the solar hemisphere.

TABLE I

Development of calcium plage, 1954 August 20–27

Date	Time (U.T.)	Maximum Intensity	Total Area*		Σ Product of Excess Intensity and Area, for Isophotes	
			Disk	Hemisphere	$\Sigma I \times A_D$	$\Sigma I \times A_H$
Aug. 20	1500	1·0	0	0	0	0
	1510	1·2	34	21	7	4
	1520	1·3	95	59	20	12
	1530	1·3	112	69	24	15
	1540	1·3	157	97	36	22
	1550	1·4	202	125	48	30
	1600	1·4	258	159	62	38
	1632	1·5	325	201	88	55
	1700	1·5	280	173	80	49
	1800	1·6	426	264	126	78
	1900	1·8	672	417	234	145
	2000	1·9	706	438	241	149
	2104	1·9	806	500	289	178
	2157	2·0	974	606	361	224
21	1340	1·8	1534	961	557	348
	1700	1·7	1535	970	522	330
	2100	1·9	1725	1100	622	397
22	1500	2·2	2106	1408	933	623
	2152	2·4	2430	1682	1234	854
23	1727	2·4	3058	2333	1815	1370
24	1558	2·3	2666	2458	1415	1300
	1934	2·3	2878	2943	1554	1590
25	1524	2·3	2811	3655	1430	1865
26	1650	(1·9)	(1344)	(2953)	(506)	(1110)
27	Plage still visible, but too close to limb for photometric measurements.					

* Area is that outlined by 1.2 isophote. It is reported in millionths of solar disk and hemisphere respectively.

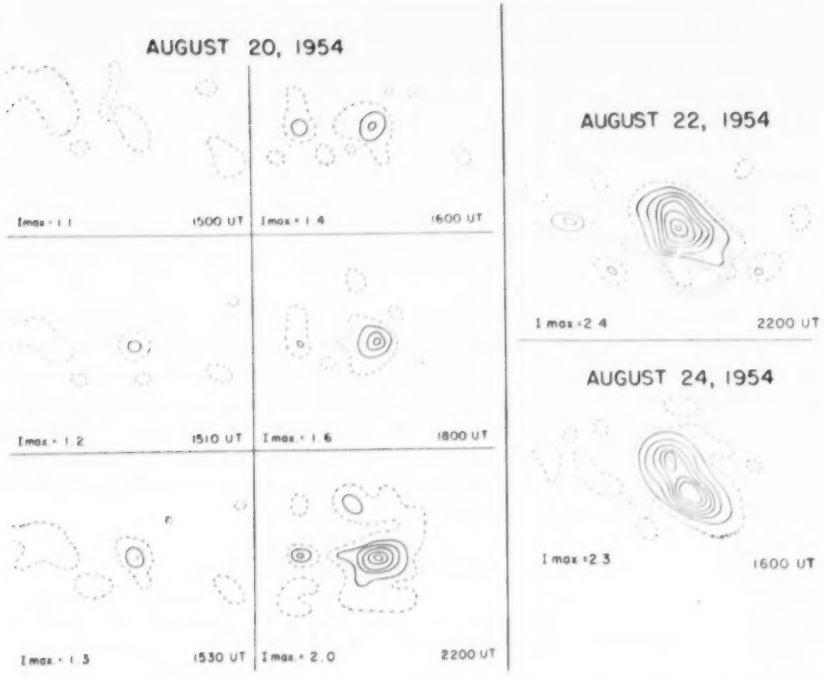

FIG. 1.—*Isophotes of calcium plage, 1954 August 20, 22, 24. In general, dotted lines indicate 1.1 isophotes. Full lines give 1.2 isophotes and those that differ by increments of 0.2. Maxima differing by 0.1 from the last-drawn isophote are shown by dotted lines.*

Radiation from the calcium plage can be expressed by the summation of the products of excess intensity and area. This product shows a steady increase through August 25 if areas have been corrected for projection effects and are in units of the hemisphere, or a levelling off after August 23 if the areas are expressed in units of the disk (Table I and Fig. 2). The plage was still visible on August 26 and 27 but too close to the limb for accurate photometric measurements.

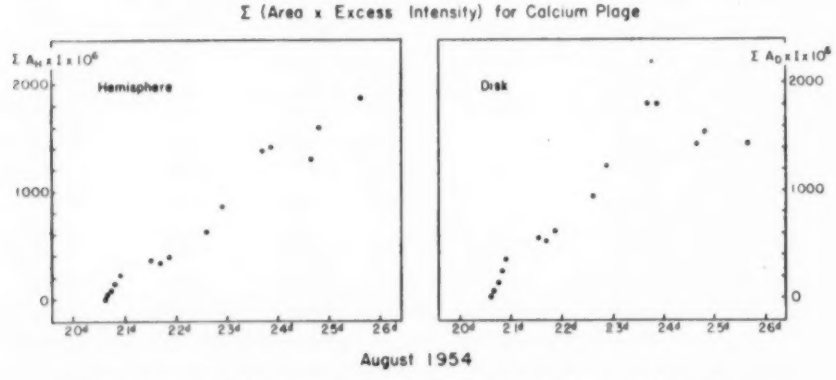

FIG. 2.—*Product of calcium plage area and excess intensity as shown by the isophotes.*

The plage underwent two distinct periods of growth. The initial development, lasting from August 20 to 21, was followed by a four-day period, August 22 to 25, during which the maximum intensity was relatively constant and distinctly greater than on the two preceding days. The plage declined in both area and intensity after August 25. For both periods of growth, the maximum intensity was attained relatively quickly, and the subsequent change in the plage was primarily an increase in area. The development of the plage is shown clearly in the plot in Fig. 3, where for each day intensity is shown as a function of the distance across the plage. For this diagram,the isophotes of irregular shape were replaced by circles equal to them in area. In general, the intensity profile of the mature plage was bell-shaped with a broad maximum.

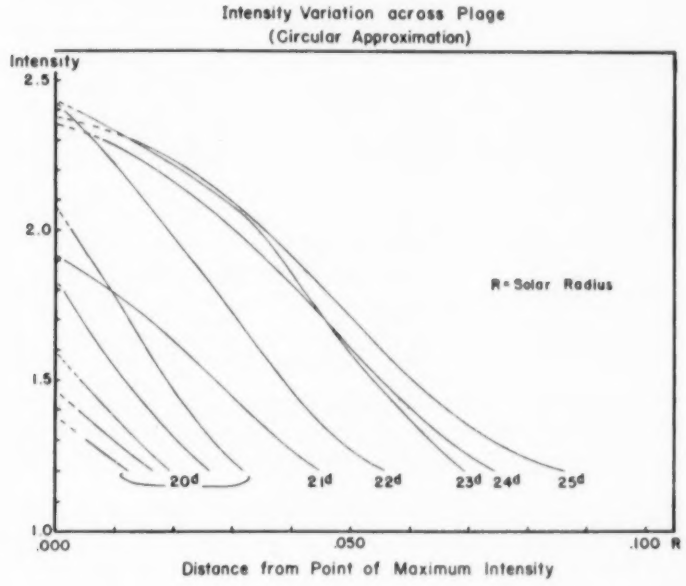

FIG. 3.—*"Intensity profile" for calcium plage—circular approximation. In these measures, corrections have been made for projection effects.*

The same type of general development is apparent in the intensity profiles for E–W and N–S cuts across the actually measured isophotes. In addition, the detailed profiles show that there was continuous growth of the plage in the E–W direction, but that a spread in the N–S direction took place only when the maximum intensity was increasing (Fig. 4).

Sunspots.—On August 20 at about $18^h\,00^m$ U.T., at the McMath–Hulbert Observatory, a small sunspot was observed to have formed within the new plage. A telephone call was made to the Mount Wilson Observatory for confirmation and cooperation in observing the newly formed plage and spot. Dr Seth B. Nicholson was good enough to make special records of the spot and of the hydrogen and calcium plages on August 20 and to put this material at our disposal.

The Mount Wilson photograph for $13^h\,50^m$ U.T. and our detailed visual examinations of the solar disk at $13^h\,20^m$ and $14^h\,50^m$ U.T. all indicate that the

spot was not present at these times. A single spot was observed by us at Lake Angelus at $18^h 00^m$ U.T. A Mount Wilson photograph taken at $21^h 28^m$ U.T. shows that a second member had developed. At that time Dr Nicholson measured the magnetic field and found the spots to be of new-cycle polarity, with leader V5 and follower R3. The position was S30° E01°. By $21^d 02^h 02^m$ the bipolar group was well formed and the combined area of the two components, as measured at Mount Wilson, was 20 millionths of the solar hemisphere.

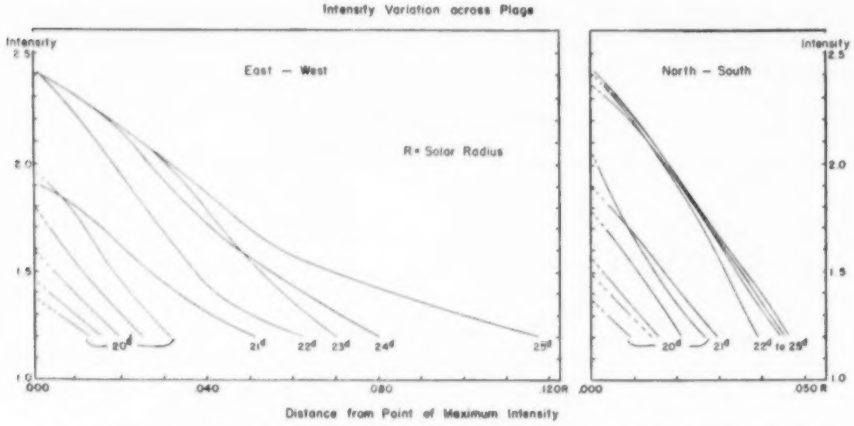

FIG. 4.—*"Intensity profile" for calcium plage—east–west and north–south directions. In these measures, corrections have been made for projection effects.*

The initial outbreak of the plage and the formation of the first spot took place in the heliographic longitude corresponding to the leading portion of the mature plage. In general, the spots were located near the east–west extremities of the plage.

Areas of the spot group from August 20 to 27 as measured at the Royal Greenwich Observatory, at the U.S. Naval Observatory (both Naval Observatory and Mount Wilson plates are used), and at Lake Angelus are given in Table II. The differences in the reported areas for this relatively simple spot group illustrate the difficulties inherent in making such measurements and the problems encountered in trying to put together data from different observatories. Although there is some ambiguity, maximum area probably took place on August 23. If one interprets the observations literally, the spot group disappeared on August 26 between $13^h 56^m$ and $14^h 50^m$ U.T.

Magnetic field.—The spot group was classified at Mount Wilson as β 20 with new cycle polarity. Detailed magnetic measures, made by Drs Nicholson and Babcock at Mount Wilson and the Hale Laboratories respectively, are summarized in Table III.

It is of interest to note that the two periods of growth shown by the plage are reflected also in measurements of spot area and magnetic field. In the first period the leading spot was the larger and had the greater magnetic field. In the second period the reverse was true. Although a number of the plage isophotes show two distinct maxima, they do not reflect clearly the systematic changes and differences suggested by spot areas and magnetic fields.

TABLE II

Area of spots ($L = 175°$, $B = -30°$) in millionths of hemisphere

Date (U.T.) Aug.	Greenwich ($0^d.3\pm$)	U.S. Naval Obs. ($0^d.6\pm$)			Mount Wilson[a] ($0^d.6\pm$)			McM–H Obs.[b] ($0^d.6\pm$)	Average
		Leader	*Follower*	*Total*	*Leader*	*Follower*	*Total*		
20	0	0	0	0		(0–20)		(0–10)	0–20
21	23	...	...	...	24	12	36	30	30
22	98	146	170	316	68	93	161	100	169
23	187	100	140	240	145	121	266	250	236
24	162	61	134	195	108	76	184	200	185
25	73	18	28	46	40	40	80	75	69
26[c][d]	16	0	22	22	0	48	48	0	22
27[c]	0	...	...	...	0	0	0	0	0

(*a*) Measurements made at U.S. Naval Observatory.

(*b*) Measurements of daily large scale drawings.

(*c*) Spots are present in another part of solar disk on these days.

(*d*) The Service of Solar Physics and Radio Astronomy of the Royal Observatory of Belgium reports that on August 26 a single spot in this region was visible at $09^h\ 35^m$ U.T. but had disappeared by $15^h\ 45^m$ U.T. The spot was photographed at Mount Wilson Observatory at $13^h\ 56^m$ U.T. It was not visible at the McMath-Hulbert Observatory at $14^h\ 50^m$ U.T.

TABLE III

Summary of magnetic observations of active centre 1954 August 18–25

Date	Mount Wilson Observatory		Hale Laboratory
	Leading Spot	Following Spot	
Aug. $20^d.89$	−500 gauss	+300 gauss	BM region with " new polarity ".
$21^d.62$	−1500	+500	...
22	−1000	+2000	...
	(" Following spot grows and develops field stronger than that of leader.")		
$23^d.72$	−400	+2100	...
	−2000	+1800	...
24	−700	+1000	*Positive field* recorded as region approaches west limb; record is imperfect.
	−1000	+1000	
25	−500	+800	Positive field recorded; negative field does not show. Why?

Coronal emission.—There was no indication of unusual coronal radiation in the position of this active region when it traversed the east limb about August 13, a week before the appearance of the plage near the central meridian. At west limb passage, the excess radiation associated with the region was detected from August 25–30. All coronal stations with observations during these days agree in the existence of maxima in both the red and green coronal emission lines for the general region of the Sun in which this active area was located.

Coronal isophotes have been prepared especially for this study by Drs J. Rösch and M. Trellis from the calibrated data at the Pic-du-Midi. The maximum green line intensity was 54 in units of 10^{-6} times the intensity at the same wave-length for one angstrom of the photospheric spectrum. The red line maximum was 22 in similar units. According to Dr Rösch, the ratio of the intensity of the green coronal emission to that of the red is much smaller during periods of low solar activity than near maximum in the solar cycle, and the ratio 54/22 should be considered as normal. The Pic-du-Midi isophotes shown in Fig. 5 are projected

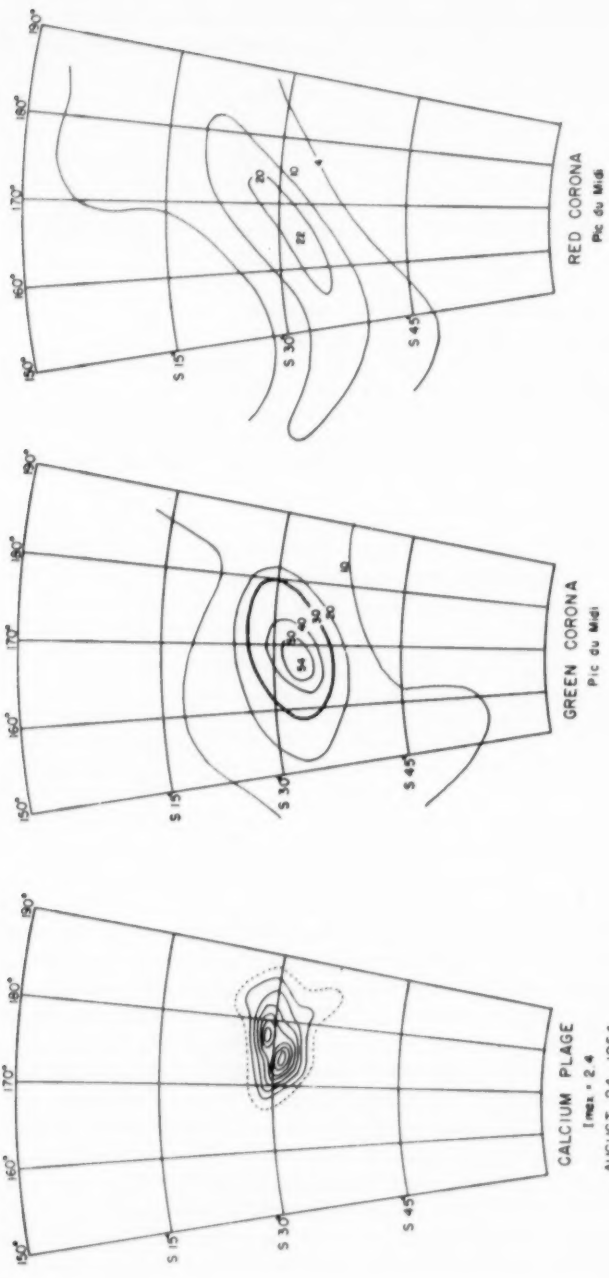

FIG. 5.—*Comparison of coronal and calcium plage isophotes. Heavy line marks isophote "30", considered to circumscribe the region of excess green coronal emission.*

on a cone tangent to the Sun at latitude S 30°. The isophote for the calcium plage for August 24 is shown in a similar projection. Although there is marked similarity between the plage and the region of green coronal emission, the latter is larger and is centred about 7° to the east, and about 2° to the south of the plage. These differences in position may reflect the relatively greater importance of the following member of the spot group as the active region approached the west limb. The size of coronal isophotes of this type is necessarily influenced by the height as well as by the lateral extent of the emitting region. According to Dr Rösch, isophote "30" probably circumscribes the region of excess green coronal emission that should be associated with the active area, since the "background" intensity of the green line during the minimum years falls between 15 and 25×10^{-6}. With this criterion, the calcium plage and green coronal region are strikingly similar in size and shape. They both have an east–west extent of about 2·7′.

According to isophotes prepared at the High Altitude Observatory, Boulder, Colorado, and published in Report No. HAO-25, the green coronal emission over the region was "moderately bright" and the red emission "very bright." These statements should be interpreted as referring to the intensity range for the separate lines and not to an absolute scale. The heliographic longitude of the HAO coronal isophote for the region is similar to that of the calcium plage but the latitude is 5° less.

Flares.—The first flare observed in the region took place on August 22, only 48 hours after the initial formation of the calcium plage. There is evidence for the occurrence of at least five flares and subflares before the region traversed the west limb. Of the four flares that we observed, that of August 23 at $13^h\,25^m$ was the greatest. Information relating to the flares is summarized in Table IV.

TABLE IV

Flares observed in active centre, 1954 August 20–27

Date	U.T.	Imp.	Position		Observers	Remarks
Aug. 22	1525–1650	1	S30	W17	Capri, Meudon, McMath	Accompanied by high velocity dark flocculus
	2125–2140	1–	S30	W20	McMath	
23	1325–1420	1	S30	W31	McMath	Accompanied by high velocity dark flocculus
26	0443–0500	1	S30	W65	Kodaikanal	
27	1724–1736	1–	S30	W90	McMath	On calcium spectroheliogram.

Prominences.—The Solar Report No. HAO-25 states for the region here studied that "the most definite active-region-prominences of the period (July 10–September 30, 1954) were seen at the east limb passage preceding the appearance of the spot group." Small filaments were visible on the disk near the region. The report of prominences at the east limb is the earliest indication of activity in the area in which the plage and spot later developed.

Radio-Frequency emission: (a) decimetre wave-lengths.—At Nagoya, Ottawa, and Sydney the high resolution instruments recording at approximately 7, 10, and 60 cm showed a region of excess flux traversing the solar disk from close to the central meridian on August 20–21 to August 26, 27, and 25 for the respective frequencies. The maximum excess flux at these wave-lengths was

about 6 per cent of the flux from the quiet Sun. There is some indication from the Sydney record that excess 60 cm radiation was being emitted from the location of the active area one to three days before the spot and plage became visible.

The three records at decimetre wave-lengths essentially agree with each other as to the location of the source of the enhanced radio radiation. Furthermore, these positions correspond to the successive daily positions of the spot and plage within the accuracy of the data.

Mr Covington, at Ottawa, reports that the drift curves taken between 1954 August 22 and 25 indicate that the 10 cm emissive region "was very unlikely to have been as wide as 3 minutes of arc and can be regarded as a point source. The antenna half power width was 8 minutes of arc". For the spot group, the maximum east–west extent was about 1·5′. The calcium plage was larger. The greatest east–west chord of the 1·1 isophote of the plage corresponded to about 2·7′. For the more certain 1·2 isophote, the maximum east–west extent was 2·3′. The great similarity between the extent of the calcium plage and the region of excess green coronal emission has already been pointed out.

Although the active region here studied is not well suited for clarification of the detailed relationships between plage area, spot area, and excess decimetre radiation, it does provide further evidence that the 2800 Mc/s radiation follows very closely the development of the calcium plage (**1**) (Fig. 6). When the plage areas are measured in units of the disk, the agreement between plage area and 2800 Mc/s flux is better than when the areas are measured in units of the hemisphere and corrected for projection. The use of both area and intensity ($\Sigma A_{\text{Disk}} \times I_{\text{Excess}}$) as a measure of the calcium plages gives only slightly better agreement, in this case, than does the use of area alone. Sunspot areas diminished more rapidly after August 23 than did either the excess 2800 Mc/s radiation or the plage area. The high resolution 2800 Mc/s records indicate that excess emission from the region under consideration was observed up to and including August 27. On the 27th the calcium plage was still visible though greatly reduced in size and intensity. The sunspots, however, had disappeared or ceased to be visible before $14^{h}\,50^{m}$ on August 26.

It is of interest to report that, in addition to the region studied, the high resolution instruments at Nagoya, Ottawa, and Sydney also recorded the presence of another newly formed, very small, plage and spot, visible on August 26 and 27 in the eastern part of the solar disk (Plate 3). Radiation from the small second region was detected and reported by the three radio-frequency observers even though the excess flux associated with it was only one to two per cent of the quiet Sun radiation at the respective frequencies.

(*b*) *Metre wave-lengths.*—At metre wave-lengths the excess radiation was associated more with flare activity than with the general development of spot and plage. For the time interval under consideration, there was no significant increase in flux until after flares had started to occur in the region. A 200 Mc/s noise storm with increase in flux and many superposed bursts began on August 23. The flux increased slowly from $12^{h}\,15^{m}$ U.T to the outbreak of a flare at $13^{h}\,25^{m}$ U.T., after which the flux increased rapidly for several hours and then slowly declined. The noise storm was still in progress throughout August 24. On these two dates the active centre was between 50° and 65° from the centre of the solar disk (Plate 3 and Fig. 7). The 81 Mc/s records did not show a noise storm during this period.

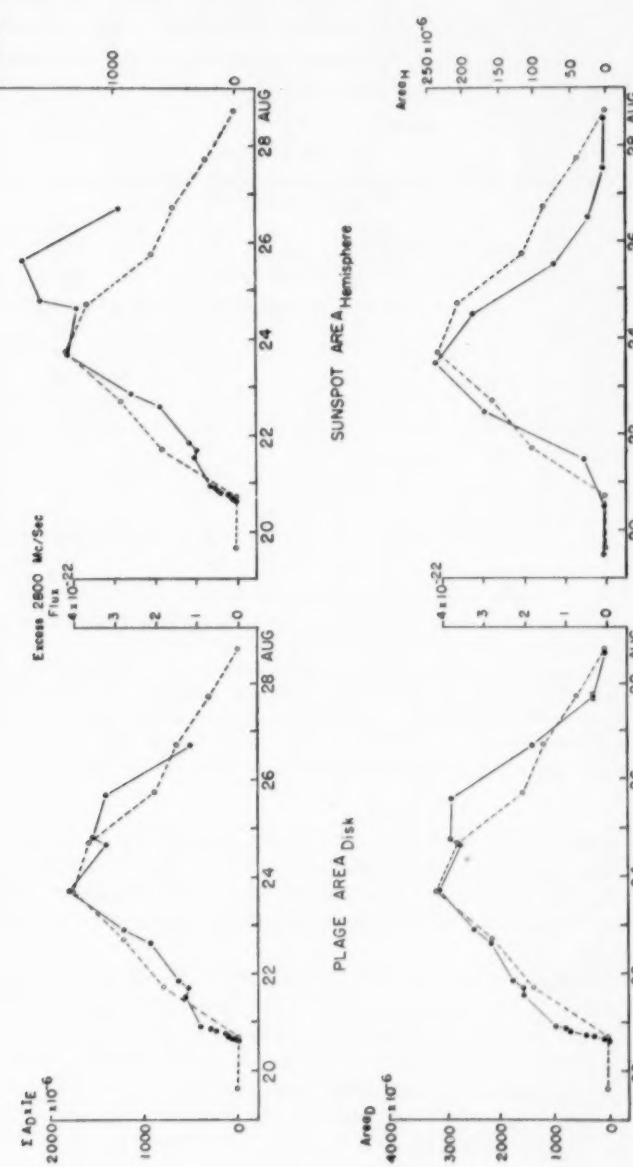

FIG. 6.—*Comparison of excess 2800 Mc/s flux with plage and sunspot data, 1954 Aug. 20–28. Dotted curve gives 2800 Mc/s data. Full line shows plage and sunspot data. Scales have been chosen to provide equal ordinates for August 23.*

The foregoing variations in the excess flux at radio frequencies are summarized in Table V and presented graphically in Fig. 7. The 6 per cent increase in flux at 3750 and 2800 Mc/s associated with the August 20–27 active centre is clearly evident in the plot of the average daily values, but on the same scale, the comparable increase recorded at 500 Mc/s is scarcely detectable. The ten-fold greater increase at 200 Mc/s illustrates the greater sensitivity of this frequency to solar activity than is the case for its neighbouring frequencies.

TABLE V

Summary of daily values of flux at radio frequencies, 1954 August 18–28 Quarterly Bulletin of Solar Activity

Mc/sec		81	200					460	500	545	2800	3750
Observatory		Cav.	Syd	Tok	Ned	Cor	Sun	NBS	Syd	Ned	Ott	Nag
Average U.T.		$12^h{\cdot}5$	02^h	03^h	$12^h{\cdot}5$	$16^h{\cdot}5$	$19^h{\cdot}5$	$18^h{\cdot}5$	02^h	$12^h{\cdot}5$	18^h	04^h
Date		*Average Daily Flux in Units of 10^{-22} Watts Meter^{-2} $(C/S)^{-1}$*							(*a*)		(*b*)	
Aug.	18	1·1	16	8	8	...	9	21	16+·16	26	69(0)	81
	19	1·0	13	...	8	11	...	20	·08	25	67(0)	80
	20	1·2	19	8	7	10	...	21	·27	24	69(0)	79
	21	1·1	16	8	7	10	...	20	...	24	—(1·8)	81
	22	...	14	8	...	11	8	20	...	...	70(2·8)	81
	23	1·2	15	8	14	24	22	21	1·23	25	72(4·1)	84
	24	1·0	16	11	10	16	11	20	·17	25	72(3·6)	84
	25	0·9	20	8	9	10	7	19	·04	25	72(2·0)	82
	26(*c*)	...	18	8	8	10	8	20	...	25	72(1·5)	80
	27(*c*)	...	18	7	8	10	8	20	...	25	70(0·7)	81
	28(*c*)	...	19	7	8	10	8	20	...	25	—(0)	80

(*a*) Data from special observations of excess flux made by Swarup and Parthasarathy with Christiansen's interferometer operating at 60 cm. Quiet Sun is 16×10^{-22}.

(*b*) Values in parentheses give flux assigned by Covington specifically to region here studied, on basis of data from 150-ft. array. Reference quiet days were August 28 and 29. Peak value of 4·1 units is difference in total flux on August 23 and 29 as measured by 4-ft reflector. Only one region of excess 10-cm emission on disk on August 23.

(*c*) Additional active regions are present on the solar disk on these dates.

(*c*) *Distinctive events.*—During the period August 20–27 there were four burst-type events and one noise storm onset. The two principal bursts occurred at both metre and decimetre wave-lengths and were associated in time with known flares. Data relating to these outstanding occurrences are summarized in Table VI.

At metre wave-lengths, the relationship between flares and certain well defined increases in flux is often masked by the use of average daily flux values rather than those made at closer time intervals. For this study an attempt was made to provide as complete a coverage at 200 Mc/s as possible. Table V shows that there is a considerable scale difference between the several observatories reporting at this frequency. In order to use consecutively the hourly values provided by Cornell University, Nederhorst den Berg Radio (NERA), and Tokyo Observatory, the values from the latter two stations were multiplied by a scale factor of 1·4. The hourly values in Fig. 7 show clearly the distinct rise in flux on August 23 that followed the largest and brightest flare observed in the region.

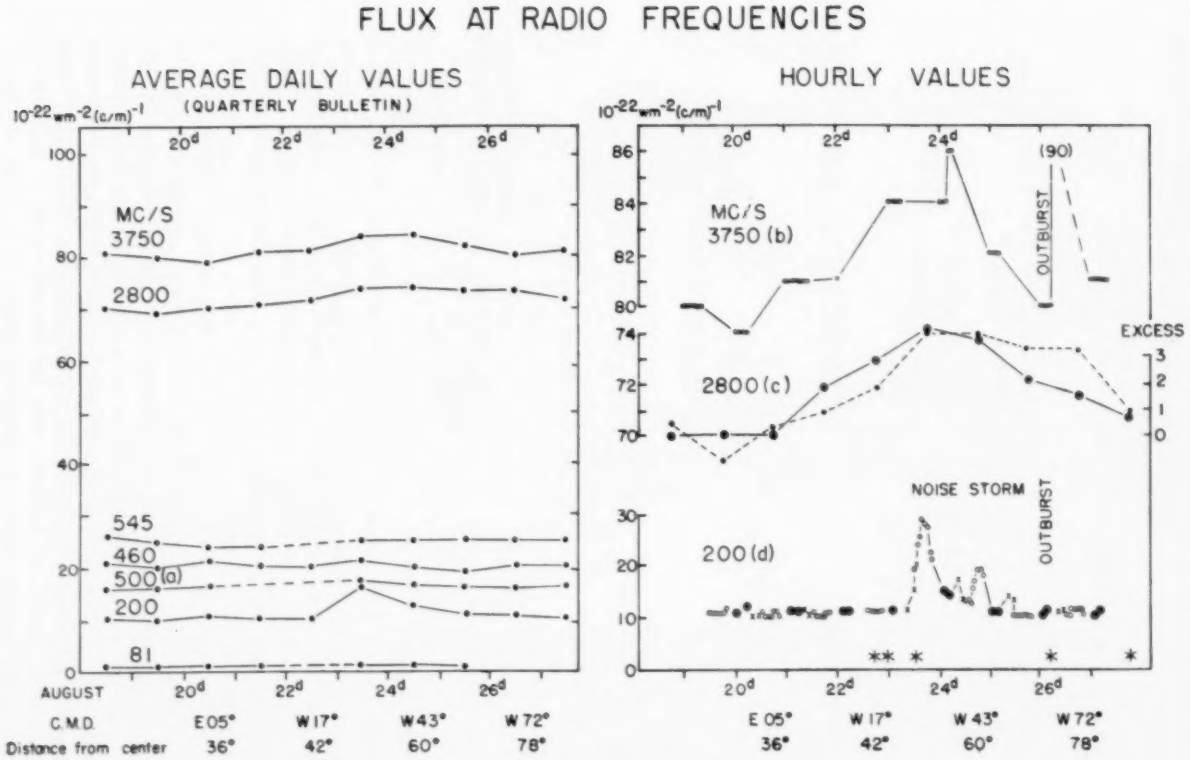

FIG. 7.—*Flux at radio frequencies, 1954 Aug. 18–28.*

(a) Special 500 Mc/s (60 cm) interferometer measures at Sydney, Australia, by G. Swarup and R. Parthasarathy.
(b) Data from Nagoya University, Toyokawa, Japan.
(c) Data from National Research Council, Ottawa, Canada. Dotted line, data from 4-foot reflector. Full line gives excess flux assigned studied region on basis of data from 150-foot array.
(d) Open circles, filled circles, and crosses show data from Cornell, Tokyo, and Nederhorst stations respectively.

TABLE VI

Outstanding Occurrences or Distinctive Events at Radio Frequencies 1954 August 20–26

(Summarized from Quarterly Bulletin of Solar Activity and Special Reports)

Date	Frequency Mc/s	Start (U.T.)	Duration (Min.)	Max. Inten. (Inst.) 10^{-21}wm^{-2} (c/s)$^{-1}$	General Description	Flares
Bursts						
Aug. 23	100	0314	0·2	15	Minor burst of short duration.	None reported.
	60	0314	0·2	10		
23	2800	1323	6+50	1·5	Burst followed by temporary increase in flux.	1325–1420 Imp. one. S30° W31°
	460	1324	35	5		
	200	1327	2+4^h	...		
	81	1327	1·5+>1^h	0·4		
24	3750	0240	1	...	Minor burst.	No observations.
26	3750	0434	3	weak	Outburst.	
		0440	30	strong		
	1200	0439	17	2·0		
	600	0441	15	3·0		In progress. 0443–0500 Imp. one. S30° W65°
	200	0437 or 0448	22 or 9	48 or 120		
	100	0441	10	30		
	98	0440	16·5	>64		
	60	0441	31	>60		
Noise storms						
Aug. 23–24	200	<1200	>2^d	Continuum >4× quiet Sun, 100–500 burst/hr with amplitude about 1/2 the continuum.		Storm reaches maximum 2 hours after flare Aug. 23^d 13^h 25^m.

Terrestrial effects.—The region here studied was the first of the new cycle to attain a moderately high degree of activity. Did the development of this active centre have any measurable effect upon the Earth? In seeking an answer to this question, we have access only to ionospheric and geomagnetic data. To the best of our knowledge, ionospheric disturbances did not accompany the observed flares. Geomagnetically the story is more interesting.

The four months, 1954 May–August, marked the minimum in the cycle of geomagnetic disturbances. During these months there was no disturbance great enough to be reported as a storm. However, during September, when the Sun again exhibited only the most limited activity, three geomagnetic storms took place (Fig. 8). It is possible that these storms reflect only the well known increase in geomagnetic disturbances in March and September (**2**). On the other hand, if one seeks a solar cause, one is faced with the recrudescence of geomagnetic disturbances in September after the definite resurgence of solar activity in August. More specifically, it can be pointed out that the solar flare at CMD 65° W on August 26, accompanied by an outburst at radio frequencies, is the last known major solar event prior to the geomagnetic storm of September 1, the first such

storm in more than four months. The attempt to explain the September geomagnetic disturbances in terms of preceding solar activity for the very simple Earth–Sun case here considered involves time relationships far from those generally considered acceptable in such matters.

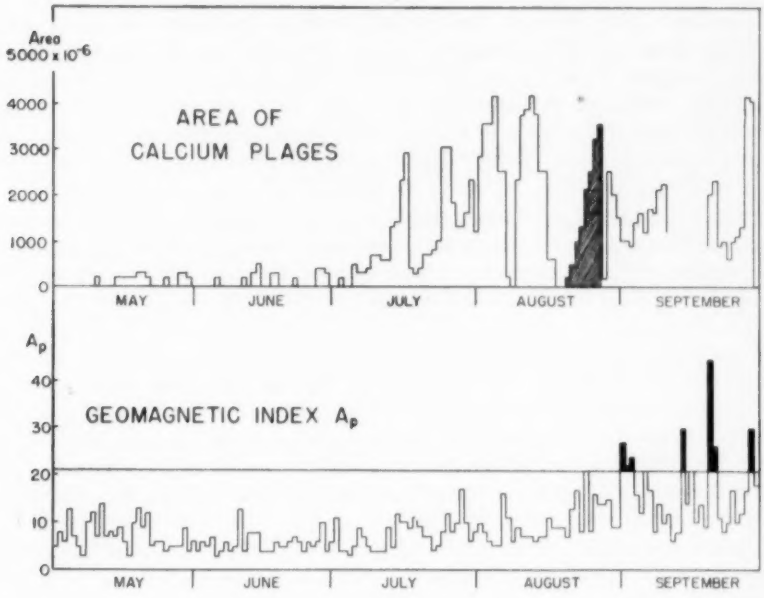

FIG. 8.—*Resurgence of solar activity after minimum, as shown by total calcium plage areas, and geomagnetic activity, May–September* 1954.

Shaded region shows calcium plage here studied. Black portions of A_p curve show periods reported as "storms" by geomagnetic stations. Plage areas are corrected for projection and measured in units of the hemisphere.

Conclusions.—It has been possible to assemble a comprehensive and partially quantitative account of the formation, growth, and decline of an isolated centre of solar activity. The material has been gathered together from many sources. The problems encountered are illustrative of those that will be met on a grander scale in the solar studies of the International Geophysical Year in 1957–58. Where there are several sources of comparable data (spot areas, coronal measurements, 200 Mc/s flux) the apparent differences between reporting stations can be absorbed in daily averages provided one does not wish to take advantage of the time spread in observations for 24-hour coverage. If the latter is sought, acceptable methods of reconciliation for data from different instruments are needed. Where there is only a single measure of a solar feature its "uncertainty" is comfortably masked by lack of information.

Study of the active region of 1954 August 20–27, has provided additional evidence for the concomitant growth of plage, spot, and magnetic fields. The two distinct periods of development were clearly marked in these three types of observations. The flares and excess radiation at *metre* wave lengths took place

entirely within the second period in which the "following" spot and magnetic field had become dominant and the spots reached maximum and then diminished in area. The principal outburst at radio frequencies occurred just eleven hours before the spots are known to have disappeared completely. The great simplicity of the solar disk during this period permitted the one dimensional sweeps of the high resolution radio-frequency instruments to provide data unusually free from ambiguities. The coronal observations, though excellent, all refer to the declining phase of the region and should, therefore, not be compared directly with peak values of plage, spot, and radio flux obtained between August 22–24.

Finally, although the sequence of events here reported is believed to be illustrative for active regions in general, there is evidence that the development of the region was unusually swift. The time interval between the formation of the plage and spot was only three hours, whereas Dr Nicholson writes, and the authors concur, that "when most spots form, the K plage develops a day or more ahead of the spots." The complete lifetime of the spot group was slightly less than six days. Even though the coronal measures were made during the declining phase of the region, the Boulder group comments: "It is unusual for the coronal lines to reach so strong a level so soon after the outbreak of the region."* The lifetime for the region as a whole was also very short. The plage was not visible during the next rotation. The only trace of the region in September was a faint green coronal maximum observed at the east limb. The fact that the time of the initial outbreak of the plage is known within ten minutes, and the times of both formation and disappearance of the spots within three hours, is another atypical aspect of the region, but it is one that the growing series of solar observations may soon eliminate.

Acknowledgments.—The authors wish to express their very great appreciation to the astronomical friends and associates in many parts of the world who made possible the comprehensive nature of this study by their generosity in sharing their data and in preparing special studies. They wish to acknowledge especially the material prepared by Dr Seth Nicholson, Dr Jean Rösch, M. M. Trellis, Dr Horace Babcock, Mr Arthur Covington, Dr Takeo Hatanaka, Dr A. Kimpara, Mrs Winifed S. Cameron, Dr Patrick Wayman, and the Messrs. G. Swarup and R. Parthasarathy.

McMath–Hulbert Observatory
of the University of Michigan,
Pontiac 4, Michigan,
U.S.A.:
1956 *March.*

References

(1) H. W. Dodson, *Ap. J.*, **119**, 564, 1954. T. Hatanaka, K. Akabane, F. Moriyama, H. Tanaka, T. Kakinuma, *Pub. Ast. Soc. Japan*, **7**, 161, 1955.
(2) S. Chapman, and J. Bartels, *Geomagnetism*, Vol. 1, 365, 1940.

* HAO Report No. 25, p.7.

THE RELATION BETWEEN INTERSTELLAR GAS, DUST AND THE EMISSION FROM NEUTRAL HYDROGEN AT 21 CM

R. D. Davies

(Received 1956 April 6)

Summary

Observations have been made of the 21 cm emission from neutral hydrogen in the direction of dense interstellar dust clouds lying in the galactic plane. The emission in these directions is lower than in surrounding regions and appears to be due to dense HI clouds at a low kinetic temperature. These results indicate a correlation between the abundance of gas and dust in interstellar clouds; the density of neutral hydrogen is 300 times that of the dust. Furthermore, the observations confirm the mechanism proposed by Kahn and Seaton to explain the observed kinetic temperature of interstellar neutral hydrogen.

1. *Introduction*

It is of great importance in the study of the interstellar medium to obtain more detailed observations of the relation between interstellar gas and dust. The study of this problem can now be extended by observation of the emission at a wave-length of 21 cm from interstellar neutral hydrogen, the most abundant interstellar gas. It is also of interest to investigate the effect of other interstellar gases and dust upon the emission from neutral hydrogen.

Several of the studies of the relation between the occurrence of interstellar dust and 21 cm emission give apparently conflicting results. van de Hulst, Muller and Oort (**1**) found a small excess of 21 cm emission in the direction of one obscuring cloud in Taurus and a deficiency in the direction of another dust cloud. Lilley (**2**) also examined the Taurus region and found no correlation between 21 cm emission and the dust clouds shown by McCusky's (**3**) star counts but found a close correlation with the absorption regions obtained from counts of external galaxies. Heeschen (**4**) found that the density of neutral hydrogen was closely related to the colour excess of globular clusters in the vicinity of the galactic centre.

It is suggested in this paper that these results appear inconsistent for either one or both of the following reasons.

(i) The optical and radio results do not refer to matter at the same distance in the direction studied, e. g., the star counts in Taurus give information about *nearby* interstellar space, whereas the absorption of the emission from external galaxies measures the *total* amount of obscuring matter in this direction; the neutral hydrogen emission itself comes from the *full* depth of the galaxy.

(ii) The kinetic temperature of the interstellar medium varies from cloud to cloud within the galaxy so that the observed radio emission is a function of both the density and the kinetic temperature of the neutral hydrogen. The observations mentioned above have been made in regions away from the galactic

plane where the neutral hydrogen is not optically thick. This paper describes an investigation of the relation between dust and neutral hydrogen in interstellar clouds lying within the galactic plane and points (i) and (ii) are elucidated. In order to obviate the uncertainties introduced by (i), a radio and optical study was made of one region in Auriga which was otherwise free of large obscuration features.

2. *The observational data*

2.1. *Equipment.*—The aerial used in this experiment had a beamwidth of 1°·6, and was a focal plane paraboloid 30 ft in diameter with a dipole feed and reflector. This was combined with a hydrogen line spectrometer of the double-comparison type. Spectra and drift curves across the Galaxy in Auriga were obtained with a bandwidth of 40 kc/s and a time constant of 30 seconds. The survey in Cygnus was made using a bandwidth of 20 kc/s.

2.2. *The Auriga region.* (*a*) *A radio investigation.*—A clearly defined region with 21 cm emission lower than its surroundings was found in the galactic plane in Auriga at Dec. = 40°·5 and R.A. = $05^h\,06^m$ ($l = 134°{\cdot}5, b = 3°$). Its angular extent was determined from drift curves across the region with the spectrometer set at the frequency which showed the maximum fall in temperature at the centre of the region. Mean drift curves for the range Dec. = 39° to 45° are shown in Fig. 1.

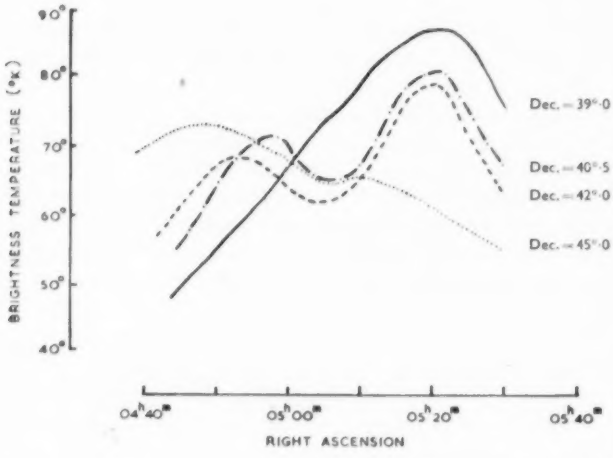

FIG. 1.—*A set of drift curves across the cloud in Auriga between Dec.* = 39° *and* 45°.

The temperature scale used in this investigation is derived from a comparison with the peak temperature of the spectrum at $l = 50°$ and $b = 0°$ which is taken as 100 deg. K. After the removal of the broadening effect due to the beamwidth of the aerial, the region which is elongated in declination, was found to extend from 39°·5 to 44°. Its extent to half power points is 2°·5. Its width in right ascension, which resulted in only a slight broadening of the beam pattern, was estimated to be less than 1°.

Further information about the low temperature region can be obtained from the difference spectrum, $T_D(v)$, in the direction of the cloud. $T_D(v)$ is defined as the difference between the observed spectrum and the spectrum expected if

the cloud were not present, $T_B(v)$. $T_B(v)$ is obtained by extrapolating across the cloud from spectra taken on either side of it. The mean of three sets of spectra taken at Dec. $= 40°{\cdot}5$, R.A. $= 04^h\,50^m$, $05^h\,06^m$ and $05^h\,22^m$ are shown in Fig. 2(*a*). A mean difference spectrum was obtained by combining the results for sets of spectra at Dec. $= 40°{\cdot}5$ and $42°$ with a set taken diagonally across the region It was then corrected for receiver bandwidth and added to two sets of observations obtained at Dec. $= 40°{\cdot}5$ using a 20 kc/s bandwidth to give the resultant difference spectrum shown in Fig. 2(*b*). The accuracy of any point on this difference spectrum due to observational errors was calculated to be less than 1 deg. K. The centre of $T_D(v)$ is displaced 8 km/sec relative to the frequency zero, compared with 15 km/sec for the centre of the background hydrogen line emission spectrum, $T_B(v)$, in this direction. $T_D(v)$ has a half-width of 6 km/sec compared with 20 km/sec for $T_B(v)$.

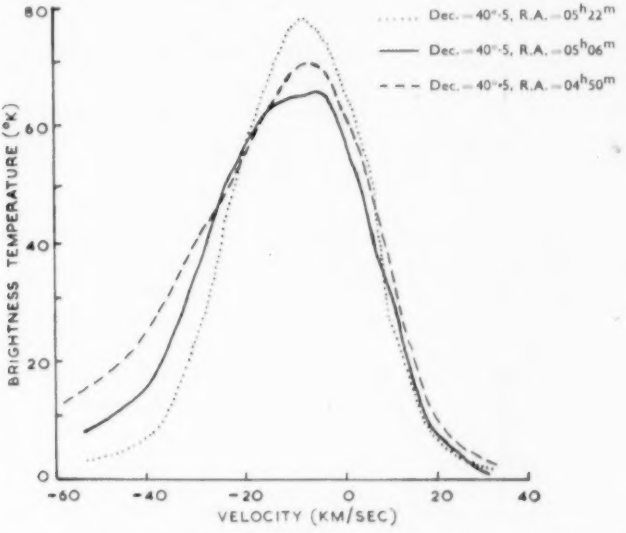

FIG. 2(*a*).—*Mean spectra obtained across the Auriga cloud centred on Dec.* $= 40°{\cdot}5$ *and R.A.* $= 05^h\,06^m$.

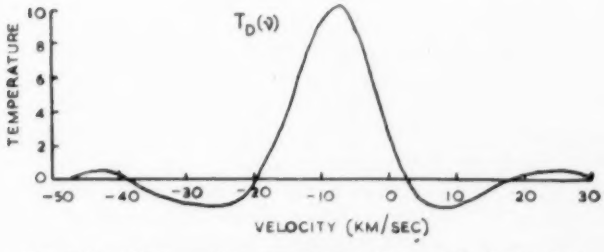

FIG. 2(*b*).—*The mean difference spectrum,* $T_D(v)$ *of the Auriga cloud.*

(*b*) *Optical data.*—Since there is no detailed analysis of the distribution of stars or obscuring matter in this part of the Milky Way, an analysis was made of the available information in the Henry Draper and Henry Draper Extension catalogues. This data was extended by using photographic plates of different

exposure times kindly taken by Dr J. Cisar with the 18″ Schmidt telescope at the St. Andrews University Observatory.

An inspection of a high contrast print from a long exposure (60 minutes) plate revealed the existence of a clearly defined absorbing region 2° long in declination, and $0^h\,7^m$ in R.A., which coincided in position and shape with the radio feature described above.

Star counts were taken across the plates at a number of limiting magnitudes whose values were obtained by comparing the number of stars observed per square degree with the number for each magnitude on the galactic equator given by Trumpler and Weaver (**5**). The absorption produced by the dust cloud was $0^m{\cdot}25$ and was calculated from a comparison of the observed number of stars near the cloud and the number in the direction of the cloud. Its distance was deduced from the magnitude at which absorption attained half its maximum value, and was found to be 200 parsecs, thus making its dimensions 8 parsecs by

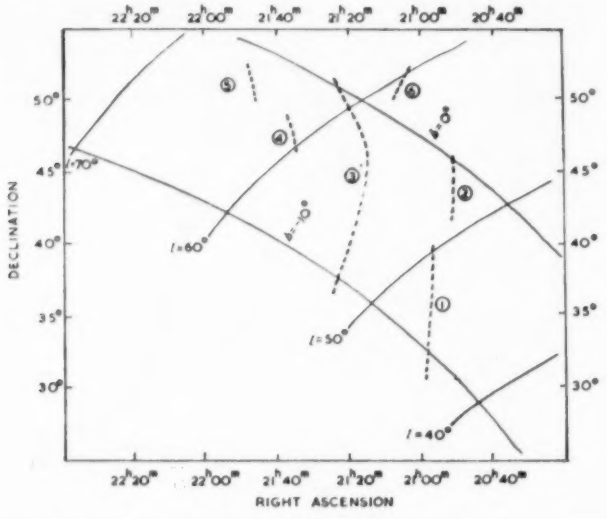

FIG. 3.—*A map showing the position and extent of six dust and neutral hydrogen clouds in and near the constellation of Cygnus.*

2 parsecs. This region of the sky was found to contain no further dense obscuring matter out to a distance of 1 kiloparsec (the limit of the longest exposure plate), thus confirming the original supposition that this part of the Milky Way is relatively free of obscuration. It is concluded that the Auriga cloud lies between the Sun and the bulk of the Milky Way in this direction.

2.3. *The Cygnus region.* (*a*) *A radio investigation.*—A region including the constellation of Cygnus was first studied by Williams (**6**) using a receiver bandwidth of 40 kc/s and taking drift curves for each 2° in declination at only one frequency. Several low temperature regions were detected. A more complete investigation was therefore considered desirable.

The area of the sky surveyed extended from $19^h\,00^m$ to $23^h\,00^m$ in right ascension and from 25° to 55° in declination. Drift curves were obtained across the area at intervals of two degrees in declination with the receiver tuned to the

frequency of maximum emission in the galactic plane. The absolute intensities of the drift curves were obtained by taking spectra at 2° intervals along the galactic plane and calibrating them against the peak intensity of the spectrum at $l = 50°$ and $b = 0°$ which is assumed to be 100 deg. K. Six separate low temperature emission regions were discovered and their positions are plotted in Fig. 3. Because of the sharply changing background temperature in the vicinity of these regions, the frequency dependence of the emission was obtained by taking transits across the region at 30 kc/s intervals instead of taking spectra as in the Auriga region. The difference spectra could be reconstructed from this data and were checked with the difference spectra obtained for regions Nos. 5 and 6 where the background is changing less sharply.

(*b*) *Optical data.*—Pannekoek (**7**) has made a photometric survey of the distribution of visual surface brightness of galactic star-light in the Northern Milky Way. This distribution shows a number of discrete absorbing clouds which coincide in position with the regions of low radio emission observed above. An approximate estimate of their absorption can be derived from his results. More detailed information regarding the distance and absorption of these clouds was obtained from star counts made by Pannekoek (**8**) and Miller (**9**). A complete study of the cloud at Dec. = 31°, R.A. = $21^h\,00^m$ has been made by Franklin (**10**). All the optical information derived for the clouds in Cygnus is given in Table II.

3. *Interpretation of results*

3.1. *The correlation between the distribution of dust and neutral hydrogen.*—The 21 cm results presented above differ in nature from those already published in that they refer to conditions near the galactic plane where the clouds appear as a fall in temperature relative to the surrounding neutral hydrogen emission. In both Cygnus and Auriga the regions of lower neutral hydrogen emission fit closely to the regions of dust absorption. These 21 cm phenomena can only be adequately* explained in terms of dense neutral hydrogen clouds which are at a lower kinetic temperature than their surroundings. These results suggest, at least qualitatively, that neutral hydrogen and dust occur together in clouds near the galactic plane.

3.2. *A model interstellar cloud.*—A simple model of an interstellar cloud will be assumed and its effects on the emission of 21 cm neutral hydrogen radiation will be discussed and compared with the observations reported in this paper and elsewhere.

The model interstellar cloud is assumed to contain dust and the various interstellar gases in the same proportion as they are found in the remainder of the interstellar medium. Such conditions are demanded by the theoretical considerations of Spitzer (**11**), Seaton (**12**) and Savedoff (**13**). The constancy of the ratio of neutral hydrogen to dust is suggested by the 21 cm results presented in this paper and is also demonstrated by the hydrogen-line observations of the galactic centre (**4**) of the anticentre (**2**) and of the local subsystem of the Galaxy (**14**). Supporting optical evidence for the close relationship between gas and dust comes from studies of the external galaxies (**15**), of the Andromeda Nebula (**16**), of the Carina section of the Milky Way (**17**), of individual emission nebulae (**18**)

* The dust particles themselves, with dimensions $\simeq 10^{-5}$ to 10^{-4} cm, will not absorb or scatter 21 cm radiation. Furthermore, the results cannot be explained in terms of a deficiency of neutral hydrogen in these regions for even if the volume of the dust cloud were completely devoid of neutral hydrogen the emission would not be sufficiently reduced.

and of the observed correlation between the equivalent width of interstellar lines and stellar reddening (**19**). Although departures from this correlation between the occurrence of gas and dust are found, the model assumed can be regarded as representative of conditions in the interstellar medium.

The effect of an increase in the density of the model cloud upon its kinetic temperature will now be discussed. Spitzer (**20**) has shown that molecular hydrogen is an effective cooling agent for interstellar neutral hydrogen. The considerations used by Kahn (**21**) to explain the observed kinetic temperature of interstellar neutral hydrogen in terms of heating due to cloud collisions and subsequent cooling by molecular hydrogen are now applied to determine the concentration of molecular hydrogen required to give interstellar clouds of various harmonic mean temperatures. The results are given in Table I. The cloud concentration factor, which has been included in the Table, is the density of dust and gas in a cloud relative to the average cloud which has a kinetic temperature of 125 deg. K (the observed value for interstellar neutral hydrogen). Since the density of molecular hydrogen, $N(\text{H II})$, varies as the square of the density of neutral hydrogen atoms the concentration factor will be given by the square root of $N(\text{H II})$ relative to the average cloud. It is clear that a large increase in the concentration factor is required to reduce the temperature significantly below 50 deg. K.

TABLE I

Harmonic mean temperature (deg. K)	No. of hydrogen molecules/cm^3 N (H II)	N (H II) relative to average cloud	Cloud concentration factor
250	$5{\cdot}5\times10^{-3}$	0·19	0·44
200	$9{\cdot}1\times10^{-3}$	0·31	0·56
150	$1{\cdot}7\times10^{-2}$	0·59	0·77
125	$2{\cdot}9\times10^{-2}$	1·00	1·00
100	$5{\cdot}2\times10^{-2}$	1·8	1·3
80	$1{\cdot}3\times10^{-1}$	4·5	2·1
60	$4{\cdot}2\times10^{-1}$	14	3·7
50	1·8	62	7·9
40	15·1	520	23

Another cooling mechanism which is more effective at these low temperatures has been suggested by Seaton (**22**); it involves the electron excitation of the gaseous metal constituents of the clouds, principally singly ionized carbon. Again, the temperature falls with increasing concentration factor. Thus if one or both of these cooling mechanisms are operative the kinetic temperature of the model interstellar cloud will be lower, the higher the density.

3.3. *The 21 cm results compared with the cloud model.*—Most of the information about the physical conditions in interstellar neutral hydrogen clouds can be derived from the difference spectrum as defined in Section 2.2(*a*). The effect of a cloud lying between the Sun and the Milky Way will now be considered. If the brightness temperature of the neutral hydrogen emission from the Milky Way is $T_B(\nu)$ at a frequency ν, then it will be reduced on traversal of the cloud to $T_B(\nu)e^{-\tau(\nu)}$ where $\tau(\nu)$ is the 21 cm optical depth of the cloud at frequency ν. The observed emission in the precise direction of the cloud will then be

$$T_c(\nu) = T_B(\nu)e^{-\tau(\nu)} + T_c'[1 - e^{-\tau(\nu)}] \qquad (1)$$

where T_c' is the kinetic temperature of the cloud. The difference spectrum is then

$$T_D(\nu) = T_B(\nu) - T_c(\nu)$$
$$= [T_B(\nu) - T_c'][1 - e^{-\tau(\nu)}]. \quad (2)$$

(*a*) *The Auriga cloud.* (i) *The kinetic temperature.*—The kinetic temperature of an interstellar cloud can be obtained from its difference spectrum. From equation (2), $T_D(\nu)$ is zero at frequencies where $T_B(\nu)$ equals the kinetic temperature of the cloud. Inspection of the difference spectrum for the Auriga cloud yields two estimates of the kinetic temperature, the average of which is 60 deg. K.

The width of the emission spectrum from a neutral hydrogen cloud is also related to its kinetic temperature. If $T_B(\nu)$ does not vary by more than 20 per cent, say, over the frequency range of emission from the cloud, the shape of the spectrum $T_D(\nu)$ will be similar to that for the cloud. The half-width of the emission from the Auriga cloud is accordingly 30 kc/s. Temperature broadening alone would be ± 8 kc/s for hydrogen at 60 deg. K. The larger experimental value may be attributed to the expansion of the cloud into the surrounding space which may be 3 times as great as the r.m.s. velocity of the cloud atoms (**23**).

The observed value of the kinetic temperature may be compared with that obtained using the optical results and the cloud model of section 2.2 (*a*). The dust absorption of $0^m{\cdot}25$ takes place in a cloud depth of 2 parsec (assuming the cloud to be cylindrical in shape). The concentration factor can be obtained by a comparison with an average cloud, 4 parsec in diameter (**24**), and producing $0^m{\cdot}1$ absorption, (assuming 10 clouds per kiloparsec which on the average produce $1^m{\cdot}0$ of absorption). The corresponding concentration factor of 5 would produce a kinetic temperature of 55 deg. K. This is in good agreement with the value obtained from the 21 cm results and consequently adds weight to the assumed cloud model.

(ii) *The mass of the neutral hydrogen cloud.*—From the known kinetic temperature of the neutral hydrogen cloud and the value of $T_D(\nu)$ at the centre frequency, the optical depth of the cloud at its centre frequency (τ_0) can be derived from equation (2). For the Auriga cloud $\tau_0 = 1$. The number of neutral hydrogen atoms per cm^2 in the line of sight in a cloud is given by Heeschen (**4**) as

$$N(\mathrm{H}) = \frac{\tau_0 \eta T_c' \sqrt{2\pi}}{5{\cdot}44 \times 10^{-14}} \text{ hydrogen atoms/cm}^2$$

where η is the halfwidth of the emission spectrum (6×10^5 cm/sec) of the cloud and T_c', its kinetic temperature, is 60 deg. K. Thus N(H) for the Auriga cloud is $1{\cdot}6 \times 10^{21}$ hydrogen atoms per cm^2 (250 per cm^3) compared with $2{\cdot}4 \times 10^{20}$ cm^{-2} for an average cloud 4 parsec in depth and containing 20 atoms per cm^3; N(H) is $1{\cdot}2 \times 10^{22}$ cm^{-2} for all he hydrogen on the line of sight in the anticentre region (**1**). The mass of the Auriga cloud, assuming the optical dimensions, is 200 solar masses or $4{\cdot}0 \times 10^{35}$ grm. The number of dust particles in a line of sight through the centre of a cloud producing an absorption of m magnitudes is (**2**)

$$N(D) = 3{\cdot}25 \times 10^8 m \text{ grains cm}^{-2}$$
$$= 8{\cdot}1 \times 10^7 \text{ grains cm}^{-2} \text{ for the Auriga cloud.}$$

The mass of the dust cloud, assuming grains 3×10^{-5} cm in radius and unit density, is $1{\cdot}3 \times 10^{33}$ grm. The ratio of the density of neutral hydrogen gas to dust within the cloud is therefore 300. This value may be compared with a ratio of 100 obtained by Lilley (**1**) at intermediate galactic latitudes near the galactic anticentre.

(iii) *The distance of the neutral hydrogen cloud.* The Doppler shift of a neutral hydrogen cloud relative to the Sun can give the distance of the cloud in the same way as the distance of spiral arms of the galaxy are obtained. The velocity displacement for the Auriga cloud relative to the Sun is 8 km/sec compared with 15 km/sec for the spiral arm in this direction. Since the random cloud velocity at this distance from the centre of the galaxy is 6 km/sec (**25**) the cloud is significantly nearer than the bulk of the hydrogen in this direction, which is at a distance of 1·5 kiloparsec. A distance of the cloud based on the Oort rotation model is 0·7 kiloparsec but since the random motions are appreciable this quantitative result will be unreliable. It is clear that both the neutral hydrogen cloud and the dust cloud lie between the Sun and the spiral arm in this direction. In principle, the observation of the difference spectrum of a neutral hydrogen cloud leads to an estimate of its distance.

(*b*) *The Cygnus clouds.*—It has not been possible to study each of the six clouds in the Cygnus region as thoroughly as the Auriga cloud because of the complex spectrum in this region which has three narrow peaks; in addition, the clouds lie slightly away from the galactic plane where the brightness temperature is changing rapidly. All the information which could be obtained for each cloud is given by Table II. The position tabulated is that of the centre of the cloud as shown in Fig. 3. The kinetic temperature is a maximum value only, being the actual temperature recorded at the centre frequency of the cloud spectrum. This value would be accurate if the optical depth of the cloud were greater than unity. η is the half-width of the emission spectrum of each cloud. The "radio" distance was calculated in the manner described in the previous section. The optical data has been discussed in Section 2.3 (*b*).

TABLE II

Cloud	Position			Radio Results				Optical Results	
	Dec.	R.A.		kinetic temp.	η	T_c' max.	distance	dust absorption	distance
No.	°	h	m	(deg. K)	km/s	(deg. K)	kps	m	kps
1	31–38	21	00	50	8·0	30	1·2	1·5	1·6
2	42	20	50	60	7·3	25	1·5–2·5	4·0	remote
3	38–51	21	20	45	9·3	22	0	>1	remote
4	47	21	35	27	8·0	12	0·8–1·8	>1	remote
5	51	21	48	31	7·0	12	1·9–2·8	>1	remote
6	50	21	10	44	7·3	10	0·5–1·5	>1	0·3

The distances obtained from the two methods, both of which are liable to large errors, agree as well as may be expected. In these dense dust clouds it is likely that the kinetic temperature of the neutral hydrogen should be very low, as in fact the 21 cm results show. The actual temperatures are lower than anticipated on the Kahn model and could be more readily explained by the presence of ionized carbon (Seaton's model).

The cloud at Dec. = 42°, R.A. = 20^h 50^m, may be associated with the Cygnus rift at about 2 kiloparsec. The two distant dust clouds at Dec. = 50° exhibit only a small fall in temperature on the 21 cm records. This is probably because the main body of the hydrogen emitting at their characteristic frequencies lies in front of and not behind them.

4. *Conclusion*

The study of the relation between dust and neutral hydrogen emission in Auriga and Cygnus shows clearly that regions containing excess dust are cooler than surrounding regions. This result adds weight to the mechanisms proposed by Kahn and Seaton to explain the high kinetic temperature of interstellar neutral hydrogen.

Equation (2) indicates that a dense neutral hydrogen cloud will appear either hot or cold relative to its surroundings, depending upon the values of $T_B(\nu)$ and T_c'. In the galactic plane it will nearly always appear cool as in the observations presented above, while away from the plane it may appear bright or cold, as in the results obtained by van de Hulst, Muller and Oort (**1**) for several regions in Taurus.

It has been suggested that the kinetic temperature of neutral hydrogen is likely to vary throughout the Galaxy (see for example (**21**)). The observations by Williams and Davies (**26**) of absorption of the radio sources at a wave-length of 21 cm gave evidence for a variation from 60 deg. K to 250 deg. K in the kinetic temperature of the spiral arms. The present observations show that the kinetic temperature of individual interstellar clouds can be definitely lower than the mean value.

Acknowledgments.—The author wishes to thank Professor A. C. B. Lovell, the Director of the Station, for his interest in the investigation and Mr Hanbury Brown for helpful discussions during the course of this work. Particular thanks are due to Dr D. R. W. Williams for his assistance during the initial stages of this work and to Dr F. D. Kahn for stimulating discussions on the interpretation of the results.

University of Manchester,
Jodrell Bank Experimental Station:
1956 *April* 5.

References

(1) van de Hulst, H. C., Muller, C. A. and Oort, J. H., *B.A.N.*, **12**, 117, 1954.
(2) Lilley, A. E., *Ap. J.*, **121**, 559, 1955.
(3) McCusky, S. W., *Ap. J.*, **88**, 209, 1938.
(4) Heeschen, D. S., *Ap. J.*, **121**, 569, 1955.
(5) Trumpler, R. J. and Weaver, H. F., "Statistical Astronomy", p. 418, 1953.
(6) Williams, D. R. W., Ph.D. thesis, Manchester University, 1954.
(7) Pannekoek, A., *Pub. Astron. Inst. Univ. of Amsterdam*, No. 3, 1933.
(8) Pannekoek, A., *Pub. Astron. Inst. Univ. of Amsterdam*, No. 7, 1942.
(9) Miller, F. D., *Harvard Annals*, **105**, 297, 1937.
(10) Franklin, F. A., *Astron. J.*, **60**, 351, 1955.
(11) Spitzer, L., *Ap. J.*, **95**, 329, 1942.
(12) Seaton, M. J., *M.N.*, **111**, 368, 1951.
(13) Savedoff, M. P., *Gas Dynamics of Cosmic Clouds, A Symposium*, p. 218, 1955.
(14) Lilley, A. E. and Heeschen, D. S., *Pub. Nat. Acad. Sci.*, **40**, 1095, 1954.
(15) Baade, W. and Mayall, N. J., *Problems of Cosmical Aerodynamics, A Symposium*, p.165, 1949.

(16) Baade, W., *Coordination of Galactic Research, A Symposium*, 1953.
(17) Bok B. J. and Wade, C. M., *Gas Dynamics of Cosmic Clouds, A Symposium*, p. 273, 1955.
(18) Shajn, G. A., Hase, V. T. and Pickelner, S. B., 6th International Astrophysical Colloquium Liège, p. 441, 1955.
(19) Spitzer, L., *Ap. J.*, **108**, 276, 1948.
(20) Spitzer, L., *Ap. J.*, **107**, 6, 1948.
(21) Kahn, F. D., *Gas Dynamics of Cosmic Clouds, A Symposium*, p. 60, 1955.
(22) Seaton, M. J., *Annales d'Astrophysique*, **18**, 188, 1955.
(23) Rach, D. C., *M.N.*, **113**, 43, 1953.
(24) Oort, J. H., *Ap. J.*, **116**, 233, 1952.
(25) Schmidt, M., Jodrell Bank Radio Astronomy Symposium, August 1955.
(26) Williams, D. R. W., and Davies, R. D., *Phil. Mag.*, **1** (Series VIII), 622, 1956.

ON THE DIFFERENTIAL GALACTIC ROTATION OF THE SYSTEM OF CEPHEID VARIABLE STARS

D. W. N. Stibbs

(Communicated by the Director, University Observatory, Oxford)

(Received 1956 March 3)

Summary

The radial velocities of cepheid variable stars, recently augmented by observations of fifty-five southern Cepheids (**10**), are analysed for solar motion, galactic rotation near the Sun, and a K-term due to a general expansion of the system parallel to the galactic plane. Solutions are carried out with an approximate form for the radial velocity equation for two values of the longitude l_0 of the galactic centre, 325° and 328°, suggested by optical and radio data, using a correction $\Delta M = -1{\cdot}4$ magnitudes to Shapley's 1940 zero-point of the period-luminosity curve, and Baade's distance R_0 to the galactic centre of 8·2 kiloparsecs. It is shown that there is no evidence in the cepheid motions for a K-term if $l_0 = 325°$, and only slight evidence in the solution for $l_0 = 328°$ for a negative K-term of the form $k_0 r \cos^2 b$, corresponding to a uniform contraction of the system, the value of k_0 being $-2{\cdot}6 \pm 1{\cdot}1$ km/sec/kpc. The solution for $l_0 = 325°$ with no K-term gives $u_0 = +8{\cdot}7 \pm 2{\cdot}1$, $v_0 = +12{\cdot}1 \pm 1{\cdot}4$, $w_0 = +7{\cdot}3$ (assumed), for the components in km/sec of the solar motion with respect to the circular velocity of the cepheid system, u_0 being directed towards the galactic centre, v_0 in the direction of rotation, and w_0 perpendicular to the galactic plane. The value of the Oort constant A is found to be $19{\cdot}5 \pm 1{\cdot}9$ km/sec/kpc., in agreement with a determination from a group of nearby Cepheids given in an earlier paper (**20**) on the intrinsic colours of cepheid variables. These two determinations of A refer to a cepheid distance scale in which the photographic absorption averages approximately 2 magnitudes per kpc.

The rotation of the cepheid system as a function of distance R from the galactic centre is then examined by means of Camm's method (**4, 11**). Weighted mean values of the function $f(R, R_0) = R_0[\omega(R) - \omega(R_0)]$ are obtained from the radial velocity data for 189 cepheid variables arranged in 15 groups according to distance R, the weighted mean distance of the groups from the galactic centre ranging from the nearest at 5·4 kpc to the farthest at 11·9 kpc. The angular velocity $\omega(R_0)$ of the system at the solar distance R_0 is then found from the $f(R, R_0)$ curve and the proper motions of the objects in galactic longitude. Reliable proper motions are available for only 18 variables. These are found to yield a value of $\omega(R_0)$ which does not differ significantly from the value of $A - B = 26{\cdot}4$ km/sec/kpc obtained by Morgan and Oort (**34**) from the proper motions of early type stars and faint stars in general. It is emphasized that the angular velocity of the cepheid system should be assessed from the cepheid data alone as the velocity of rotation is not necessarily the same as the average for a heterogeneous collection of nearby objects.

The paper concludes with a comparison between the rotation $f(R, R_0)$ from cepheid variables, and the rotation given by 21 cm radio data and schematic models of the mass distribution in the galactic system, the most comprehensive being a model recently constructed by Schmidt (**38**). The cepheid groups at large distances from the galactic centre appear to rotate more rapidly than the model, and the groups nearest the centre more slowly. The latter discrepancy represents a striking disagreement between radio and optical methods both of which purport to give an observational determination of the same quantity.

Introduction.—In 1937 Joy published his monumental work on the *Radial Velocities of Cepheid Variable Stars* (**1**) followed by a discussion of galactic rotation (**2**) using all the data available. Joy's list of velocities has been further analysed for galactic rotation in several investigations (**3–9**) in which there are important differences in the treatment of the effect of galactic rotation on the radial velocities, in the method of allowance for interstellar absorption, and in the adopted zero-point of the period–luminosity curve. Valuable though these analyses have been, they have all suffered to some extent from the inadequate distribution of the observations in galactic longitude due to the absence of radial velocity data within a large sector inaccessible from the northern hemisphere. This deficiency has been remedied by the recent observations of 55 variables presented in the communication *Radial Velocities of Cepheid Variable Stars in the Southern Hemisphere* (**10**) which completes an extension of Joy's programme to southern Cepheids with photographic magnitudes brighter than 10·5 at minimum light. These observations increase the number of cepheid velocities to 195, including some objects belonging to Population II. A discussion of the augmented list of velocities is given in this communication.

1. *The scope of the work*

The object of this analysis of the data is to determine (i) the Oort constants of differential rotation near the Sun, (ii) the solar velocity with respect to the rotating system of Cepheids, (iii) the level of significance of the K-term, and (iv) the rotational structure of the system using Camm's treatment of the radial velocity and proper motion equations (**4, 11**). The data required for such an analysis are radial velocities and proper motions, absolute magnitudes from the period–luminosity law, and distance moduli corrected for interstellar absorption.

1.1. *The period–luminosity curve.*—The correlation between the periods of galactic Cepheids and their luminosities may be taken from the periods and apparent magnitudes of cepheid variables in the Small Magellanic Cloud. According to Baade, the period–luminosity curves for type I Cepheids (classical δ Cephei variables) and type II Cepheids (RR Lyrae and W Virginis stars) differ in zero-point by 1·5 photographic magnitudes. The period–luminosity curve given by Shapley (**12**) in 1930 was obtained by adjusting the zero-point of the curve for the Cloud Cepheids so as to join the RR Lyrae variables in the Galaxy at zero photographic absolute magnitude. It appears that Baade's correction $\Delta M = -1{\cdot}5$ magnitudes refers to the 1930 zero-point. In 1940 Shapley (**13**) slightly revised the shape of the curve and increased the luminosity of the classical Cepheids by 0·1 magnitudes, so that Baade's correction to the 1940 version of the curve should be taken as $\Delta M = -1{\cdot}4$ magnitudes. Support for

TABLE I

The adopted period–luminosity relation

$\log P$	0·1	0·2	0·3	0·4	0·5	0·6	0·7	0·8	0·9
M_{pg}	−1·91	−2·08	−2·25	−2·41	−2·57	−2·73	−2·89	−3·06	−3·24
$\log P$	1·0	1·1	1·2	1·3	1·4	1·5	1·6	1·8	2·0
M_{pg}	−3·42	−3·60	−3·79	−3·99	−4·20	−4·42	−4·65	−5·13	−5·64

such a large correction to the zero-point of the period–luminosity curve is to be found in some recent investigations (**14, 15, 16, 17**), and in the much earlier work of Lundmark (**18**) and Mineur (**5, 19**).

The period–luminosity relation adopted in the present work is given in Table I in which P is the cepheid period in days, and M_{pg} is the photographic median absolute magnitude defined as the average of the magnitudes at maximum and minimum light.

1.2. *Interstellar absorption.*—The most satisfactory method of correcting the distance moduli of the Cepheids for interstellar absorption is by means of colour excesses. Given a homogeneous set of magnitudes and colours, and some information as to the unreddened or intrinsic colours of the Cepheids as a function of their periods, reliable distances could be determined. The basic datum required for such a determination is the relation between intrinsic colour and period.

In a recent paper (**20**) the writer has obtained intrinsic colours for the Cepheids using Eggen's photo-electric colours, and a suitable interpolation formula for the reddening of the B stars in surrounding fields as a function of distance and the galactic coordinates. The formula

$$E_1(r, b) = \frac{c_0\beta}{\sin b}\left(1 - \exp\left(-\frac{r \sin b}{\beta}\right)\right)$$

for the colour excess on the system of Stebbins, Huffer and Whitford, with a zero-point correction of $+0{\cdot}04$, was used to estimate the reddening in the path to a given Cepheid by interpolation or extrapolation within or beyond the field of B stars used in the determination of the parameters in the reddening formula. In this way, estimates of the unreddened colours were obtained, and from these estimates the best linear relations for intrinsic colours at maximum and minimum light as a function of the logarithm of the periods were determined. These relations may be used to determine the interstellar absorption for the calibrating stars with greater accuracy for a single star than that obtained directly from the formula, and to obtain reliable corrections for absorption for more distant Cepheids. We have, however, used practically all the available photo-electric data in the calibration of the intrinsic colours. In the circumstances, pending the completion of further photo-electric work on cepheid colours, the only course to follow in order to keep the distance scale as uniform as possible is to determine the interstellar absorption for the remaining Cepheids by the method used in the determination of the intrinsic colours. Accordingly, the cepheid distance moduli have been corrected for interstellar absorption using (i) $A_{pg} = \chi E$, where $\chi = 4{\cdot}75$ and E is the colour excess on the ***P, V*** system, and (ii) the solution by successive approximation in the distance modulus equation with

$$A_{pg} = \frac{a_0\beta}{\sin b}\left(1 - \exp\left(-\frac{r \sin b}{\beta}\right)\right),$$

using $\beta = 100$ pc, and the values of a_0 given by Parenago (**21**) for small zones bounded by circles of galactic latitude and longitude. The distances of the Cepheids determined by these methods are given in Table II.

As a check on the absorption, it may be shown (**22**) that the distances of the Cepheids in the table satisfy the test proposed by Bottlinger and Schneller (**23**) that the half-thickness of the z-distribution should not correlate with heliocentric distance. It has already been demonstrated by the writer (**20,** p. 330) that the

cepheid distances calculated from colour excesses, using the intrinsic colours determined as above, also satisfy the condition that heliocentric distances and periods of Cepheids are likewise not unduly correlated.

1.3. *Observational data.*—The data required in the analysis of the radial velocities are summarized in Table II which gives the galactic coordinates (l, b) of the Cepheids referred to Ohlsson's pole ($\alpha = 190°$, $\delta = +28°$); the median apparent magnitudes m_{pg} from Eggen's photo-electric observations where available, otherwise the revised magnitudes given by Parenago (**6**); the median absolute magnitudes M_{pg} from Table I, using the periods given in the Russian *Catalogue of Variable Stars*; the heliocentric distances r in kpc; the normal radial velocities ρ from Joy's work (**1, 2**) revised by Parenago (**6**) by means of improved ephemerides, and from the writer's radial velocity observations of cepheid variables in the Southern Hemisphere (**10**). The data on cepheid distances and radial velocities should be supplemented by the accurate proper motions of eighteen variables published by Blaauw and Morgan (**17**).

The explanation of the notes in the last column of Table II is as follows: 1, absorption determined from colour excess; 2, absorption determined by

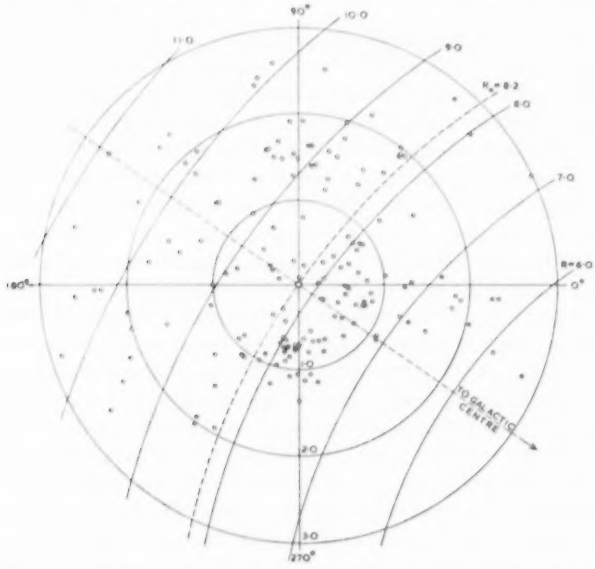

FIG. 1.—*Distribution of cepheid variables with known radial velocities and within 3 kpc of the Sun shown projected on the galactic plane. The scale of the projected heliocentric distances is indicated by complete circles centred on the Sun with radii 1·0, 2·0, and 3·0 kpc, the galactocentric distance scale being given by arcs of circles drawn from the galactic centre distant 8·2 kpc from the Sun and in longitude 325°.*

successive approximation in the formula for the distance modulus; 3, Cepheids used in the solutions for the solar motion and Oort's constant A in Section 2 of the paper; 4, Cepheids with accurate proper motions used in the solution for the velocity of rotation of the system in Section 3.2; and 5, Population type II Cepheids. Six of the variables in the table are assigned to this class: W Virginis, and five Cepheids provisionally identified as type II by Eggen. The distances of these objects have been calculated for an assumed period–luminosity relation

1·5 magnitudes fainter than that given by Table I for all periods. Type I galactic Cepheids within 3 kpc of the Sun are shown projected on the galactic plane in Fig. 1.

TABLE II

Cepheid data for analysis

Star	l	b	m_{pg}	M_{pg}	r	ρ	Notes
	°	°					
V336 Aql	1·9	−3·6	10·8	−3·2	1·32	+11·5	2
SZ Aql	3·4	−3·8	9·7	−3·8	1·67	+9·5	1
TT Aql	3·6	−4·6	8·1	−3·7	0·80	+0·5	1, 3
FN Aql	6·3	−4·5	9·4	−3·4	1·01	+6·6	1
BH Oph	7·5	+11·9	12·0	−3·5	7·52	+32·5	2
η Aql	8·8	−14·4	4·6	−3·2	0·25	−12·9	1, 3, 4
BB Her	11·0	+5·4	11·0	−3·2	3·04	+91·0	1
FM Aql	12·0	−0·4	9·3	−3·0	0·72	−10·0	1, 3
BL Her	12·6	+18·1	10·5	−1·3	1·25	+16·5	1, 5
AP Her	14·7	+6·1	11·9	−3·4	4·51	−29·5	2
FF Aql	16·8	+5·0	6·0	−2·8	0·30	−19·0	1, 3, 4
KL Aql	22·8	−8·8	11·2	−3·0	3·13	−1·5	2
S Sge	23·0	−7·3	6·4	−3·3	0·54	−10·0	2, 3, 4
U Vul	23·8	−1·5	8·2	−3·2	0·64	−10·8	2, 3
CN Lyr	25·4	+13·5	11·3	−2·4	3·09	+17·0	2
X Vul	31·6	−2·4	10·0	−3·1	0·80	−13·0	1, 3
SV Vul	31·6	−0·8	8·5	−4·8	1·56	−0·5	1, 3
SU Cyg	32·4	+1·5	7·2	−2·7	0·89	−30·6	1, 3
GH Cyg	34·2	−1·1	11·3	−3·2	0·87	−19·5	2, 3
MW Cyg	38·6	−1·5	10·8	−3·0	0·80	−13·6	2, 3
CD Cyg	38·7	+0·6	9·6	−3·8	1·20	−10·3	2, 3
T Vul	40·1	−11·1	6·3	−2·8	0·55	−1·3	1, 3, 4
V383 Cyg	41·7	−3·6	12·8	−2·8	2·67	−20·0	2, 3
V343 Cyg	42·8	+3·4	14·8	−3·6	18·28:	−90·5	2
GL Cyg	42·9	+3·4	14·6	−2·6	10·76	−60·5	2
DT Cyg	44·5	−11·6	6·2	−2·4	0·40	+0·6	1, 3, 4
X Cyg	44·7	−5·1	7·3	−3·8	0·82	+9·3	1, 3
VX Cyg	50·0	−4·2	11·5	−4·0	2·85	−18·0	2, 3
VY Cyg	50·7	−5·2	10·7	−3·2	1·96	−9·8	2, 3
MZ Cyg	51·3	−9·5	12·4	−4·0	9·13	−53·5	2
SZ Cyg	52·1	+3·3	10·8	−3·8	1·92	−11·7	2, 3
TX Cyg	52·1	−2·9	11·0	−3·7	1·92	−20·7	2, 3
BZ Cyg	52·5	+0·7	11·7	−3·4	1·65	−13·2	2, 3
V386 Cyg	53·3	−5·5	11·0	−2·9	2·01	−10·0	2, 3
VZ Cyg	59·5	−9·0	9·5	−2·9	1·39	−16·5	2, 3
BG Lac	60·9	−9·6	9·5	−2·9	1·56	−19·5	1, 3
Y Lac	66·5	−4·3	9·7	−2·8	2·17	−18·0	1, 3
AK Cep	72·7	+0·2	12·7	−3·2	1·78	−45·6	2, 3
δ Cep	72·9	+0·4	4·5	−2·9	0·24	−17·4	1, 3, 4
RR Lac	73·4	−2·1	9·6	−3·1	1·98	−34·5	1, 3
Z Lac	73·5	−1·7	9·3	−3·5	1·56	−25·0	1, 3
V Lac	74·2	−2·6	9·5	−2·9	1·29	−20·0	2, 3
X Lac	74·3	−2·6	9·1	−3·0	1·17	−25·0	2, 3
SW Cas	77·4	−1·6	10·5	−3·0	1·60	−38·0	2, 3
RS Cas	82·2	+0·9	11·1	−3·1	1·41	−24·5	2, 3
RY Cas	83·1	−3·1	11·1	−3·6	2·55	−70·5	2
DD Cas	84·2	+0·5	10·9	−3·4	1·41	−69·5	2, 3
CG Cas	84·6	−1·1	12·1	−2·8	1·64	−87·0	2
SY Cas	86·0	−3·9	10·6	−2·7	1·63	−43 0	2

Star	l	b	m_{pg}	M_{pg}	r	ρ	Notes
	°	°					
TU Cas	86·9	−11·2	8·4	−2·3	0·82	−20·3	2, 3
AP Cas	88·6	+0·4	12·4	−3·1	1·92	−44·5	2
α UMi	90·3	+26·8	2·6	−2·7	0·10	−17·4	2, 3, 4
XY Cas	90·5	−2·4	10·6	−2·8	1·49	−42·0	2
VW Cas	92·3	−0·7	11·1	−3·0	1·53	−58·5	2
BP Cas	93·0	+3·2	12·5	−2·0	1·28	−46·5	2
UZ Cas	93·2	−1·1	12·3	−2·8	1·91	−51·0	2
RW Cas	96·8	−4·1	10·5	−3·7	2·61	−64·5	1
BY Cas	97·3	−0·2	11·6	−2·6	1·49	−45·5	2
VV Cas	98·1	−1·6	11·2	−3·0	1·69	−50·5	2
VX Per	100·6	−2·4	10·0	−3·5	1·52	−33·0	2
SU Cas	100·8	+9·0	6·5	−2·2	0·29	−8·0	1, 3, 4
UX Per	101·3	−2·5	12·6	−2·8	2·47	−41·5	2
SZ Cas	102·6	−0·6	10·8	−3·7	1·62	−41·0	2
VY Per	102·8	−1·1	12·3	−4·0	2·38	−39·5	2
UY Per	103·6	−0·7	12·4	−3·9	1·62	−59·0	2
RW Cam	112·4	+4·7	9·7	−3·8	1·33	−26·0	2
RU Cam	112·9	+28·9	9·9	−4·1	4·57	−23·9	2
RX Cam	113·7	+5·7	8·7	−3·2	0·73	−36·5	1, 3
AS Per	121·8	+0·2	10·6	−2·9	0·99	−25·5	2
SX Per	126·7	−5·2	12·0	−2·8	1·97	+5·5	2
SV Per	130·3	−0·3	9·7	−3·5	2·30	−9·0	1
SY Aur	132·4	+3·4	10·0	−3·4	1·77	−2·0	2
AN Aur	132·5	+0·1	11·8	−3·4	1·93	−9·5	2
RX Aur	133·5	−0·1	8·5	−3·5	1·33	−21·3	1
Y Aur	134·3	+5·6	10·3	−2·7	1·36	+8·5	2
AW Per	134·4	−4·1	8·5	−3·1	0·59	+13·5	2, 3
YZ Aur	135·0	+2·2	10·9	−3·9	2·27	−20·5	2
AO Aur	145·3	+3·4	11·7	−3·1	2·68	−14·5	2
SZ Tau	147·4	−17·4	7·2	−2·6	0·42	−3·2	1, 3, 4
AS Aur	150·0	+5·1	12·8	−2·6	3·73	+16·0	2
RT Aur	150·7	+10·3	6·0	−2·7	0·36	+21·0	2, 3, 4
AA Gem	152·3	+4·1	10·6	−3·5	2·10	+9·5	2
RZ Gem	155·4	+1·4	10·6	−3·0	1·24	+6·5	2
SW Tau	158·0	−28·4	10·2	−0·6	0·98	+16·5	1, 5
ST Tau	160·8	−6·6	9·0	−1·2	0·78	+1·4	1, 5
AD Gem	161·0	+9·1	10·0	−2·7	1·59	+36·0	2
ζ Gem	163·5	+13·4	4·7	−3·4	0·25	+6·8	1, 3, 4
CR Ori	163·7	−2·4	13·1	−2·9	4·10	+40·5	2
RS Ori	164·3	+1·8	9·3	−3·2	1·43	+40·5	2
W Gem	165·1	+4·8	7·7	−3·2	0·74	0·0	2, 3, 4
CS Ori	165·7	−3·0	11·6	−2·7	2·68	+15·5	2
WW Mon	170·4	+1·8	13·6	−2·8	4·05	+56·5	2
T Mon	171·3	−1·1	7·1	−4·3	0·85	+32·5	1, 3
SV Mon	171·4	−2·2	9·4	−3·8	1·77	+26·5	2
TZ Mon	181·7	+2·7	11·9	−3·2	3·31	+39·0	2
SZ Mon	181·8	+0·8	11·1	−3·8	2·38	+32·0	2
TX Mon	181·8	+0·5	11·6	−3·3	2·30	+51·0	2
XX Mon	183·3	+0·3	12·8	−2·9	2·60	+63·5	2
AC Mon	189·5	−0·5	11·8	−3·2	2·02	+40·5	2
RY CMa	193·7	+1·6	9·0	−2·8	1·05	+37·5	2, 3
TV CMa	194·9	−1·0	11·9	−2·8	2·01	+39·0	2
TW CMa	196·8	+1·4	10·4	−3·1	1·60	+66·5	2
WW CMa	196·8	−15·1	10·2	−2·7	2·88	+53·5	2
RW CMa	199·7	−2·6	12·7	−3·0	3·19	+50·0	2
VW Pup	203·1	+0·6	12·4	−2·8	3·17	+24·0	2

Star	l	b	m_{pg}	M_{pg}	r	ρ	Notes
	°	°					
X Pup	203·8	+0·4	9·4	−4·2	2·14	+64·0	2
WW Pup	205·1	+2·2	11·6	−3·0	3·41	+87·0	2
SS CMa	206·9	−3·0	11·4	−3·6	4·47	+60·0	2
WX Pup	209·2	−0·3	10·7	−3·3	2·34	+53·4	2
WY Pup	209·5	+3·8	11·8	−2·9	4·52	+44·0	2
AD Pup	209·6	+1·1	11·4	−3·7	3·32	+67·5	2
WZ Pup	209·6	+4·4	11·4	−2·9	4·04	+64·0	2
VZ Pup	211·1	−2·2	11·6	−4·1	5·02	+49·0	2
AQ Pup	213·9	+1·1	9·8	−4·4	2·64	+59·8	2
RS Pup	220·1	+0·7	8·4	−4·7	1·27	+21·3	2, 3
AT Pup	222·0	−0·7	8·7	−3·1	0·94	+28·8	2, 3
AP Pup	223·0	−4·9	8·1	−2·9	0·86	+17·9	2, 3
AH Vel	230·0	−6·3	6·1	−2·8	0·46	+26·0	1, 3
RZ Vel	230·5	−0·8	7·9	−4·0	1·54	+25·5	2, 3
AX Vel	230·8	−7·0	8·8	−2·4	1·07	+24·2	1, 3
T Ant	232·5	+11·6	9·6	−3·0	2·00	+29·5	2, 3
T Vel	233·1	−3·2	8·7	−2·8	1·06	+8·0	1, 3
SX Vel	233·2	−1·6	9·2	−3·4	2·03	+30·9	2, 3
β Dor	238·5	−32·3	5·1	−3·4	0·38	+8·1	2, 3, 4
BG Vel	239·5	−2·1	9·3	−3·1	1·95	+10·9	2, 3
V Car	242·6	−11·9	8·6	−3·1	1·02	+16·1	2, 3
V Vel	244·2	−3·8	8·5	−2·8	0·91	−28·7	2, 3
l Car	250·7	−6·8	5·0	−4·5	0·47	+1·4	2, 3, 4
UX Car	252·5	+0·3	8·8	−2·7	0·72	+10·4	2, 3
Y Car	253·4	−0·2	8·4	−2·7	0·65	−5·8	2, 3
SV Vel	253·8	+2·5	9·7	−3·7	1·21	+4·5	2, 3
VY Car	254·3	+1·3	8·8	−4·0	0·98	−1·2	2, 3
U Car	256·8	+0·1	7·2	−4·6	0·76	+0·4	2, 3
ER Car	257·8	+1·5	7·8	−3·2	0·66	−18·1	2, 3
GI Car	258·0	+2·5	8·9	−2·8	0·81	−21·4	2, 3
IT Car	259·1	−1·1	8·5	−3·2	0·76	−14·0	2, 3
V419 Cen	259·9	+4·2	9·0	−3·0	0·91	−17·2	2, 3
AZ Cen	260·5	−0·3	9·1	−2·6	0·74	−12·3	2, 3
UZ Cen	262·6	−1·1	9·6	−2·6	0·85	−5·1	2, 3
RT Mus	264·1	−5·4	9·6	−2·6	1·02	−1·8	2, 3
T Cru	267·1	+0·1	7·8	−3·1	0·73	−6·0	2, 3
S Mus	267·1	−7·8	7·4	−3·4	0·72	+11·8	2, 3
R Cru	267·4	+0·8	7·8	−3·0	0·72	−13·5	2, 3
AG Cru	269·4	+2·8	9·4	−2·7	1·06	−4·5	2, 3
R Mus	269·6	−6·9	7·6	−3·2	0·72	+3·8	2, 3
X Cru	270·1	+3·4	9·7	+3·0	1·37	−25·0	2, 3
S Cru	271·1	+4·1	7·6	−2·8	0·70	−6·6	2, 3
V378 Cen	273·8	−0·1	9·7	−3·1	1·13	−17·7	2, 3
CPD−60°4739	275·4	+0·5	7·4	−3·0	0·63	−12·8	2, 3
XX Cen	277·3	+4·1	8·4	−3·5	1·07	−15·7	2, 3
V381 Cen	278·6	+3·8	8·1	−2·9	0·80	−30·8	2, 3
V339 Cen	280·9	−1·1	9·6	−3·4	1·17	−24·3	2
V Cen	284·2	+2·6	7·6	−3·0	0·68	−22·3	2, 3
R TrA	284·5	−8·4	7·5	−2·6	0·57	−9·1	2, 3
W Vir	289·3	+57·6	10·6	−2·4	3·37	−65·4	1, 5
S TrA	289·6	−9·0	7·3	−3·1	0·71	+6·6	2, 3
U TrA	290·7	−8·9	8·4	−2·4	0·85	−13·7	2, 3
S Nor	295·3	−6·3	7·1	−3·4	0·71	+3·3	2, 3
κ Pav	295·4	−26·3	5·0	−1·8	0·19	+37·6	1, 5
AL Vir	299·8	+44·2	10·0	−1·9	1·97	+22·5	1, 5

Star	l	b	m_{pg}	M_{pg}	r	ρ	Notes
	°	°					
V636 Sco	311·1	−6·4	7·7	−3·1	0·80	+0·8	2
RX Lib	316·2	+25·5	12·6	−4·2	14·06:	−58·0	2
RV Sco	318·2	+4·4	7·5	−3·0	0·57	−18·3	2, 3
V482 Sco	322·1	−1·2	8·5	−2·8	0·64	+11·1	2, 3
RY Sco	324·2	−4·8	9·0	−4·0	1·12	−18·4	2
BF Oph	324·9	+7·2	8·2	−2·7	0·79	−31·4	2
V500 Sco	326·7	−2·7	10·0	−3·4	1·09	−13·8	2
X Sgr	328·9	−1·2	5·4	−3·2	0·31	−13·7	2, 3, 4
W Sgr	329·2	−5·4	5·5	−3·2	0·33	−26·4	2, 3, 4
AP Sgr	335·8	−3·9	7·7	−2·9	0·52	−18·0	2, 3
VY Sgr	337·8	−2·5	13·0	−3·7	2·81	−6·0	2
WZ Sgr	339·8	−2·8	9·0	−4·1	1·57	−10·0	1
Y Sgr	340·5	−3·6	6·4	−3·0	0·46	−3·8	1, 3, 4
AY Sgr	340·9	−3·9	12·0	−3·1	2·40	−26·5	2
V350 Sgr	341·3	−9·2	8·0	−2·9	0·79	+9·0	1
U Sgr	341·4	−5·9	9·6	−3·1	1·36	+3·9	1, 4
V377 Sgr	342·2	−9·8	14·3	−3·8	14·86:	+6·0	2
BB Sgr	342·3	−10·5	7·9	−3·1	0·82	+7·5	2
XX Sgr	342·7	−3·4	9·8	−3·1	1·23	+2·0	1
YZ Sgr	345·4	−8·6	8·1	−3·4	0·80	+19·3	1
V410 Sgr	345·6	−12·9	13·3	−3·7	12·02:	+0·0	2
X Sct	346·7	−3·1	9·6	−2·8	0·88	+7·0	2
UZ Sct	346·9	−3·0	12·6	−3·7	2·04	+12·0	2
Y Oph	348·3	+8·6	7·4	−3·8	0·56	−6·1	2, 3
Y Sct	351·7	−2·3	10·9	−3·4	1·80	+6·5	2
SS Sct	352·9	−3·3	8·8	−2·7	0·85	−14·0	1
Z Sct	354·5	−2·2	11·0	−3·6	1·90	+29·0	2
TY Sct	355·8	−1·4	12·4	−3·5	2·27	+6·5	2
V496 Aql	355·9	−7·3	8·8	−3·1	0·58	+5·2	1, 3
BW Sct	355·9	−2·7	12·7	−2·7	2·44	+2·0	2
RU Sct	355·9	−1·2	11·0	−4·0	1·83	−12·0	2
BX Sct	356·6	−3·2	13·9	−3·1	4·13	−17·5	2
AA Ser	358·5	+0·3	14·6	−3·8	1·24	−9·0	2
U Aql	358·6	−13·1	7·3	−3·2	0·57	−6·8	1, 3
PZ Aql	358·6	−3·8	13·0	−3·3	3·94	−32·0	2

In addition two parameters, the distance to the galactic centre R_0 and the longitude of the centre l_0, are required in the analysis. We shall adopt the distance $R_0 = 8{\cdot}2$ kpc obtained by Baade (**24**) from the maximum in the line of sight distribution in the density of RR Lyrae variables in the vicinity of the galactic nucleus. Although the value of R_0 determined from the distance to the maximum density depends upon an adopted longitude of the galactic centre, probably the most important factor affecting the certainty of the result is the absorption. No attempt will be made in this paper to determine the longitude of the galactic centre from the radial velocity data. Previous determinations of l_0 from cepheid velocities have given values between 325° and 326° with an r.m.s. error of about 2°. More recently, higher values of l_0 between 327° and 328° have become popular, due largely to the influence of the radio determinations (**25**). However, current work (**26, 27**) suggests that the radio position may be disturbed by a point source approximately in the direction of the centre but located between the Sun and the galactic nucleus. Since the values of l_0 suggested by the optical and radio data lie within the range $l_0 = 325°$ to 328°, we shall carry

out the analysis with these two assumed longitudes in order to set limits to the values of the parameters in the representation of the cepheid motions which are sensitive to the direction of the galactic centre.

2. *Differential rotation near the Sun*

In a previous paper (**20**) a determination of Oort's constant was given for a group of nearby Cepheids with distance moduli corrected for absorption by means of colour excesses. Using the Oort approximation to the effect of galactic rotation on the radial velocities, it was shown that in spite of Baade's revision of the zero-point of the period–luminosity curve, Joy's original value of Oort's constant $A = 20$ km/sec/kpc was recovered. The interstellar absorption adopted by Joy appears to have been unduly low by comparison with the absorption required by the reddening of the B stars, and this higher absorption was shown to compensate for the increase in the distance moduli of the Cepheids brought about by Baade's revision of the absolute magnitudes.

The solutions for differential rotation given in this section bring the earlier analysis forward in two respects. In the first place, it was previously necessary to correct the radial velocities for local solar motion since the amount of data was insufficient for a realistic determination of the velocity components. Secondly, whereas the use of the Oort approximation was a necessary part of the scale-factor method, it is now convenient to use higher order approximations which do not restrict the selection of stars to those for which the heliocentric distances are small.

2.1. *The radial velocity equation.*—Consider a galaxy containing a highly flattened system of stellar objects in differential rotation about an axis of symmetry, and let $\omega(R)$ be the angular velocity at a distance R from the axis of rotation, $\omega(R)$ being assumed to be independent of the distance z above or below the galactic plane for small values of z. If circular orbits of the objects about the galactic centre are assumed, the motions take place in a field of force $F(R) = R\omega^2(R)$ directed towards the galactic centre. The radial velocity of an object relative to a frame of reference rotating with the velocity of the system at the distance R_0 is then given by

$$\rho_c = R_0[\omega(R) - \omega(R_0)] \sin(l - l_0) \cos b, \tag{1}$$

where l and b are the galactic co-ordinates of the object. This form for the radial velocity due to differential rotation was originally introduced by Bottlinger (**28**) in order to obtain, for *empirical laws of force*, trigonometric expansions of a higher order than is given by the Oort approximation.

Let us now superimpose a general expansion of the galactic system on the pure rotation, neglecting the z-component of the velocity field of the expansion since the effect of this component on the radial velocities involves the factor $\sin b$, which is negligibly small for objects in a highly flattened system. Let Π be the radial component of the velocity of expansion at a distance R from the axis of rotation, and suppose that for small distances from the galactic plane Π is effectively independent of z. The radial velocity due to the expansion is then given by

$$k(R)r \cos^2 b - R_0[k(R) - k(R_0)] \cos(l - l_0) \cos b, \tag{2}$$

where $k(R) = \Pi/R$. The expression (2) is the K-term for a general expansion parallel to the galactic plane.

Combining the effects due to differential rotation and expansion of the system, the radial velocity equation may be written in the form

$$\rho' = kr\cos^2 b + f(R, R_0)\sin(l-l_0)\cos b - g(R, R_0)\cos(l-l_0)\cos b, \tag{3}$$

where

$$f(R, R_0) = R_0[\omega(R) - \omega(R_0)], \qquad g(R, R_0) = R_0[k(R) - k(R_0)].$$

The radial velocity ρ' is the velocity of an object relative to a frame of reference rotating with the system. Let u_0, v_0 and w_0 be the components of the solar motion referred to this frame, the components u_0 and v_0 being in the galactic plane and in the direction of longitude l_0 and $l_0+90°$ respectively, w_0 being perpendicular to the galactic plane and directed towards the north galactic pole. The observed radial velocity corrected for the solar motion is then given by

$$\rho' = \rho + u_0\cos(l-l_0)\cos b + v_0\sin(l-l_0)\cos b + w_0\sin b. \tag{4}$$

The distinction between the radial velocity ρ referred to the Sun, the radial velocity ρ' defined by equation (3), and the radial velocity ρ_c given by equation (1) for purely circular motion should be noted. The latter velocity is clearly the observed velocity corrected for solar motion and the K-term.

2.2. *Solutions for galactic rotation.*—We wish to make an analysis of the cepheid velocities which will lead to a determination of the Oort constant

$$A = -\tfrac{1}{2}\left(\frac{df(R,R_0)}{dR}\right)_{R=R_0}, \tag{5}$$

the velocity components of the solar motion, and to an examination of the level of significance of the K-term for the cepheid system by means of equations (3) and (4), using a suitably approximate treatment of the equations. The passage from the exact form (1) for the radial velocity equation for circular motion to the well-known Oort approximation has been shown by Camm (**4**, p. 166; **11**, p. 82) to involve two steps, (i) a dynamical approximation

$$f(R, R_0) = -2A(R-R_0), \tag{6}$$

and (ii) a geometrical approximation

$$R - R_0 = -r\cos(l-l_0)\cos b. \tag{7}$$

Although (i) is satisfactory for small values of $R-R_0$ so long as the curvature of $f(R, R_0)$ is not large, (ii) is rather less satisfactory since it involves a systematic error. Furthermore, if there is a change δr in r, the corresponding change δR in R is such that $|\delta(R-R_0)| \leqslant |\delta r|$, and the equality only applies to objects in the galactic plane with $l = l_0$ and $l_0+180°$. In most cases we have $|\delta(R-R_0)| \ll |\delta r|$, and the radial velocity is then by no means linearly proportional to the distance r. In this section we shall adopt Camm's linear approximation (6). By analogy with the definition (5) of Oort's constant, we define

$$C = -\tfrac{1}{2}\left(\frac{dg(R, R_0)}{dR}\right)_{R=R_0} \tag{8}$$

so that the approximation is $g(R, R_0) = -2C(R-R_0)$. The appropriate form of equation (3) is then

$$\begin{aligned}\rho' = {} & k_0 r\cos^2 b - 2A(R-R_0)\sin(l-l_0)\cos b \\ & - 2C(R-R_0)\{(r/R_0)\cos^2 b - \cos(l-l_0)\cos b\},\end{aligned} \tag{9}$$

where $k_0 = k(R_0)$. Thus, to a consistent order of approximation we may determine from equations (4) and (9), by the ordinary method of least squares, the quantities k_0, A, C, u_0, v_0, and w_0, although a determination of w_0 would be low in weight for a highly flattened system of objects. A further simplification might be made

by writing $C=0$, corresponding to an expansion parallel to the galactic plane such that Π/R is independent of R. We shall, however, retain the term in C in equation (9) in order to preserve the degree of approximation, and to decide from the observations if there is any evidence for the function $g(R, R_0)$ in the cepheid motions.

Although the linear approximation to $f(R, R_0)$ in equation (6) may be used without restriction on the heliocentric distance r, it is necessary that $R-R_0$ should not be too large if the higher order derivatives of the function are not negligible. Some idea as to the limitation of the range of values of $R-R_0$ which might be necessary may be gained by considering the rotation

$$f(R, R_0)=\tfrac{4}{3}AR_0\{(R_0/R)^{3/2}-1\} \qquad (10)$$

which holds for a system in rotation under the influence of an inverse square law of force. A comparison between the exact function and the approximate form (6) shows that the error is less than ten per cent provided $|R-R_0|<0{\cdot}1R_0$.

In Table II there are 96 Cepheids for which the galactocentric distances, given by

$$R^2=R_0{}^2+r^2\cos^2 b-2R_0r\cos(l-l_0)\cos b,$$

lie within the range $7{\cdot}5\,\text{kpc}<R<9{\cdot}0\,\text{kpc}$, comprising about half the data available, the velocities of 45 Cepheids being taken from the recent observations (**10**). We shall restrict our solutions of the approximate equations to Cepheids which lie within this annular strip of width 1·5 kpc, the Sun being located approximately at its centre. The solutions were made by the ordinary method of least squares from 96 equations of condition of the form

$$\begin{aligned} k_0r\cos^2 b-u_0\cos(l-l_0)\cos b-v_0\sin(l-l_0)\cos b \\ -w_0\sin b-2A(R-R_0)\sin(l-l_0)\cos b \\ -2C(R-R_0)\{(r/R_0)\cos^2 b-\cos(l-l_0)\cos b\}=\rho+\delta\rho, \end{aligned} \qquad (11)$$

where $\delta\rho$, the peculiar part of the radial velocity, is a correction to the observed radial velocity ρ which includes the observational error in ρ and departures from the adopted kinematics as represented on the left-hand side of equation (11). We have assumed that $\delta\rho$ is more important than the errors in r and $R-R_0$, a condition necessary for the application of the ordinary method of least squares,

TABLE III

Solutions for Oort's constant A, the components of the solar motion, and the K-term

l_0	325°			328°		
A	+18·5 ± 2·1	+18·9 ± 2·0	+19·5 ± 1·9	+18·6 ± 2·0	+18·6 ± 2·0	+19·9 ± 2·0
u_0	+7·8 ± 2·2	+8·2 ± 2·2	+8·7 ± 2·1	+8·3 ± 2·2	+8·4 ± 2·2	+9·6 ± 2·2
v_0	+11·9 ± 1·4	+11·9 ± 1·4	+12·1 ± 1·4	+11·5 ± 1·4	+11·5 ± 1·4	+12·0 ± 1·4
w_0	+7·3 ...	+7·3 ...	+7·3 ...	+7·3 ...	+7·3 ...	+7·3 ...
k_0	−0·4 ± 1·0	−1·1 ± 1·2	...	−2·4 ± 1·3	−2·6 ± 1·1	...
C	+2·7 ± 2·7	...	...	+0·7 ± 2·7	...	...
μ	11·3	11·3	11·3	11·3	11·2	11·5

and that $\delta\rho$ behaves like a random error in the construction of the normal equations. The velocity component w_0 is essentially indeterminate, and the standard value $w_0 = +7{\cdot}3$ km/sec has been adopted.

2.3. *Discussion of the solutions.*—The solutions for Oort's constant, the solar motion, and the K-term are given in Table III for the two assumed longitudes of the galactic centre, $l_0 = 325°$ and $328°$. The table also gives the r.m.s. error calculated in the usual way from the weights of the unknowns in the normal equations and the r.m.s. error μ of an observational equation. Three solutions were made for each longitude. In the first, all six unknowns were determined, in the second we have taken $C = 0$; and finally, a solution was made without any K-terms.

2.3.1. *The K-term.*—The solutions show that there is no evidence in the cepheid motions for the second part of the K-term which involves the coefficient C. Hence $g(R, R_0) = 0$, and $k(R) = k_0$, a constant independent of R, is the form of the K-term to be examined. It is evident from the size of the r.m.s. error in k_0 that we are dealing with a quantity of marginal significance. There is no warrant for retaining the term if $l_0 = 325°$. However, the size of the negative K-term increases with l_0, and thus could become more significant if higher values of l_0 were adopted. For $l_0 = 328°$, we have $k_0 = -2{\cdot}6 \pm 1{\cdot}1$ km/sec/kpc. Although it might be argued that a quantity which is two and a half times the r.m.s. error could be significant, the fact remains that the velocity dispersion is only very slightly reduced if the K-term is retained. It might be concluded that there is some slight evidence in the cepheid motions for a negative K-term corresponding to a uniform contraction of the system if the longitude of the galactic centre is $328°$. The acceptance of a negative K-term for the cepheid system has been advocated by Parenago (**6, 29**) who has considered some of the interesting consequences which arise from such a term in dynamical theory. However, it appears that the existence of the term was inferred from solutions for galactic rotation in which the lower value of the longitude $l_0 = 325°$ was assumed. The present work offers little support for the K-term in these circumstances.

2.3.2. *Solar motion.*—The solutions for the solar motion in Table III are the velocity components relative to a frame of reference moving with the circular velocity of the system at the solar distance from the galactic centre. The solar motion relative to the circular velocity should be carefully distinguished from the local solar motion which is the velocity of the Sun with respect to the centroid of the space motions of the nearby stars. Now the well-known asymmetry in the frequency distribution of the space motions in the direction of galactic rotation gives a centroid which differs for different groups of stars. But it has been pointed out by Vyssotsky (**30**) that whereas the centroids of the space motions for the various groups differ, the *maximum* of the frequency function for each group occurs at approximately the same value of the space velocity. The position of the maximum has been identified by Vyssotsky with the solar motion with respect to the circular velocity. In order to distinguish between the solar motion defined in this way, and the *local solar motion*, we shall use Vyssotsky's term *basic solar motion*.

A comparison between the velocity components for the standard value of the local solar motion (20 km/sec towards $l = 23°{\cdot}5$, $b = +21°{\cdot}6$), the basic solar motion of Vyssotsky and Janssen (**30**), and the velocity components obtained

in the present work is given in Table IV. In addition to the velocity components u_0, v_0, and w_0, the table gives $(u_0^2+v_0^2)^{1/2}$, the projection of the solar velocity on the galactic plane. Special consideration should be given to v_0, that is the component in the direction of galactic rotation. It is found that the solar motion obtained for the Cepheids gives a rotation of the system which makes the average value of the function $f(R, R_0)$ equal to zero for Cepheids for which $\bar{R}=R_0$. Camm has shown (**11**, p. 84) that this condition is rather sensitive to the value of the v_0-component. If the condition is not satisfied, the v_0-component of the solar motion is incorrect. A recent determination by Raimond (**31**) is deficient in this respect as it gives $f(R_0, R_0)=+7$ km/sec. The discrepancy in $f(R_0, R_0)$ is not so marked in the case of the local solar motion.

The last line in Table IV shows that the components of the solar motion obtained in the present work are practically the same as the components of the basic solar motion given by Vyssotsky and Janssen. Since the motion of the Sun with respect to the circular velocity of rotating systems of objects is a reflection of their speed of rotation, the system of stars to which Vyssotsky and Janssen's determination refers must be sharing the same rotation as the cepheid system at the solar distance from the galactic centre.

TABLE IV

Comparison between velocity components of the solar motion for $l_0=325°$

Component	u_0	v_0	w_0	$(u_0^2+v_0^2)^{1/2}$
Local Solar Motion	+9·7	+15·9	+7·3	18·6
Present work	+8·7 ± 2·1	+12·1 ± 1·4	+7·3 ...	14·2 ± 1·8
Basic Solar Motion	+9·7 ± 0·6	+10·6 ± 1·0	+5·9 ± 0·3	14·4 ± 0·9
Present work *minus* Basic Solar Motion	−1·0 ± 2·2	+1·5 ± 1·7	...	−0·2 ± 2·0

2.3.3. *Oort's constant.*—In an earlier paper (**20**) Oort's constant was determined from a group of nearby Cepheids at a mean distance of 0·87 kpc from the Sun, using distance moduli corrected for absorption by means of colour excesses. The solution $A=19·8 \pm 2·3$ km/sec/kpc was obtained by means of the Oort approximation. Since the reddening of the B stars which was used for the determination of the intrinsic colours in (**20**) is essentially the same as that used in the calculation of the distances of the Cepheids in Table II for which colours are not available, the determinations of Oort's constant given in Table III and in the previous paper differ only in method and weight. The solution for Oort's constant in Table III for the case $l_0=325°$ and no K-term, namely $19·5 \pm 1·9$ km/sec/kpc, is practically identical with the value of A found in the earlier paper by means of the Oort approximation with $l_0=325°$ and no K-term. The present work therefore strongly reinforces the earlier conclusion that Baade's revised distance moduli for the Cepheids, corrected for absorption by means of the reddening of B stars in surrounding fields, gives an Oort constant

$A = 20$ km/sec/kpc approximately. These determinations refer to a distance scale in which the average absorption $\Sigma A_{pg}/\Sigma r$ is approximately 2 magnitudes per kpc near the galactic plane.

3. *The rotation of the cepheid system*

In the preceding section, Camm's linear approximation (6) was used for the functions $f(R, R_0)$ and $g(R, R_0)$ for small values of $R - R_0$. This step was taken so that the differential rotation at the solar distance from the galactic centre could be determined at the same time as the components of the solar motion with respect to the circular velocity of the rotating system. In this way we have obtained a solar motion which gives the correct rotation $f(R, R_0)$ at $R = R_0$, and a determination of the K-term which could be used to free the observed radial velocities from the effect of non-circularity in the mean motion about the galactic centre.

Having obtained the corrected velocities, the restriction on $R - R_0$ may now be removed, and the rotation of the entire system examined by means of a powerful general method introduced in 1938 by Camm (**11**). The method starts with the radial velocity and proper motion equations for circular motion as written by Bottlinger (**28**) for any force function. But whereas Bottlinger only used the equations to obtain higher order terms in trigonometric expansions for special laws of force, that is for *assumed* forms for the rotation as a function of distance from the galactic centre, Camm inverted the problem and determined the rotation as a function of distance directly from the radial velocities. The method was applied by Camm to cepheid variables (**4**) and planetary nebulae (**11**), and has been used extensively by Soviet astronomers with due acknowledgment. It appears, however, that the existence of the method has not been appreciated elsewhere.

3.1. *Exposition of Camm's method.*—The radial velocity and proper motion equations may be written in the form

$$\rho_c = f(R, R_0) \sin(l - l_0) \cos b, \tag{12}$$

and

$$\tau_c = f(R, R_0)[\cos(l - l_0) - (r/R_0) \cos b] - \omega(R_0) r \cos b, \tag{13}$$

where ρ_c and τ_c are the radial and transverse velocities corrected for solar motion and the K-term, the proper motion in galactic longitude $\mu_l \cos b$ being related to τ_c by the equation

$$r\mu_l \cos b = \tau_c + u_0 \sin(l - l_0) - v_0 \cos(l - l_0) + g(R, R_0) \sin(l - l_0). \tag{14}$$

Equations (12) and (13) are exact in the sense that they follow from the assumption of circular motion about the galactic centre without mathematical approximation. When applied to a system of stellar objects, a velocity dispersion is superimposed on the mean motion. Equations (12) and (13) should therefore contain terms representing the peculiar part of the radial and transverse velocities.

Camm's method may be divided into two steps, (1) the determination of the $f(R, R_0)$ curve, (2) the determination of $\omega(R_0)$ from the proper motion equation, and hence the angular rotation of the system as a function of R from the equation

$$\omega(R) = \omega(R_0) + R_0^{-1} f(R, R_0). \tag{15}$$

The determination of the $f(R, R_0)$ curve for the system consists in finding mean values of $f(R, R_0)$ and R for objects conveniently arranged in distance groups.

The following is a suitable method of weighting equation (12) to obtain the best mean value of $f(R, R_0)$ from the objects within each group. If the range of vaiues of R in the group is small, we may assume that

$$f(R, R_0) = f(R_1, R_0) + (R - R_1)(df/dR)_{R=R_1}, \tag{16}$$

where R_1 is some weighted mean value of R. Let $w = \sin(l - l_0)\cos b$, then equations (12) and (16) give

$$f_1 w + (df_1/dR)w(R - R_1) = \rho_c + \delta\rho_c, \tag{17}$$

where $f_1 = f(R_1, R_0)$, and $\delta\rho_c$ arises from the velocity dispersion. If $\delta\rho_c$ can be treated as a random error, the ordinary method of least squares applied to equation (17) gives the normal equations

$$f_1 \Sigma w^2 + (df_1/dR)\Sigma w^2(R - R_1) = \Sigma w\rho_c, \tag{18}$$

$$f_1 \Sigma w^2(R - R_1) + (df_1/dR)\Sigma w^2(R - R_1)^2 = \Sigma w(R - R_1)\rho_c. \tag{19}$$

Now the weight of the solution for f_1 in these equations is

$$\Sigma w^2 - [\Sigma w^2(R - R_1)]^2/\Sigma w^2(R - R_1)^2,$$

and when $\Sigma w^2(R - R_1) = 0$, that is when R_1 is given by

$$R_1 = \Sigma w^2 R/\Sigma w^2, \tag{20}$$

the weight of $f(R_1, R_0)$ takes its greatest value Σw^2. The mean value of $f(R, R_0)$ given by equation (18) is then

$$f(R_1, R_0) = \Sigma w\rho_c/\Sigma w^2. \tag{21}$$

This method of weighting takes two factors into account, the variation of $f(R, R_0)$ within the group, and the weight of each object as a function of the longitude. If the velocity dispersion were small and the amount of data adequate, the method would give small segments of the $f(R, R_0)$ curve. It is, however, sufficient to have established that the appropriate mean values for any distance group are given by equations (20) and (21),* the $f(R, R_0)$ curve for the system being the continuous curve through the mean points. The velocity-dispersion for the objects in each group follows directly from the radial velocity equation (12), the value of $f(R, R_0)$ for each object being taken from the smooth curve. The r.m.s. error μ_f in the weighted mean value $f(R_1, R_0)$ may then be calculated for each group from the relation

$$\mu_f{}^2 = \Sigma(\delta\rho_c)^2/(n - 1)\Sigma w^2. \tag{22}$$

Having determined the $f(R, R_0)$ curve for the system, the second step, the determination of $\omega(R_0)$ from the proper motion equation, may now be completed. From equations (13) and (14) with $g(R, R_0) = 0$, we have

$$\omega(R_0)r\cos b = V - r\mu_l\cos b, \tag{23}$$

where

$$V = u_0 \sin(l - l_0) - v_0\cos(l - l_0) + f(R, R_0)[\cos(l - l_0) - (r/R_0)\cos b].$$

Since u_0, v_0 and $f(R, R_0)$ are known from the analysis of the radial velocities, the contribution V to the mean motion transverse to the line of sight may be found for any object. The solution of equation (23) for $\omega(R_0)$ which then follows requires some consideration since the terms in the equation are subject to several sources of error. In the first place, for a system of objects with a velocity dispersion, equation (23) should contain a term representing the peculiar

* Soviet astronomers use a weight $|w|$, objects very close to the longitude of the centre and the anticentre being excluded.

transverse motion which affects the term V. Secondly, the observational term in the equation of condition contains the observed proper motion $\mu_l \cos b$ in galactic longitude and the computed distance r, both of which are subject to error. If the distances are known more accurately than the proper motions, equation (23) may be solved by the ordinary method of least squares to obtain the estimate

$$\omega_1(R_0) = \Sigma r \cos b(V - r\mu_l \cos b)/\Sigma r^2 \cos^2 b. \tag{24.1}$$

This is equivalent to weighting the individual values of $\omega(R_0)$ in equation (23) by $r^2 \cos^2 b$. Alternatively, equation (23) may be divided by r before applying least squares to obtain a second estimate

$$\omega_2(R_0) = \Sigma \cos b(V/r - \mu_l \cos b)/\Sigma \cos^2 b. \tag{24.2}$$

In this case, greater weight is given to the nearer objects by placing emphasis upon errors in V due to the velocity dispersion. Since equations (24.1) and (24.2) give estimates of $\omega(R_0)$ which fit the data from one end of the distance range at the expense of the other, it is advisable to make a third estimate to compromise between the two extremes. This may be done by introducing weights proportional to $r \cos b$, so that the weighted mean value of $\omega(R_0)$ from equation (23) is given by

$$\omega_3(R_0) = \Sigma(V - r\mu_l \cos b)/\Sigma r \cos b. \tag{24.3}$$

As a further refinement, the observational equations might be weighted according to the errors in the proper motion determinations, choosing weights proportional to the inverse of the errors in preference to their inverse squares.

3.2. *Application to cepheid variables.*—In Camm's application of the method to cepheid variables and planetary nebulae (**4, 11**), preliminary forms for the $f(R, R_0)$ curve were obtained for assumed values of the velocity components (u_0, v_0, w_0) of the solar motion, the longitude l_0 and the distance R_0. The method of differential corrections was then applied to the radial velocity equation in order to determine corrections Δu_0, Δv_0, Δw_0, Δl_0 and ΔR_0 to the assumed values by the method of least squares, the preliminary curve for $f(R, R_0)$ being used to obtain the derivative $\partial f(R, R_0)/\partial R$ required in the equations of condition. This refinement of the method has not been applied in the present work in which the $f(R, R_0)$ curve for the Cepheids is based upon an adopted longitude l_0, Baade's value of the distance R_0, and the velocity components u_0 and v_0 given by the solutions carried out in Section 2.2.

Cepheids listed in Table II as members of Population II have been omitted in this determination of the $f(R, R_0)$ curve. The remaining 189 Cepheids were conveniently grouped according to distance R, and weighted mean values of R and $f(R, R_0)$ for each distance group were calculated from equations (20) and (21), the radial velocity ρ_c for each object being given by

$$\rho_c = \rho + u_0 \cos(l - l_0) \cos b + v_0 \sin(l - l_0) \cos b + w_0 \sin b - K,$$

where ρ is the observed radial velocity in Table II. The mean values of R and $f(R, R_0)$ are given in Table V for $l_0 = 325°$ and no K-term, the values of u_0, v_0, and w_0 being given in the third column of Table III.

Having determined the $f(R, R_0)$ values we can now proceed to the determination of $\omega(R_0)$ for the cepheid system along the lines indicated in the preceding section. It is to be expected that the determination cannot be made with much weight on account of the small number of reliable proper motions which are available

at the present time. It is, however, essential to attempt a determination of the angular velocity, even from insufficient information, for two reasons. In the first place, this can only be done satisfactorily for distant objects—for there may be a local vortex—and the differential rotation effect should be carefully removed,

TABLE V

Weighted mean values of R and $f(R, R_0)$ for cepheid variables in distance groups

Range in R kpc	Number of objects	R_1 kpc	$f(R_1, R_0)$ km/sec
4·7—6·2	7	5·43	+21±25
6·2—6·9	9	6·42	+49±21
6·9—7·5	19	7·24	+32·7±6·0
7·5—7·7	14	7·59	+23·4±4·7
7·7—7·9	20	7·82	+ 9·8±3·1
7·9—8·1	20	7·99	+11·2±3·2
8·1—8·3	10	8·24	− 0·8±2·5
8·3—8·5	12	8·41	− 6·8±1·9
8·5—8·7	8	8·59	−15·8±3·7
8·7—9·0	12	8·91	−30·6±6·3
9·0—9·4	11	9·20	−58·7±4·8
9·4—9·8	15	9·53	−56·0±5·0
9·8—10·3	14	10·15	−52·9±6·7
10·3—11·3	11	10·81	−46·4±6·1
11·3—12·3	6	11·92	−51·5±7·6

as indicated in Section 3.1, and not merely thrown into another harmonic term. Secondly, there is no valid reason for supposing *a priori* that the angular velocity $\omega(R_0)$ for the Cepheids should be the same as that given by other groups of objects. Indeed, it has been established observationally by Strömberg (**32**) and envisaged theoretically by Lindblad (**33**) in the original hypothesis of galactic rotation, that the velocity of rotation is closely related to the velocity dispersion of each group or system of objects. Now the Cepheids comprise a highly flattened system in which the random motions of the objects, as indicated by the dispersion in radial velocities, are much smaller than the random motions of other groups of objects such as the early type stars. Although the proper motion data are much more extensive for these groups than for the Cepheids themselves, it is clearly desirable to determine $\omega(R_0)$ for the cepheid system from the cepheid data alone, instead for forcing agreement with other groups of objects.

The data used in this determination of $\omega(R_0)$ for the Cepheids are the proper motions of 18 variables given by Blaauw and Morgan (**17**) in their work on the calibration of the cepheid absolute magnitudes. The proper motion stars are indicated in the notes for Table II which also indicate that the distance moduli of ten of the objects have been corrected for absorption by means of colour excesses. The distances of the remaining eight Cepheids for which photo-electric colours are not available are probably less accurately known. The components of the proper motion in right ascension and declination given by Blaauw and Morgan were combined to give the proper motion in galactic longitude in seconds of arc per annum. The linear transverse velocity $\kappa r \mu_l \cos b$ was then obtained for each object in km/sec., using $\kappa = 4{\cdot}735 \times 10^3$ with the distance r in kpc. The

TABLE VI

Estimates of $\omega(R_0)$ for the cepheid system

Estimate	Solution 1.	Solution 2.
	km/sec/kpc	km/sec/kpc
$\omega_1(R_0)$	$39{\cdot}2 \pm 7{\cdot}2$	$38{\cdot}4 \pm 8{\cdot}2$
$\omega_2(R_0)$	$26{\cdot}9 \pm 6{\cdot}5$	$29{\cdot}6 \pm 7{\cdot}3$
$\omega_3(R_0)$	$28{\cdot}5 \pm 8{\cdot}0$	$32{\cdot}0 \pm 7{\cdot}0$
Mean	$31{\cdot}4 \pm 7{\cdot}2$	$32{\cdot}9 \pm 7{\cdot}5$

three estimates of $\omega(R_0)$ from equations (24.1), (24.2) and (24.3) are given in Table VI with the r.m.s. errors. The second set of solutions given in the table was obtained by weighting the equations inversely as the errors in the proper motions. The solutions were all made for the case $l_0 = 325°$, using the $f(R, R_0)$ curve defined by the mean points in Table V.

The weighted mean value of the estimates given in Table VI is $\omega(R_0) = 32 \pm 7{\cdot}5$ km/sec/kpc, the large uncertainty being due entirely to the small number of reliable proper motions. It is of interest to note that the same proper motion data which enabled Blaauw and Morgan to determine the zero-point of the P–L curve with considerable accuracy have given a determination of the rotation with low weight. The uncertainty in $\omega(R_0)$ is such that the Oort constant $B = -12{\cdot}5 \pm 7{\cdot}5$ km/sec/kpc, which follows from the relation

$$B = A - \omega(R_0)$$

with $A = 19{\cdot}5$ km/sec/kpc, does not differ significantly from the lower negative value $B = -6{\cdot}9 \pm 1{\cdot}5$ km/sec/kpc obtained by Morgan and Oort (**34**) from the proper motions of early type stars and faint stars in general, and the entirely

TABLE VII

Comparison of $f(R, R_0)$ for cepheid variables with values from 21-cm radio data and schematic models of the galactic system

R kpc	Cepheid variables	Radio data	Oort's model	Schmidt's model	Inverse square
5·43	$+21 \pm 25$	+118	...	+118	+182
6·42	$+49 \pm 21$	+71	...	+71	+94
7·24	$+32{\cdot}7 \pm 6{\cdot}0$	+38	...	+38	+44
7·59	$+23{\cdot}4 \pm 4{\cdot}7$	+24	...	+24	+26
7·82	$+9{\cdot}8 \pm 3{\cdot}1$	+15	...	+15	+16
7·99	$+11{\cdot}2 \pm 3{\cdot}2$	+9	...	+9	+8
8·24	$-0{\cdot}8 \pm 2{\cdot}5$	...	−2	−2	−2
8·41	$-6{\cdot}8 \pm 1{\cdot}9$	...	−8	−8	−8
8·59	$-15{\cdot}8 \pm 3{\cdot}7$	...	−14	−15	−14
8·91	$-30{\cdot}6 \pm 6{\cdot}3$	...	−24	−26	−25
9·20	$-58{\cdot}7 \pm 4{\cdot}8$	...	−33	−36	−34
9·53	$-56{\cdot}0 \pm 5{\cdot}0$	...	−43	−45	−43
10·15	$-52{\cdot}9 \pm 6{\cdot}7$	...	−60	−61	−58
10·81	$-46{\cdot}4 \pm 6{\cdot}1$	...	−74	−75	−72
11·92	$-51{\cdot}5 \pm 7{\cdot}6$	...	−95	−96	−92

independent value of B which follows from the axial ratio of the velocity ellipsoid, $-B/(A-B)=0{\cdot}24\pm0{\cdot}04$, obtained by Hins and Blaauw (**35**) from a study of the Radcliffe proper motions of faint stars. In the course of time, the accuracy of the determination for the Cepheids will improve as more data on proper motions become available. It may then be possible to ascertain if the Oort constant B for the Cepheids differs appreciably from these average values for heterogeneous collections of nearby objects.

3.3. *Discussion of the rotation curve.*—We shall conclude this discussion of the rotation of the cepheid system with a comparison between the observed rotation and the rotation according to schematic models of the mass distribution in the galactic system. If the differential rotation of the system near the Sun is determined largely by the mass of the Galaxy in the inner region where $R<R_0$, the $f(R, R_0)$ curve may be approximated near $R=R_0$ and at greater distances by equation (10), namely

$$f(R, R_0)=\tfrac{4}{3}AR_0\{(R_0/R)^{3/2}-1\}.$$

This gives the rotation for circular motion when the field of force $F(R)$ varies as the inverse square. Although this representation appears to involve only the distance R_0 and the Oort constant A, it is implicit in the assumption of an inverse square law that $A+3B=0$, so that the value of the Oort constant B is implied for an assigned value of A. Now the value $A=19{\cdot}5$ km/sec/kpc for the cepheid system is well determined from the analysis of the radial velocities, and a system with this value of A in an inverse square field of force would have $B=-6{\cdot}5$ km/sec/kpc. The cepheid proper motions, on the other hand, give an uncertain but greater negative value $B=-12{\cdot}5$ km/sec/kpc. Although the inverse square behaviour of the field of force near the Sun would be excluded by this greater negative value, the uncertainty is such that a decision cannot be made from the available proper motion data. Values of $f(R, R_0)$ calculated from equation (10) with $A=19{\cdot}5$ km/sec/kpc are given in Table VII for the values of R at which weighted mean values of $f(R, R_0)$ were calculated for cepheid variables in Section 3.2. A comparison is also made in the table with values of $f(R, R_0)$ for circular motion in Oort's original model of the galactic system (**36, 37**, p. 134) in which the distribution of mass is represented by the superposition of concentric homogeneous spheroids and a more recent model, constructed by Schmidt (**38**), in which both homogeneous and non-homogeneous spheroids are used. An important feature of the model adopted by Schmidt is that in the region $R<R_0$ it reproduces the circular velocities obtained from the Leiden 21-cm radio data (**39**). These models are constructed for a Galaxy in which $R_0=8{\cdot}2$ kpc, $A=19{\cdot}5$ km/sec/kpc, $B=-6{\cdot}9$ km/sec/kpc, so that the circular velocity at the Sun is $\Theta_0=216$ km/sec. Accordingly, the field of force at $R=R_0$ is practically an inverse square as $A+3B=-1{\cdot}2$ km/sec/kpc for the models, whereas $A+3B=0$ for the inverse square law. Since most of the mass is concentrated in the region $R<R_0$, it is perhaps not surprising to find in Table VII that for $R>R_0$ the rotation $f(R, R_0)$ for the models does not differ greatly from that given by the inverse square law.

A comparison is given in Fig. 2 between the rotation for Schmidt's model and the mean rotation calculated for the cepheid groups. The comparison shows that the best agreement is to be found in a comparatively small range of distances about $R=R_0$ where the agreement is guaranteed by the appropriate choice of

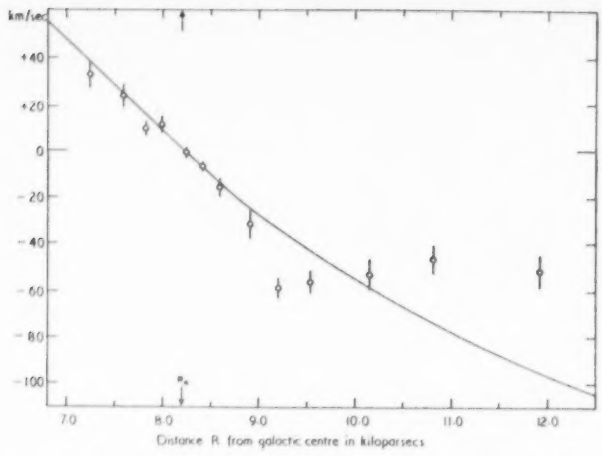

FIG. 2.—*The differential rotation $f(R, R_0)$ of the system of cepheid variable stars compared with the rotation curve for Schmidt's model. Open circles denote mean rotations computed for cepheid variables in distance groups by Camm's method, assuming $l_0 = 325°$ and $R_0 = 8{\cdot}2$ kpc. The Oort constant A for the model is 19·5 km/sec/kpc.*

the Oort constant A for the model. There are, however, three remarkable discrepancies between the rotation $f(R, R_0)$ for the Cepheids and the model. At large distances from the galactic centre the Cepheids are found to rotate much more rapidly than the model. There are, no doubt, appreciable uncertainties in the absorption at great distances in the absence of data on the colours of the faint Cepheids which comprise the outermost groups, but it appears unlikely that the cepheid rotations would be drastically modified by a revision of the distances of the objects in these groups. The second discrepancy between the Cepheids and the model is the appearance of large negative values of $f(R, R_0)$ near $R = 9{\cdot}2$ kpc. This peculiarity is also present in the rotation curve obtained by Camm (**4**) and is due, as Camm suggested, to group motions in a small sector of galactic longitude in the vicinity of the constellation Cassiopeia. The velocity dispersion within the group itself is small, but the radial velocities are systematically too negative by about 20 km/sec. The third discrepancy is perhaps the most striking. For distances $R < 7$ kpc, which are not shown in Fig. 2, the cepheid rotations given in Table VII fall well below the rotation curve from 21-cm radio data.

In particular, the group nearest the galactic centre shows a striking difference. It is rather remarkable that there should be such a large discrepancy between $f(R, R_0)$ from cepheid variables on the one hand and radio data on the other as both methods purport to give an observational determination of the same quantity. In the case of Camm's method it is possible to assign an uncertainty to the computed rotation by means of equation (22). The computed uncertainty for the two groups nearest the galactic centre is large, partly on account of the small weight which the method assigns to the objects near the longitude of the galactic centre, and partly because the velocity dispersion appears to increase towards the centre of the Galaxy. In the case of the radio method no uncertainty is assigned to the computed rotation, but the determination by Camm's method

clearly indicates that the rotation for the group nearest the centre lies significantly below the rotation given by the radio determination.

Acknowledgments.—Grateful acknowledgment is due to Dr G. L. Camm for permission to give an account in Section 3.1 of the system of weighting which was used in his earlier application of the method to cepheid variables; to Dr O. J. Eggen of the Lick Observatory for the reduction of his photo-electric observations of Cepheids to the ***P, V*** system; and to Dr J. B. Sykes for generous assistance with the Russian literature.

The work described in the paper was initiated during the author's tenure of the Radcliffe Travelling Fellowship in Astronomy at Oxford. The writer is greatly indebted to Professor H. H. Plaskett for his continued interest and stimulating advice which has contributed much to the investigation.

University Observatory,
Oxford:
1956 *March.*

References

(1) A. H. Joy, *Ap. J.*, **86,** 363, 1937.
(2) A. H. Joy, *Ap. J.*, **89,** 356, 1939.
(3) R. E. Wilson, *Ap. J.*, **92,** 170, 1940.
(4) G. L. Camm, *M.N.*, **104,** 163, 1944.
(5) H. Mineur, *Ann. d'Astrophys.*, **7,** 160, 1944.
(6) P. P. Parengo, *Variable Stars Bulletin* (USSR), **6,** 102, 1947.
(7) O. A. Melnikov, *Pulkova Obs. Publ.*, **64** (No. 2), 81 *et seq.*, 1950.
(8) N. U. Mayall, *Michigan Publ.*, **10,** 19, 1951.
(9) H. F. Weaver, *A.J.*, **60,** 202, 1955.
(10) D. W. N. Stibbs, *M.N.*, **115,** 363, 1955; *Comm. Radcliffe Obs., Pretoria*, No. 32.
(11) G. L. Camm, *M.N.*, **99,** 71, 1938; *Comm. Univ. Obs., Oxford*, No. 13.
(12) H. Shapley, *Harvard Monograph* No. 2, 135, 1930.
(13) H. Shapley, *P.N.A.S.*, **26,** 541, 1940.
(14) A. D. Thackeray and A. J. Wesselink, *Nature*, **171,** 693, 1953.
(15) H. Shapley, *P.N.A.S.*, **39,** 349, 1953.
(16) H. Shapley and V. McK. Nail, *P.N.A.S.*, **40,** 1, 1954.
(17) A. Blaauw and H. R. Morgan, *B.A.N.*, **12,** 95, 1954.
(18) K. Lundmark, *Lund Medd.*, Ser. I, No. 135, 1933; No. 163, 1946.
(19) H. Mineur, *Comptes Rendus*, **235,** 1067, 1952.
(20) D. W. N. Stibbs, *M.N.*, **115,** 323, 1955; *Comm. Univ. Obs., Oxford*, No. 48.
(21) P. P. Parenago, *A.J.* (USSR), **22,** 129, 1945.
(22) G. L. Camm, *Private communication.*
(23) K. F. Bottlinger and H. Schneller, *Zs. f. Ap.*, **1,** 339, 1930.
(24) W. Baade, *Michigan Symposium on Astrophysics*, Lecture X, 24, 1953.
(25) J. D. Kraus and H. C. Ko, *Ap. J.*, **122,** 139, 1955.
(26) R. D. Davies and D. R. W. Williams, *Nature*, **175,** 1079, 1955.
(27) E. F. McClain, *Ap. J.*, **122,** 376, 1955.
(28) K. F. Bottlinger, *Veröff. Berlin-Babelsberg*, **10,** No. 2, 1933.
(29) P. P. Parenago, *Course in Stellar Astronomy* (Moscow), 3rd Edition, Ch. VII, Section 62.
(30) A. N. Vyssotsky and E. M. Janssen, *A. J.*, **56,** 58, 1951.
(31) E. Raimond, *B.A.N.*, **12,** 99, 1954.
(32) G. Strömberg, *Ap. J.*, **61,** 363, 1925.
(33) B. Lindblad, *Arkiv. för Matematik*, **19** A, No. 21, 1925; *Upsala Medd.*, No. 3, 1925.
(34) H. R. Morgan and J. H. Oort, *B.A.N.*, **11,** 379, 1951.
(35) C. H. Hins and A. Blaauw, *B.A.N.*, **10,** 365, 1948.
(36) J. H. Oort, *Ap. J.*, **116,** 233, 1952.
(37) H. C. van de Hulst, C. A. Muller and J. H. Oort, *B.A.N.*, **12,** 117, 1954.
(38) M: Schmidt, *B.A.N.*, **13,** 15, 1956.
(39) K. K. Kwee, C. A. Muller and G. Westerhout, *B.A.N.*, **12,** 211, 1954.

CONTENTS

PAGE

Meeting of 1956 May 11

Fellows and Junior Member elected 361

Presents announced 361

Harold Jeffreys, The damping of the variation of latitude 362

D. E. Blackwell, Observations from an aircraft of the zodiacal light at small elongations 365

C. H. Costain, B. Elsmore and G. R. Whitfield, Radio observations of a lunar occultation of the Crab Nebula 380

R. G. Conway and P. A. O'Brien, The distribution of brightness at metre wavelengths across the Sun's disk 386

R. J. Bray, The centre-limb variation of the sodium D line intensities 395

C. W. Allen, Spectrophotometry of the outer corona 413

H. H. Plaskett, Excitation of chromospheric emission 419

Helen W. Dodson and E. Ruth Hedeman, Detailed study of the development of an active solar region, 1954 August 20–27 428

R. D. Davies, The relation between interstellar gas, dust and the emission from neutral hydrogen at 21 cm 443

D. W. N. Stibbs, On the differential galactic rotation of the system of cepheid variable stars 453

Printed in London by Taylor & Francis, Ltd., 1957 February